Inter- and Intracellular Effects of Traumatic Axonal Injury

Inter- and Intracellular Effects of Traumatic Axonal Injury

A dissertation presented

by

Borna Esfahani Dabiri

to

The School of Engineering and Applied Sciences

in partial fulfillment of the requirements

for the degree of

Doctor of Philosophy

in the subject of

Engineering Sciences

Harvard University

Cambridge, Massachusetts

March, 2014

Dissertation Advisor: Professor Kevin Kit Parker Author: Borna Esfahani Dabiri

Inter- and Intracellular Effects of Traumatic Axonal Injury

Abstract

Mild Traumatic Brain Injuries (mTBIs) are non-penetrating brain injuries that do not result in gross pathological lesions, yet they may cause a spectrum of cognitive and behavioral deficits. mTBI has been placed in the spotlight because of increased awareness of blast induced and sports-related concussions, but the underlying pathophysiological mechanisms are poorly understood. Several studies have implicated neuronal membrane poration and ion channel dysfunction as the primary mechanism of injury. We hypothesized that injury forces utilize mechanically-sensitive, transmembrane integrin proteins, which are coupled to the neuronal cytoskeleton (CSK) and distribute injury forces within the intracellular space, disrupting CSK organization and reducing intercellular neuronal functionality. To test this, magnetic beads were coated with adhesive protein, allowing them to bind to integrins in the neuronal membrane *in vitro*. To apply forces to the neurons via the bound beads, we built custom magnetic tweezers and demonstrated that focal adhesions (FACs) formed at the site of bead binding. We showed that the beads were coupled to the CSK via integrins by measuring the disparate adhesion of the soma and neurite to their underlying substrate. The soma also required more force to detach than neurites, correlating with the FAC density between each

neuronal microcompartment and substrate. We then utilized the magnetic tweezers to test whether beads bound to integrins injured neurons more than beads that bound to neurons nonspecifically. Integrin-bound beads injured neurons more often and the injury was characterized by the formation of focal swellings along axons, reminiscent of Diffuse Axonal Injury. While integrin-bound beads initiated swellings throughout neurons, beads bound nonspecifically only caused local injury where beads were attached to neurons. To demonstrate the electrical dysfunction of integrin-mediated injury forces, we adapted Magnetic Twisting Cytometry to simultaneously apply injury forces to beads bound to multiple cells within neuronal networks *in vitro*. The formation of focal swellings resulted in reduced axonal electrical activity and decreased coordinated network activity. These data demonstrate that the mechanical insult associated with mTBI is propagated into neurons via integrins, initiating maladaptive CSK remodeling that is linked to impaired electrical function, providing novel insight into the underlying mechanisms of mTBI.

Table of Contents

List of Figures

Acknowledgments

It has been said that successfully completing one's PhD has little to do with having the best grades, the highest IQ, or the best resources. In fact, finishing a PhD has everything to do with grit, determination, and perseverance. I have found this to be true in my case as well. The source of these attributes has been my family and friends. First and foremost, I must thank my parents, Hassan and Azar, for exemplifying grit and determination. Immigrating to a new country and having to learn a new language and a new way of life in the middle of one's career is no small task. I am forever thankful and indebted for their endless love and sacrifice. They've taught me many important lessons through their actions that have directly impacted my ability to succeed. I'd also like to thank my younger brother, Pouya. He has been my best friend and confidant ever since he was born and I was lucky to have him in Boston for some time as well. He has also been a beacon of perseverance and has inspired me greatly through his actions. I also need to thank my older brother, Dana, for helping pave the way for me and being a great resource to turn to whenever I've needed anything. I love my family very much and would have never reached this point (or even gotten through elementary school) without them. Thank you.

During my nine years at Harvard as an undergraduate and a graduate student, I've had the privilege of meeting some of the most genuine and caring people. I consider my college roommates to be part of my family and I love each and every one of them like a brother. They've helped pull me through the tough times over the past decade and have been there to celebrate my best of times. Without their love and support, I would not have survived Boston. Because I had begun working in my future lab as an undergraduate, I

also had the pleasure of becoming close with many former and present members of the Disease Biophysics Group. Throughout my years in this lab, I have never known a more dedicated group, willing to extend help to others at a moment's notice. Without them, none of my work was possible and I am grateful to count them as my colleagues and friends.

During my time at Harvard, I was also lucky enough to meet the love of my life. Kyle has been a constant throughout my time here and has been an important part of my formative college and post-college years. She has been a steadfast supporter throughout my PhD and has put up with late nights at lab, long periods of questionable hygiene, and has shown compassion when I was feeling down. She has also been a source of jubilation for my successes and reminds me daily of what is important in life. I was lucky to marry the love of my life just weeks ago, and as I am writing this, we are embarking on a new journey together and I cannot imagine anyone else by my side.

I first met my advisor, Kit, as a junior in college. Ever since then, he has pushed me to accomplish feats that I never imagined possible. We never compromised our goals and dreams despite the obvious obstacles in our way. He has taught me to aim high. From my first project in the lab, where we attempted to use tumor cells to build heart tissue, to our work in understanding new mechanisms in traumatic brain injury for my dissertation, we never compromised. Our work even extended beyond the lab, where I had the opportunity to help Kit with teaching and projects beyond just the classroom. Thank you for teaching me to be creative and uncompromising, and that with hard work and planning, nearly anything is possible. I'd also like to thank Professors Maurice Smith, Dave Weitz, and Ross Zafonte for their input and support as part of my PhD committee.

Lastly, I need to thank Dr. Prislin, the Associate Dean for student affairs at the U.C. Irvine School of Medicine, for being open minded and allowing me to take a leave of absence from medical school in order to pursue my PhD.

1 Neurodegeneration and the Neuronal Cytoskeleton: A Role for Integrin Signaling in TBI

1.1 Introduction

Traumatic Brain Injury (TBI) is a complex disease process initiated by mechanical insults ranging from explosive blasts to sports-related concussions. It is characterized by a spectrum of outcomes, from lifelong cognitive dysfunction to mild impairments that resolve within weeks. TBI affects 1.7 million people annually in the United States, which is comparable to the number of heart attacks per annum [1, 2], yet unlike the multiple treatment options for cardiovascular distress, therapies for TBI are scarce. TBI is categorized into mild, moderate, and severe classes, which are determined clinically by scores from the Glasgow Index – a physical examination that assesses simple reflexes and cognitive function. In this context, mild TBI (mTBI) comprises 75% of TBI cases and refers to non-penetrating head injuries like concussions, and is not typically characterized by gross pathological findings such as skull fracture, hemorrhage, or contusions [3]. Post-mortem analysis of brain tissue from individuals who have suffered multiple mTBIs throughout their lifetime has revealed neuropathology with similarities to those found in patients with dementias like Alzheimer's Disease (AD) [4-7]. Currently, definite clinical confirmation of the histological features of mTBI relies purely on post-mortem analysis of brain tissue; however, emerging imaging modalities such as Diffusion Tensor Imaging have revealed lowered fractional anisotropy in mTBI

patients, suggesting structural abnormalities due to injury [8-10]. Declining cognitive capabilities indicate a progressive degeneration of brain function and place mTBI in the context of other progressive neurodegenerative diseases that are also faced with limited treatment strategies [11]. Thus, mTBI has emerged as a significant disease process associated with initiating neurodegenerative processes that are poorly understood and an unmet need for effective therapeutics.

The neurodegenerative process that leads to dementia, whether caused by mTBI or AD, is marked by maladaptive remodeling of the neuronal cytoskeleton (CSK), which ultimately hinders neuronal function. The neuronal cytoskeleton functions in a myriad of developmental and physiological capacities, and comprises actin, intermediate filaments (neurofilaments), and microtubules [12-14]. These structures are especially pertinent in the axonal and dendritic extensions of neurons, where they support vesicular transport to and from the soma in addition to providing structural integrity (Figure 1-1). Post-mortem analysis of brain tissue of subjects with history of repeated mTBI highlights the aggregation of microtubule-associated tau protein into neuro-fibrillary tangles (NFTs) [15, 16]. In addition to the cytotoxic effects of NFTs, aggregated tau can no longer bind and stabilize microtubules. These destabilized microtubules hinder proper transport, further contributing to neuronal dysfunction. Brain tissue from AD patients is also replete with NFTs similar to those found in brains of those with repeated mTBIs. Given the importance of CSK dysfunction in these disease processes, closer examination of the CSK may offer mechanistic insight and novel therapeutic options for mTBI and related dementias.

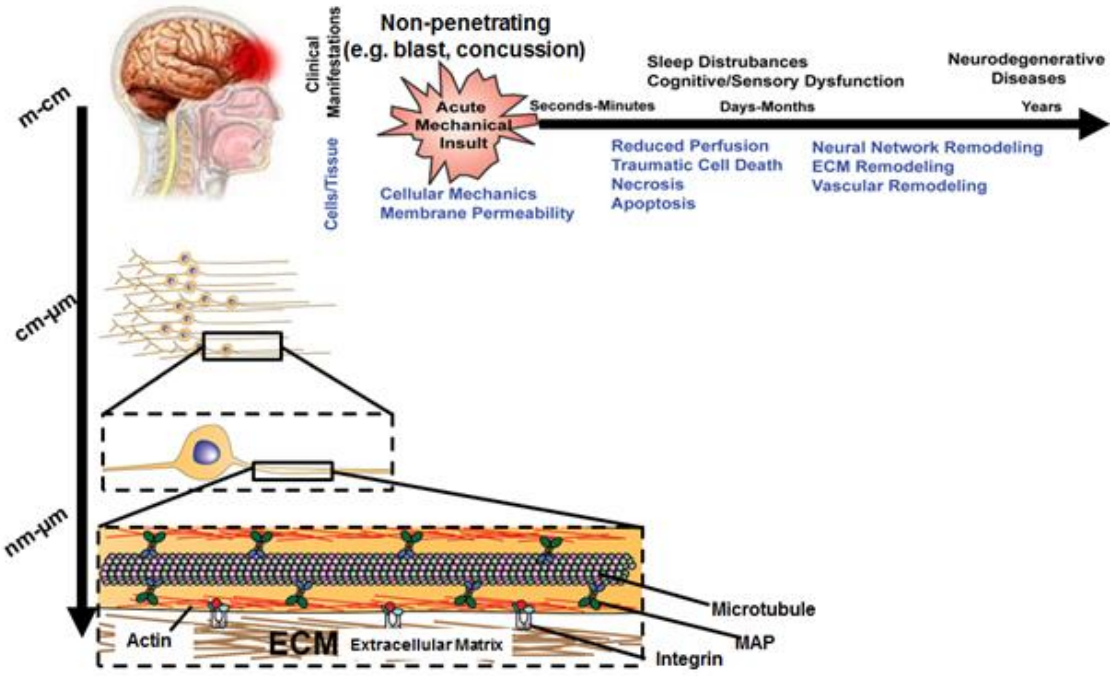

Figure 1-1: mTBI is a Multidimensional Disease. Injury forces from mTBI have short term and long term sequela, and they are transmitted through nine orders of spatial magnitude, ranging from the brain to the cytoskeleton of neurons.

In order to assess the role CSK plays in the pathological conditions associated with neurodegeneration, it is important to consider how the CSK integrates with the neuronal microenvironment (i.e., surrounding cells and extracellular matrix proteins). The CSK is intrinsically linked to the neuronal microenvironment via various transmembrane cell adhesion molecules that serve both structural and signaling functions. Integrins are a

member of the family of cell adhesion molecules, serving to link the neuronal CSK to the surrounding cellular microenvironment [17]. As transmembrane proteins, integrins are integral to the cellular machinery that couples extracellular mechanical cues to the cellular CSK and helps translate mechanical signals into intracellular biological cascades, a process called cellular mechanotransduction [18, 19]. Integrins are responsible for both ligand-mediated (e.g., T-cell receptor activity) and mechanical (e.g., forces at the cellular level) signaling to and from the CSK [20-23]. In neurons, integrin activity has been implicated in various processes, ranging from axonal pathfinding [24-26] to long term memory potentiation [27-29]. Moreover, recent reports have highlighted how integrin signaling is a component in the initiation and progression of neuronal disease processes, including mTBI (mechanical integrin signaling) [30] and AD (ligand-mediated integrin signaling) [31]. In light of the importance of the CSK in neurodegenerative disease processes like mTBI and AD, and the fact that integrins mediate the CSK's interactions with the neuronal microenvironment, it is important to consider integrin-mediated mechanisms of injury. Herein, we review the common CSK features of neurodegenerative diseases (e.g., mTBI and AD), highlight the role of integrin signaling in both disease processes, and argue that insight gained from integrin signaling and mechanotransduction may generate novel therapeutic approaches.

1.2 mTBI and Alzheimer's Mediated Dementia: The Role of the Cytoskeleton

CSK-related pathology in mTBI-induced neurodegeneration has been highlighted primarily by post-mortem analysis of brain tissue from individuals with a history of mTBI in various settings that range from blast to sports-related concussion [16, 32, 33]. Therefore, CSK-related pathology may represent a fundamental response of neurons to injurious mechanical forces, regardless of the specific event generating forces within the brain. Repeated mTBI can lead to neurological deficits and a constellation of histological features that together are referred to as Chronic Traumatic Encephalopathy (CTE). A major feature of these findings is the accumulation of neurofibrillary tangles (NFTs), which are made up of hyperphosphorylated tau protein. These NFTs are similar to those found in neurodegenerative diseases like AD and are found throughout the brain with higher densities appearing at the depth of sulci and in perivascular regions [5]. These structures are thought to contribute to the dementia-like aspects of CTE, a conjecture further supported by the fact that a dose-dependent relationship has been shown because increased incidence of mTBI correlates with higher risk of dementia later in life [34]. Though the majority of mTBI-induced neurodegenration has been linked to history of repeated mTBI, it is important that single mTBI events may also predispose individuals to early-onset AD [34, 35]. Taken together, the neuropathological findings of mTBI posit an injury mechanism that hinders CSK function via the formation of NFTs, which can directly impact microtubular stability and function.

The CSK is also disrupted in AD, where the accumulation of various protein aggregates correlate with neuronal dysfunction and death. Similar to the neuropathology of CTE, protein aggregates in AD include NFTs that are made up of hyperphosphorylated tau protein [36, 37]. Although the mechanisms by which NFTs disrupt neuronal function have remained elusive, it is clear that tau pathology is an important hallmark of neurodegeneration, as multiple reports have shown that tau mutations alone can lead to dementia [38, 39]. The NFTs found in AD are distinguishable from those of CTE in several aspects. In AD, NFTs may be found throughout the frontal cortex, whereas NFTs are located more superficially in CTE and are typically located at the depth of the sulci. Moreover, NFTs found in CTE tend to accumulate in the parenchyma in close proximity to the vasculature, a distribution pattern that is not found in AD [5]. Lastly, CTE does not always exhibit amyloid beta pathology, which is pathognomonic for AD. Amyloid beta pathology and tau pathology are the classical findings in confirmed cases of AD. Taken together, the results indicate tau pathology is common to both AD and CTE induced dementia; however, key differences in distributions of NFTs and the inconsistent amyloid beta pathology in CTE offers insight into the neuronal signaling pathways at work in both disease processes. Thus, a shared injury mechanism may entail biological cascades sensitive to the mechanical injury of CTE and to the aberrant protein processing (e.g., amyloid beta) found in AD.

1.3 Integrins Mediate Mechanical and Ligand Based Signaling

Integrins are transmembrane proteins that transmit mechanical information from the extracellular space to the internal CSK of cells. They are heterodimers, made up of various α and β dimer combinations, that together form unique binding domains (reviewed in [40]). Integrins can directly bind to extracellular proteins or ligands on other cells, linking these extracellular moieties to the cytoskeleton via the focal adhesion complex (FAC). FACs form the basis for multiple signaling cascades, including various kinases that mediate the activity of integrin activation in neurons [41-43]. The role of integrins as mechanical sensors is ubiquitous and provides for physiological and pathophysiological signaling in multiple tissues, ranging from cardiovascular function to important features of neurodevelopment [44]. Thus, integrins are the primary means of mechanical signaling between the cytoskeleton and the cellular microenvironment.

Integrins are also responsible for transducing ligand-binding mediated signals into the intracellular space. In addition to being a conduit for mechanical signaling, integrins play important roles in receptor-mediated processes, such as immune cell adhesion. Leukocyte binding to the vascular wall through vascular cell adhesion molecules (VCAMs) is dependent on integrin signaling [45], and T-cell induced inflammation in the nervous system is predicated on α4 integrin signaling [46, 47]. In addition to immune cell adhesion dynamics, integrins can modulate synaptic function in neurons. The αVβ8 integrin is important for long-term memory potentiation and maintaining synaptic integrity [48, 49]. Therefore, in addition to being an important mediator for mechanical

signaling at the cellular level, integrins also serve to convey ligand-binding signaling cascades to the CSK.

1.4 Integrin Signaling in Dementia: mTBI and Alzheimer's

As a mechanically-initiated disease process, mTBI generates forces within the brain that are capable of utilizing integrins as conduits for injury in neurons. Though severe TBI may result in traumatic failure of neurons (e.g., axonal shearing), more subtle injury forces associated with mTBI may be sensed and transduced by integrins. Since they are coupled to the neuronal CSK via the FAC, injury forces are immediately distributed through the neuron (Figure 1-2), affecting several mechanically-sensitive elements of neurons, including NMDARs [50-52]. Furthermore, direct mechanical pertubation of the FAC can activate a number of kinases [53, 54].

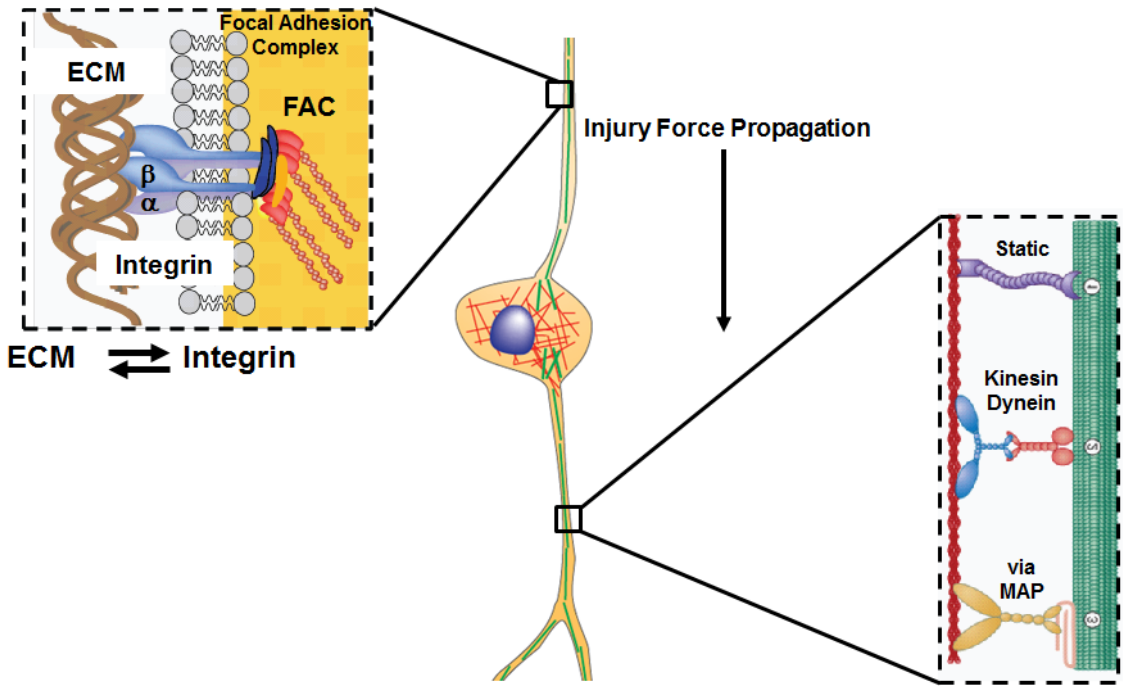

Figure 1-2: Injury Force Propagation in Neurons. Integrins serve as conduits that transfer injury forces from the extracellular matrix (ECM) to the cytoskeleton (CSK) of neurons. The CSK distributes forces throughout the neuron via cross-linking proteins such as kinesin, dynein, and microtubule associated proteins (MAP).

A well-known substrate of src kinase is tau protein, which may be hyperphosphorylated in response to src kinase activity [55, 56]. In addition, activation of the Rho/ROCK pathway may further increase CSK tension, exacerbating ongoing mechanical signaling and CSK remodeling [30, 57]. The net result of these processes can cause microtubule instability, and cause the formation of focal swellings along injured axons [30]. Thus, mechanical integrin signaling provides a means for the injury forces of mTBI to

efficiently gain access to the intracellular space and to initiate the maladaptive remodeling of the neuronal CSK.

Integrin signaling has also been implicated as one of the mechanisms of tau pathology in AD. Multiple reports have focused on the relationship between amyloid pathology and tau pathology, and although research into the relationship between these phenomena is ongoing, there are several indicators of the involvement of integrin signaling. In AD, amyloid precursor protein is inappropriately cleaved to form amyloid beta plaques, which can form aggregates in both the intracellular and the extracellular space (reviewed in [58]). Amyloid beta plaques are also known ligands of integrins [59], forming the basis for a mechanistic relationship between amyloid beta plaques and tau pathology in neurons. Several reports have shown that amyloid beta plaque integrin binding can activate kinases associated with the FAC (e.g., src kinase, integrin-linked kinase, and focal adhesion kinase) [60, 61]. These kinases can mediate tau hyperphosphorylation, causing its dissociation from microtubules and the formation of aggregates that makeup NFTs [31, 62, 63]. Taken together, these results highlight the role of integrin ligand signaling, where the tau pathology of AD is initiated by amyloid beta 42's pathological activation of integrin signaling in neurons.

1.5 Conclusion

The similarities between mTBI and AD neuropathologies suggest related injury pathways, where pathological integrin signaling mediates downstream tau pathology. Since brain tissue from those affected by mTBI induced dementia (CTE) and AD exhibit dysfunction of proteins associated with the CSK, it is important to consider how the

neuronal CSK interacts with the extracellular microenvironment. The integrin family of proteins plays important roles in mediating communication between the CSK and extracellular space, which is underscored by the fact that integrin signaling has been shown to play a role in the mechanisms underlying mTBI and AD (Figure 1-3). Current treatment strategies for mTBI and AD are only supportive and provide symptomatic relief. For example, sleep aids are provided for individuals who have suffered from sleep disruption following mTBI [64] and medications that increase acetylcholine availability (e.g., cholinesterase inhibitors) help replace lost neuronal function in AD [65]. Integrin signaling offers a plethora of therapeutic targets, many of which are currently in clinical trials. For instance, natalizumab (α4 integrin antibody) is under investigation for treating multiple sclerosis [66], and Cilengitide (αV integrin antagonist) is undergoing trials for treating glioblastomas [67]. As such, targeting integrin signaling represents novel set of tools to slow or halt the progression of neurodegeneration in the setting of mTBI.

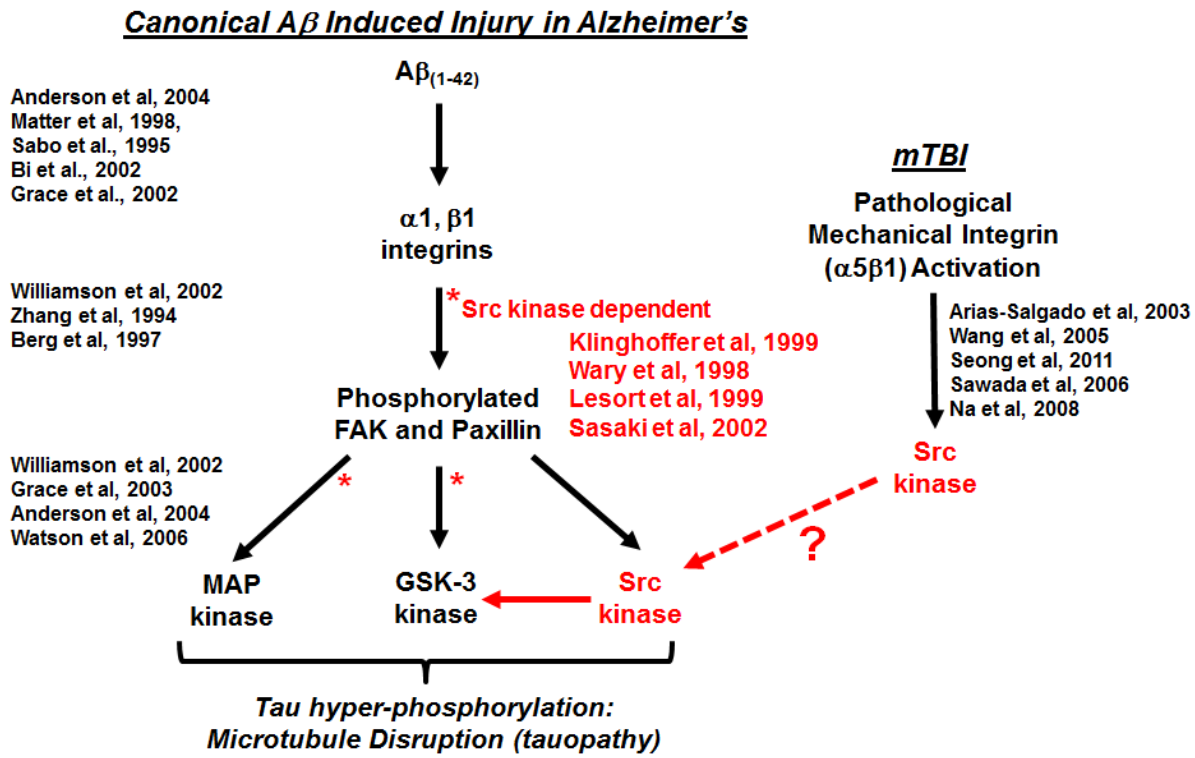

Figure 1-3: Integrin Signaling in Alzheimer's and mTBI. Proposed relationship between integrin signaling in Alzheimer's and mTBI.

2 Measuring Adhesive Properties of Neuronal Microcompartments

The brain's anatomical organization gives rise to various microenvironments, as foci of neurons extend axons far from somas individually and in bundles. Although the adhesive interactions between neurons and their microenvironment are pivotal in physiological (e.g., development and growth) and disease processes (e.g., Traumatic Brain Injury), current methods do not account for the inherent structural heterogeneities of neuronal microcompartments (i.e., soma and neurite). To address this problem, we built custom magnetic tweezers that were able to manipulate transmembrane integrin proteins in the neuronal membrane via the attachment of matrix-coated paramagnetic beads. The paramagnetic beads bound to the neuronal surface were mechanically displaced when a magnetic field was applied via the tweezers. Using this method, we applied nanoNewton forces to neurons and measured their peeling dynamics and the adhesion of specific microcompartments within the same neuron. This method is a reliable means of measuring the adhesive properties of neurons and elucidating the cellular and subcellular dynamics of how neurons physically interact with their microenvironment.

2.1 Introduction

Neurons physically interact with their local microenvironment through adhesion molecules in the cell membrane that serve as attachments points, anchoring the neuronal cytoskeleton to both the surrounding extracellular matrix (ECM) and to neighboring cells

(reviewed in [68, 69]). In addition to contributing to the mechanical integrity of neurons, adhesion molecules integrate and transmit forces necessary for a variety of processes, including neuronal growth [70-72] and migration [73-75]. These adhesions also play pivotal roles in pathophysiological processes, including Traumatic Brain Injury [30], autism [76], and schizophrenia [77]. Because adhesion molecules can propagate information, encoded as mechanical forces, into neurons [78, 79], it is important to understand how neuronal microcompartments (i.e., somas and neurites) interact with the ECM.

One method to probe neuronal adhesion and its dynamics is to generate forces at the single cell level while simultaneously measuring cellular deformation. Previous reports have primarily relied on the application of forces via fluid shear forces in various settings [80-82]. In microfluidic platforms, cell geometry and attachment can be precisely controlled and visualized while laminar flow conditions have been used to generate shear forces on cells ranging from fibroblasts to osteosarcoma cells [80, 83, 84]. Shear forces can also be generated within rheometers, where spinning cone and plate systems apply fluid shear forces directly to fibroblasts in culture [81, 85]. Lastly, suction with a large bore pipette has provided a means for controlling the rate of applied shear forces, allowing for dynamic peeling of myocytes or bacteria [82, 86]. However, fluid shear systems apply forces to cells and are further complicated by their potential to induce injury in neurons [87, 88]. Though fluid shear systems have provided insight into the adhesion dynamics of morphologically homogenous cells (e.g., fibroblasts, myocytes), similar gains have not been realized in neurons, which are also highly polarized and divided into soma and neurite microcompartments.

To address these challenges, we used magnetic tweezers to selectively apply forces to beads bound to specific microcompartments of neurons, providing a means for measuring the disparate adhesion strengths and peeling properties found within the *same* neuron. Similar to other adherent cells, neurons are mechanically connected to the ECM of the brain and adjoining cells by specialized adhesive transmembrane integrins proteins that couple the intracellular cytoskeleton of cells to the ECM [19, 89]. Integrins are important in neuronal function and they contribute to the structural integrity of neural tissue [90-92]. Integrins also confer disparate cytoskeletal dynamics on different microcompartments within the same cell [93]. Thus, we used magnetic beads to bind integrins on the apical surface of neurons to interrogate the properties of specific microcompartments. Though magnetic tweezers have been used previously to measure the adhesion strength of cells, we used them to dynamically peel neurons, demonstrating a sigmoidal behavior that indicated the unique properties of neuronal microcompartments. This finding was accompanied by experiments that discretely measured the adhesion strengths of the soma and neurite microcompartents within single neurons, revealing greater adhesion strengths of the soma relative to that of neurites. This technique provides important insight into neuronal adhesion properties, which are integral to processes ranging from axonal pathfinding to force transduction during Traumatic Brain Injury.

2.2 Materials and Methods

2.2.1 Neuron Harvest and Culture

Cortical neurons were obtained from 2-day old neonatal Sprague-Dawley rats (Charles River Laboratories, Boston, MA) and all animals were treated in compliance

with the guidelines of the Institutional Animal Care and Use Committee of Harvard University under animal experimentation protocol 24-01. The protocol meets guidelines for the use of vertebrate animals in research following recommendations included in the NIH guide for care and use of laboratory animals. Cortical tissues were surgically removed and minced into 1-2 mm^3 pieces and placed into 0.1 % trypsin solution (USB, Santa Clara, CA) overnight at 4^oC. The trypsinized tissue was triturated and filtered through a 40 µm nylon filter (BD Bioscience**,** Franklin Lakes, NJ). Then neurons were suspended in fresh DMEM culture medium (Invitrogen, Carlsbad, CA) supplemented with 10% (v/v) heat-inactivated fetal bovine serum (Invitrogen), 30 mM Glucose, 2 mM L-glutamine, 25 mM KCl, 50 mU Insulin, 7 mM p-Aminobenzoic acid, 100 U/mL penicillin, and 100 mg/mL streptomycin. Neurons were preplated for 45 minutes in a T-75 flask (VWR, Radnor, PA) and incubated in a cell culture incubator at 37°C and 5% CO_2. Neurons were seeded at a density of 10,000 neurons per cm^2 on laminin (LM) (Invitrogen, Carlsbad, CA) micropatterned polyacrylamide hydrogels, supplemented with 10 mM cytosine arabinoside (Sigma, St. Louis, MO) for the first 48 hours of culture. After 48 hours, neurons were gently rinsed three times with Phosphate Buffer Saline (PBS) (Invitrogen, Carlsbad, CA) to remove non-adherent neurons. Media was replaced every 48 hours and all experiments were performed on either day four or five after neurons were plated.

2.2.2 Polyacrylamide Hydrogel Fabrication

Magnetic tweezers experiments were performed on primary neurons grown on soft polyacrylamide (PA) hydrogels. Acrylamide and bis-acrylamide (Fisher Biotech, Loughborough, Leicestershire, UK) solutions were mixed to achieve apolymer mass of

5% and a bis-acrylamide concentration of 0.2%. This mixture resulted in a gel with a final modulus of 6 kPa, as compared to the varying stiffness of E~0.1–1 kPa measured in the brain [94]. The solutions of acrylamide, bis-acrylamide, ammonium persulfate, and N,N,N,N-tetramethylethylenediamine (TEMED) under a nonaqueous layer of toluene with 0.5% acrylic acid N-hydroxy succinimide ester (Sigma) were polymerized between two coverslips chemically modified as previously described [95]. The freshly polymerized gels were washed with HEPES buffer to remove unpolymerized solvent. The gels were then placed in wells containing sterile water and kept at 4°C until use. To activate the gel surface for protein binding, 50 μL of 1 mM Sulfo-SANPAH (sulfosuccinimidyl-6- (4-azido-2-nitro- phenyl-amino) hexanoate) (Pierce/ThermoFisher Scientific, Waltham, MA) in 200 mM HEPES were added to activate the free surface of the gel. The system was then irradiated with the UV light of a sterile hood (254 nm wavelength) for 5 min to link the Sulfo-SANPAH to the gel by photoactivation and the solution containing excess Sulfo-SANPAH was removed by aspiration. The process of adding Sulfo-SANPAH and exposing to vacuum and UV light was repeated again and the excess Sulfo-SANPAH was again removed by aspiration.

2.2.3 Micropatterning of Polyacrylamide Hydrogels

We used microcontact printing to control the neuronal and extracellular matrix interactions in order to impose bipolar morphology on neurons. The robust control of neuronal morphology allows for reproducible magnetic peeling experiments at the single cell level. Silicon (Si) master templates of 10 μm wide etched lines separated by 10 μm gaps were manufactured by standard lithography techniques, as reported previously [96]. Briefly, a thin negative photoresist (MicroChem Corp., Newton, MA) layer was spun

onto a Si wafer and exposed to UV light through an optical mask containing the desired pattern to degrade the photoresist. The exposed areas were then etched away, leaving a template mold of recessed wells with the desired patterns. Polydimethylsiloxane (PDMS) precursor (Sylgard 184, Dow Corning, Midland, MI) and curing agent were mixed (10:1 ratio) and poured over the template in a dish and cured at 65°C for 4 hours after degassing. Finally, cured PDMS stamps containing the desired array of lines were peeled from the Si wafer.

PDMS stamps with 10 μm wide micropatterns were used to pattern desired ECM proteins onto gels as previously reported [30]. Briefly, confined 10 μm wide channels were formed above the gel surface by gently pressing stamps onto the Sulfo-SANPAH activated PA hydrogels. Subsequently, 100 μL of solution containing the ECM protein to be patterned was added along the outside edges of the stamp. The stamp was constructed so that suction applied to a cavity at the top of the stamp pulled the ECM solution of 50 μg/mL LM from the edges into the confined channels formed by the bottom of the stamp and the gel surface. This concentration of LM has been shown to saturate the substrate, ensuring neuronal adhesion [97]. LM was incubated with the hydrogels overnight at 4°C and excess solution was removed by rinsing the hydrogels the next day.

2.2.4 Magnetic Tweezers Fabrication and Calibration

A magnetic tweezer is an electromagnet designed to induce a magnetic field when electric current flows through wire coiled around a metallic core. The flow of current in the wire generates a magnetic field according to the right-hand rule, where the field is generated in the direction of the right thumb as the rest of fingers wrap around the coiled

wire. The relationship between current and the induced magnetic field is described mathematically by the Biot-Savart law,

$$\vec{B}_z = \frac{\mu_0}{4\pi}\int_C \frac{Idl \times \hat{r}}{|\vec{r}|^2}, \qquad (1)$$

where μ_0 denotes the permeability of free space, I is the prescribed current in a segment of wire (dl) that is summed over path (C) of the coiled wire, and $\vec{r}$ represents the vector to the point where the magnetic field ($\vec{B}$) is calculated along the axis of the solenoid (z). In order to maximize the magnetic field of the tweezers, a custom system with two solenoids was constructed. This horseshoe magnet inspired form [98], where opposite magnetic cores are located in close proximity, was designed to facilitate the induction of large magnetic field gradients. The magnetic tweezers consisted of three linked permalloy (MμShield, Londonderry, NH) core sections that were 5 mm in diameter and 45 mm in length, connected through a permalloy base (Fig. 2-1A). In order to generate the magnetic field, two 720-turn solenoids (Magnetic Sensor Systems S-16-50, Van Nuys, CA) were fitted around each pole of the tweezers. The solenoids were supplied by a power supply (Kepco Model # BOP 100-4M, Flushing, NY) that was voltage controlled by a data acquisition board (Model # USB-6211, National Instruments, Austin, TX) programmed by a LabVIEW software (National Instruments). The tweezer set-up was fitted onto manual micromanipulators (Newport, Irvine, CA) to finely adjust the *x*, *y*, and *z* positions of the tip and attached to the stage of an inverted Axiovert 200 microscope (Carl Zeiss, Germany) (Fig. 2-1B). This assembly allowed for simultaneous cell imaging and tweezers operation.

Before conducting experiments with the magnetic tweezers, the magnetic forces produced by the system must be determined. The force is a function of both the strength of the magnetic field and the magnetic moment of the object subjected to the field. This relationship is described mathematically as:

$$\overrightarrow{F} = \nabla(\vec{m} \cdot \vec{B}), \qquad (2)$$

where $\overrightarrow{m}$ is the magnetic moment of the object reacting to $\vec{B}$, which is the magnetic field at the object's location. The magnetic tweezers in our experiments were used to generate forces on 5 μm diameter paramagnetic beads (Bioclone, San Diego, CA), which maintain magnetism only in the presence of an external magnetic field while also having high magnetic susceptibility. In order to maximize the forces on the beads, the bead's magnetic moment and the magnetic field gradient must be increased. However, this maximization faces several practical limitations. The magnetic moment of the bead is dependent on several factors including the bead's material properties, its volume, and the surrounding magnetic field strength. Although related to magnetic field strength, the gradient of the magnetic field itself depends on several factors, including the tweezers' geometry. Given the complexity of a dipole system and the presence of other factors such as the cores of the magnetic tweezers, we modeled the field gradient at the tip of the tweezers. The magnetic tweezers' bipolar, cylindrical geometry and material properties were encoded in electromagnetic field simulation software (ANSYS Maxwell, Canonsburg, PA). The 720-turn solenoids were modeled as cylinders surrounding the permalloy cores and each prescribed a 5 Amp current. The model confirmed that the

magnetic field gradient also changed as a function of distance from the tips of the tweezers (Fig. 2-1C). Given the dynamic nature of these variables, forces on the beads were empirically determined. Force calibration was conducted by measuring the velocity of the paramagnetic beads moving in a 99% glycerol solution (Sigma), as described elsewhere [99]. The force-distance relationship (Fig. 2-1D) for the beads was calibrated for coil currents of 1, 3 and 5 Amp. Bead displacement was captured using a Cascade 512B camera (Photometrics, Tuscon, AZ) during repeated current on-off cycles, each lasting 1 s (Fig. 1D inset). Since settling of the viscous fluid caused beads to drift, bead motion was also captured during current off cycles. The force acting on a bead during the current-on phase was then computed from the drift-corrected velocities according to the Stoke's formula for viscous drag at low Reynolds number flow:

$$\vec{F} = 6\mu\pi r_{bead}\vec{v}, \qquad (3)$$

where $\vec{F}$ describes the friction force of a bead with a radius r_{bead} moving with a velocity $\vec{v}$ in a fluid with dynamic viscosity μ. Under steady state bead velocity, the friction forces equal the force exerted on the bead, allowing magnetic forces acting on beads to be tabulated. To ensure the repeatability of the magnetic force produced by the dipole magnetic tweezers, we measured the velocities of at least seven beads for each current level. This calibration ensured that the forces exerted on neurons were readily determined as a function of the current applied to the tweezers and the distance between the bead and the tweezers.

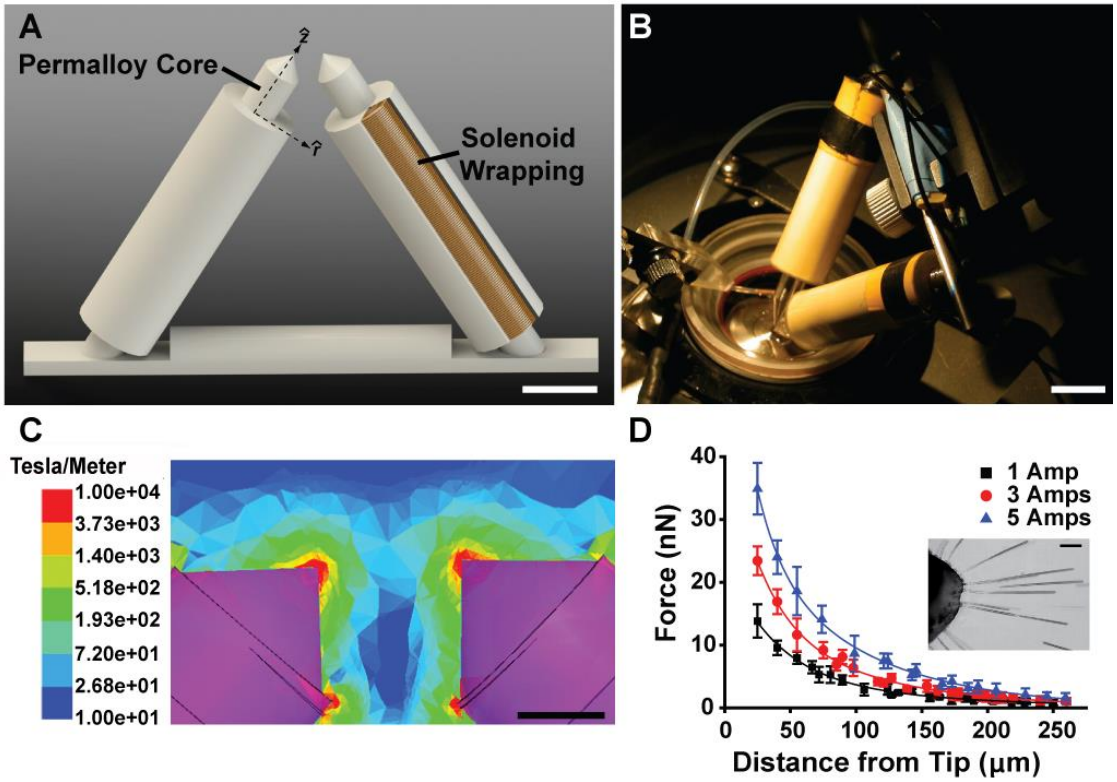

Figure 2-1: Design and assembly of dipole magnetic tweezers.

Design and assembly of dipole magnetic tweezers. (A) Schematic of dipole tweezers depicting solenoids fitted with two permalloy cores. Cut-out depicts wire wrapping of solenoid. (B) Dipole tweezers were fixed to a micromanipulator device and placed on an inverted microscope. Scale bars = 10 mm. (C) Computational modeling of the magnetic field gradient generated at both tips of the dipole tweezers. Scale bar = 2.5 mm. (D) Force-distance calibration curves recorded at different currents with sample time-lapse bead pull image (inset, scale bar = 50 µm). The force acting on beads decreased as a function of the distance from the microneedle tip and increased as a function of the electromagnetic current. Shown here: 1 A (black squares, black curve), 3 A (red circles, red curves) and 5 A (blue triangles, blue curve). At least 7 beads were analyzed for each current (error bars indicate SEM).

2.2.5 Bead Functionalization and Attachment

In order to bind paramagnetic beads specifically to the cytoskeleton of neurons, beads were coated with fibronectin (FN) (Sigma) by following the bead manufacturer's protocol for bead functionalization. Briefly, beads were first rinsed in PBS buffer (Invitrogen) and subsequently incubated in 10μg/mL FN overnight on ice. The beads were gently (0.5 Hz) agitated on rocker overnight in order to disperse beads without precipitating FN still in solution. The epoxy-activated beads bind nucleophiles such as hydroxyl groups within proteins. After rinsing beads with PBS buffer again, they were seeded onto neurons in culture medium for 20 minutes at a ratio of 4 beads per neuron. Subsequently, neurons were gently rinsed in order to wash away any unbound beads and experiments were started within 10 minutes. This process resulted in the stochastic attachment of beads to cultured neurons. It is important to note that longer bead incubation times increased the chance of bead endocytosis.

FN-coated beads bind neurons via integrins and induce the formation of the focal adhesion complex between the bead and the neuron (FAC_{bead}) at the cytoplasmic tail of clustering integrins [100] (Fig. 2-2A). The focal adhesion is comprised of several proteins responsible for mechano-chemical signaling that serve to transduce extracellular mechanical signals to the neuronal cytoskeleton. This relationship creates mechanical continuity between the bead and the internal scaffolding of the neuron. Before adding beads to neurons, zeta potential analysis [101-103] was used to confirm that beads were coated with FN. Relative to the negatively charged epoxy-coated surface of uncoated beads, FN-coated beads exhibited less negative zeta potentials (Fig. 2-2B), indicating that FN had bound to the bead's surface, reducing its net negative charge. By seeding beads

sparsely on cultured neurons and allowing binding before rinsing away unbound beads, we increased the probability of individual beads binding localized regions of neurites, permitting us to probe the properties of the local cytoskeleton. After adding beads to the neuronal cultures, the beads bound to the apical surface of neurites (Fig. 2-2C-D) while also eliciting the accumulation of focal adhesion proteins to the bead binding site, which was evidenced by the crest-shaped formation of vinculin intracellularly adjacent to the bead (Fig. 2-2E). As such, the magnetic beads were mechanically linked to the intracellular cytoskeleton of neurons via the FAC_{bead}.

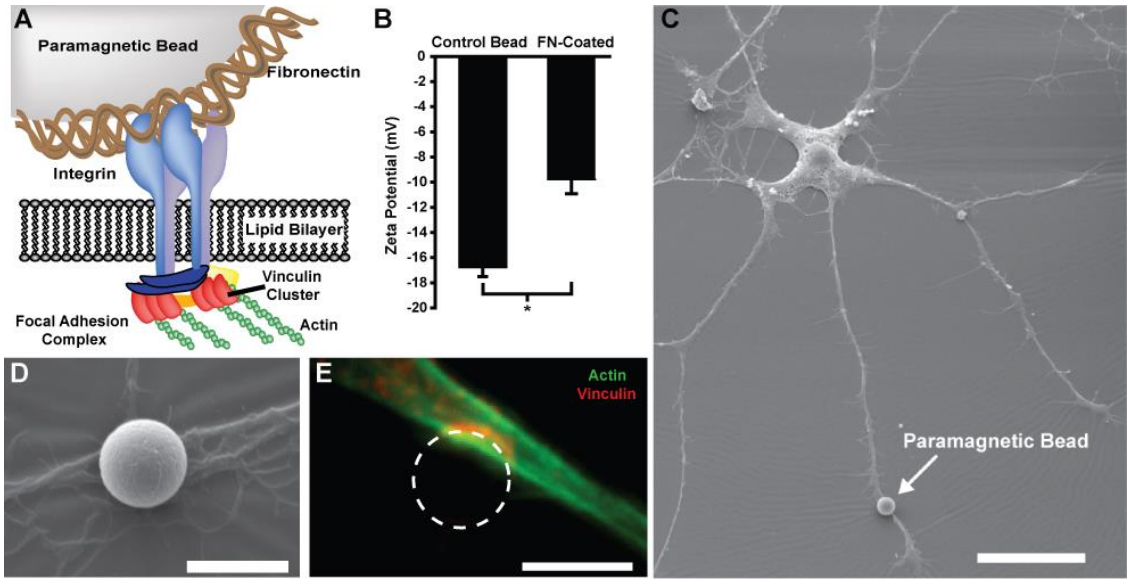

Figure 2-2: FN-coated paramagnetic beads bound specifically to neurons.

(A) Schematic of the interaction between bead, fibronectin, and the neuronal cytoskeleton through the recruitment of transmembrane integrin proteins to form the focal adhesion complex. (B) Magnetic bead coating was confirmed by measuring the zeta potential of uncoated (control) beads and FN-coated beads. n = 7 bead reactions per condition (error bars indicate SEM). (C) SEM image depicting a FN-coated paramagnetic bead bound to a neurite after beads were seeded onto neurons for 20 minutes. Scale bar = 25μm. (D) SEM image depicting a 5 μm diameter paramagnetic bead bound to single neurite. (E) Immunostaining for vinculin (in red) and actin (in green) revealed focal adhesion formation at site of bead binding. Scale bars = 5μm.

2.2.6 Neuron Peeling Experiments

Bipolar-shaped neurons were peeled controllably from the substrate as the ascending force supplied by the magnetic tweezers exceeded the failure strength of the underlying adhesion to the substrate. Magnetic tweezers were positioned at a 45° with respect to the substrate and the projected distance between the bead and the tweezers' tip was used to calculate the true distance between bead and tip (maintained between 10 – 30 μm). Only experiments whose out of plane bead motion was minimal were used to tabulate forces. The magnetic tweezers force calibration curves were utilized in order to apply forces ascending from 1nN to 10nN. As previously reported, the heat induced by current in the coils was negligible [30]. Neurons were imaged in phase contrast with an Axiovert 200 inverted optical microscope (Carl Zeiss, Oberkochen, Germany) and recorded using the Cascade 512B camera (Photometrics, Tuscon, AZ) to determine peeling speed and detachment. Images were captured at 12 frames/second and peeling speed was defined as the instantaneous velocity of the bead as neurons were peeled from their substrate. All experiments were conducted in normal Tyrode's solution at 37°C.

2.2.7 Immunocytochemistry

Neurons were fixed in a solution consisting of 4% paraformaldehyde and 0.05% Triton X-100 in PBS buffer that cooled from 37°C to room temperature during the 15 minute incubation. Neurons were stained with DAPI (Invitrogen) for DNA, FITC-phalloidin for actin (Alexa 488 Phalloidin, Molecular Probes, Eugene, OR) and incubated one hour with mouse-derived IgG1 vinculin antibody (clone hVN-1, Sigma-Aldrich) at a dilution of 1:200. Neurons were then incubated for one hour with secondary antibody tetramethylrhodamine-conjugated anti-mouse IgG (Alexa Fluor 594, Molecular Probes)

at a dilution of 1:200. Immunostained neurons were visualized with a Coolsnap camera (Photometrics, Tuscon, AZ) mounted on an inverted microscope (DMI 6000B, Leica Microsystems, Germany) with a 63x objective (HCX Plan APO, NA 1.4, Leica).

2.2.8 Scanning Electron Microscopy

Neurons and bound paramagnetic beads were rinsed twice with PBS and fixed with 2.5% glutaraldehyde for 2 hours. After another round of rinsing with PBS, neurons were incubated with 1% OsO_4 for 2 hours. Neurons were then rinsed again and were gradually dehydrated with ethanol. Following critical point drying, neurons were gold sputter coated for 2 minutes at 30 mA. Samples were imaged with a Quanta 200 scanning electron microscope (FEI, Hillsboro, OR).

2.2.9 Zeta Potential Analysis

Zeta potential analysis reveals the electric potential difference between the surface of the magnetic beads and their surrounding medium, indicating bead surface charge, which reflects bead coating [101-103]. Uncoated or FN-coated Bioclone beads were suspended in deionized water (8,500 beads/100 µL) and placed in Dip Cell kit cuvettes (Malvern Instruments, Worcestershire, UK). Zeta potentials were recorded with the Zetasizer Nano ZS system (Malvern Instruments).

2.2.10 Data Analysis and Statistics

Statistical significance was analyzed through ANOVA and appropriate pairwise comparisons when comparing multiple values. $p < 0.05$ for all statistically significant differences.

2.3 Results

2.3.1 Local Neuron Mechanics

Few studies explore the mechanical properties of the soma [104, 105]. Although these studies applied forces locally to neurons, the stimulus was delivered nonspecifically through uncoated AFM tips or hydrostatically via a pipette. To determine how neurons behave when forces are applied specifically, we asked how neurons responded to forces that are applied via magnetic beads coated to bind integrins in the neuronal membrane. To this aim, neurons were grown on 10 μm wide lines of LM separated by 10 μm wide non-adhesive gaps and extended neurites that were aligned with respect to the LM line axis (Fig. 2-3A). The neurons exhibited bipolar morphology, where neurites extend in opposite directions along the track of LM without branching. We then placed the tweezers adjacent to the culture surface in order to apply a force directly orthogonal to and in the plane of the neurite's long axis (Fig 2-3B). If one considers the neurite as a homogeneous elastic rope of initial length L_x subjected to a force applied at its center. As the neurite began to deflect, its midpoint moved towards the tweezers and the axon elongated by $\Delta L = L_0 - L_x$ (Fig. 2-3C). Only neurons whose attachment points to the substrate remained fixed throughout the experiment were analyzed. The equilibrium between the pulling force F and neurite tension T, as well as the deflection angle θ, can be measured optically and corresponds to the relation: $F = 2T\sin\theta$. By considering the neurite as an elastic rope, its tension is therefore $T = \kappa \Delta L$, where κ is the spring constant of the neurite and ΔL is the elastic elongation. Multiple studies have reported that eukaryotic cells are characterized by viscoelastic properties and that the neurite might sustain an initial tension T_0 due to the action of molecular motors and that $\sin(\theta) \ll 1$, the equilibrium becomes [106]:

$$F = \kappa \frac{L_x}{2} \theta^3 + 2T_0\theta. \qquad (4)$$

Although neurons *in vivo* exhibit initial T_0 [107, 108], the initial tension of neurons *in vitro* is negligible relative to their elastic tension [109]. Since the viscoelastic relaxation time of neurites has been reported to be greater than 12 seconds [106], we only considered neurite deformation over 10 seconds so that viscous effects could be neglected. Therefore, the evolution of the pulling force as a function of neurite angle deflection, θ (Fig. 2-3D), captured deformations representative of the pure elastic regime and allowed viscous effects to be neglected in order to extrapolate κ. The experimentally tabulated spring constant, κ, was then plotted as a function of the ratio of neurite cross section area to the initial axon length A/L_x, revealing a linear trend (Fig. 2-3E), whose slope represents the Young's Modulus (E) of the neurite such that $\kappa = EA/L_x$. This relationship was used to obtain a value of 15 ± 3 kPa for E averaged over several neurons (n = 8). By pulling on a bead bound to the cytoskeleton of the neurite through the FAC_{bead}, the value determined for E of primary cortical neurons was comparable to similar deflection experiments conducted with glass microneedles on PC12 neurons [106], confirming that beads were not simply bound to the neuronal membrane but were mechanically coupled to the cytoskeleton. Therefore, matrix-coated beads mechanically engage the neuronal cytoskeleton and permit direct interrogation of the local cytoskeletal properties of neuronal microcompartments.

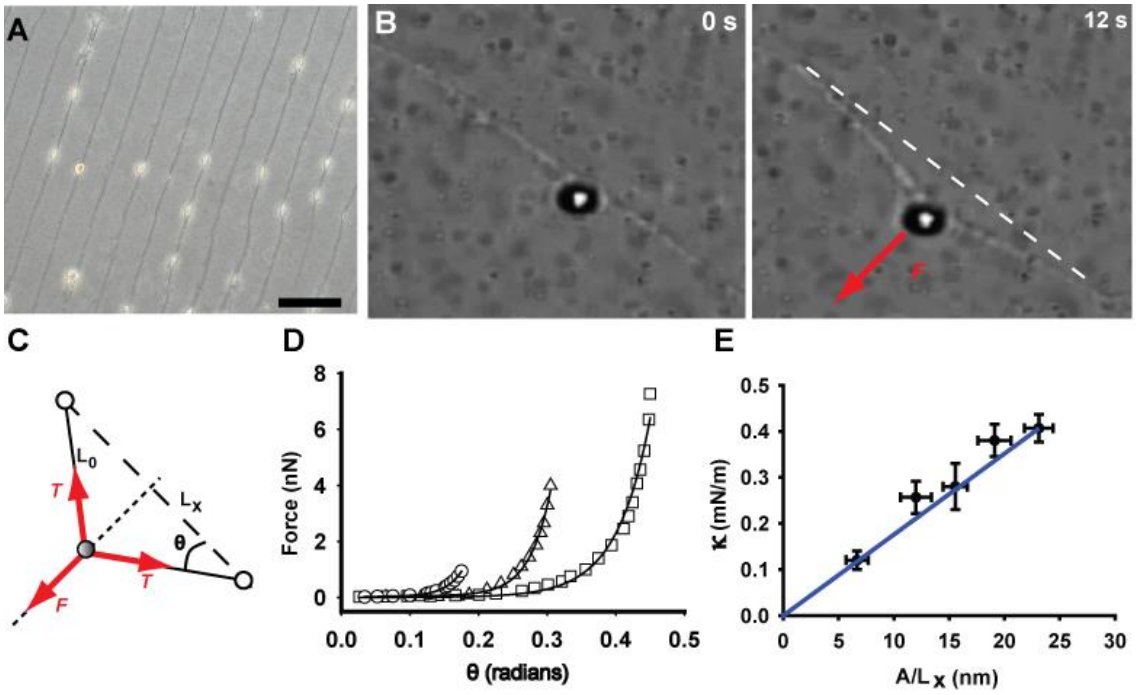

Figure 2-3: Mechanical properties of neurites.

(A) Extended, well-aligned neurites on 10 µm wide LM lines. Scale bar = 50µm. (B) A paramagnetic bead is specifically bound to a neurite (t = 0) and a constant magnetic force, F, is applied in the direction orthogonal to the neurite (t = 12s). Scale bar = 5 µm. (C) The schematic representation of neurite deflection shows the equilibrium between the normal force, F, and neurite tension, T, by creating an angle θ (D) Tension within different neurites as a function of the angle of deflection, θ, during deformations at short time. (E) The evolution of spring constant of the neurite, κ, as a function of the ratio A/Lx, where A represents neurite cross-section area and Lx represents its original length. n = 8 neurons (error bars indicate SEM).

2.3.2 Whole Neuron Peeling

To test the ability of the magnetic tweezers to determine whole cell characteristics in real-time, we controllably peeled neurons from the substrate by beginning from one extremity and continuing through the elongated neuron. Due to elongated neuron shapes imposed by micropatterning, the experimental procedure is somewhat akin to peeling adhesive tape along its length. Consistent with this analogy, when peeling force exceeds an apparent threshold, a portion of the adherent neuron could be visualized as it was peeled with the tweezers positioned above the neuron at a 45° angle (Fig. 2-4A). This led to a microscopic peeling front characterized by a moving contact line between the neuronal membrane and the substrate located in the immediate neighborhood of the dynamic detachment. The range of imposed peeling forces was between 1 and 10 nN. Below this range, peeling arrested and bead displacements indicated that a minimum tension of about 1 nN was required to overcome neuron attachment on LM substrates. Moreover, the contribution of vinculin-containing $FACs_{substrate}$ in the adhesion strengthening of the soma versus the neurite was clearly illustrated by the sigmoidal behavior in the speed with which neurons were peeled (Fig. 2-4B-C). Interestingly, no visible reattachment was observed after ~40 minutes, suggesting that the peeling process was irreversible and characterized by a general failure of neuronal reattachment. This observation may reflect a damaged cytoskeletal network. It may also reflect the inability of the cell to reattach due to its collapsed cytoskeleton since FACs between the neuron and the substrate were disconnected. These results indicate that magnetic tweezers may also be utilized to explore dynamic adhesive properties of neurons, where real-time

peeling thresholds for the soma and the neurite can be compared directly in the same neuron.

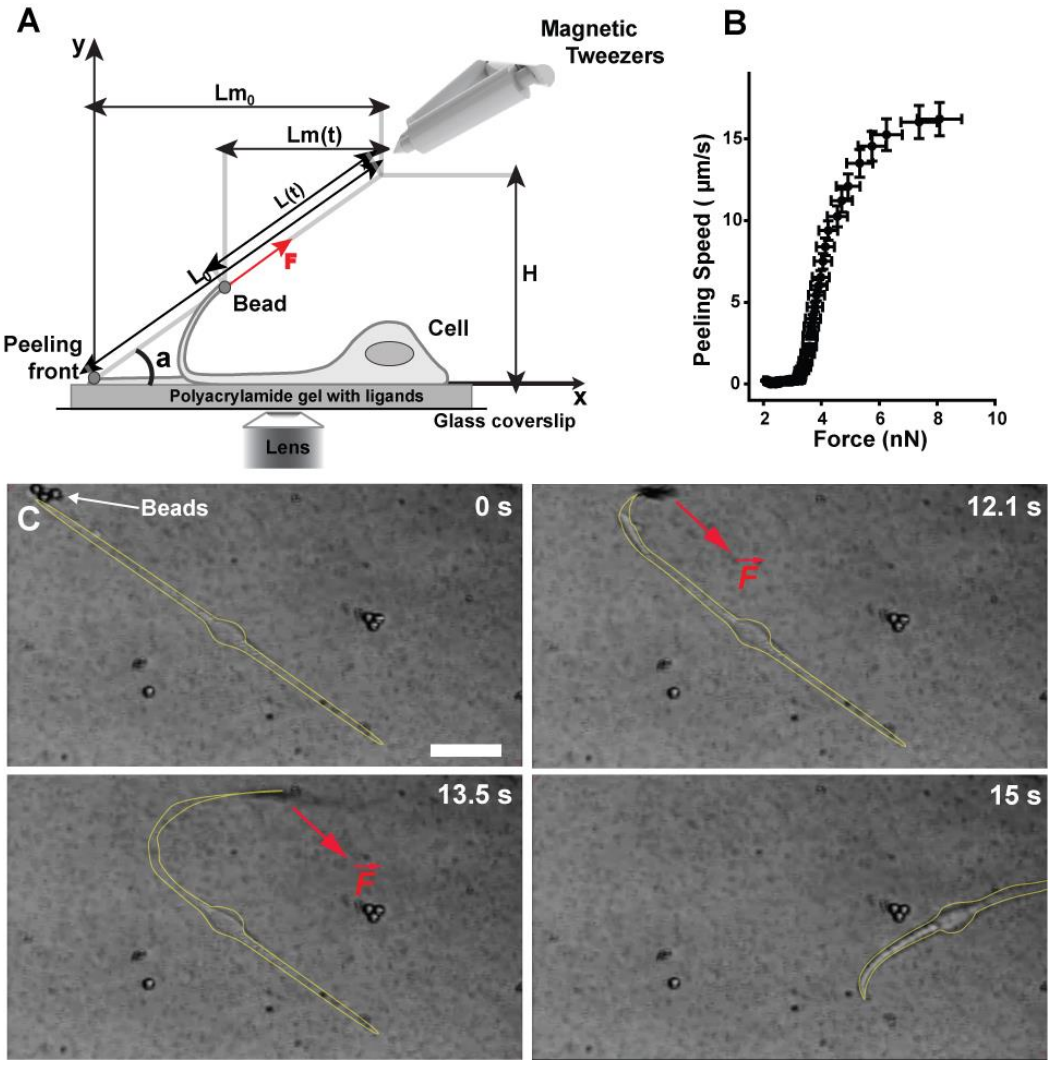

Figure 2-4: Neuron adhesion strengthening by peeling experiments.

(A) Schematic of peeling experiment. Dipole magnetic tweezers were oriented at 45° and placed at a distance L0 and a height H from the paramagnetic bead by using the micromanipulator. (B) The evolution of the peeling speed as a function of the applied force is sigmoidal. n = 3 neurons (error bars indicate SEM). (C) Representative sequence of a peeling experiment of a bipolar neuron grown on a LM micropatterned line. The yellow trace outlines the neuron. Scale bar = 25µm.

2.3.3 Neuronal Subcompartment Substrate Adhesion

To highlight the disparate adhesion properties of the soma and neurite subcompartments within the same neuron, we assessed how neurons adhered to the underlying substrate. Immunostaining for filamentous actin in patterned neurons revealed a polarized structure with neurites emanating from a central soma (Fig. 2-5A). Antibodies directed to vinculin indicated sites of neuron-gel attachment through the focal adhesion complexes between the neuron and the substrate ($FAC_{substrate}$) (Fig. 2-5A). It is important to note that $FAC_{substrate}$, which represent neuronal anchor points to the underlying gel, were not continuous and appeared as discrete puncta (Fig. 2-5B). A consequence of this form of cell adhesion was that when neurons were peeled from the substrate, increasing magnetic force on the attached bead did not immediately result in peeling (Fig. 2-5C). Thus, controlled neuron spreading through micropatterning revealed disparities in how different regions of the same cell bound the underlying substrate.

We sought to quantify cellular adhesion strength as a function of individual neuronal subcompartments (i.e., soma and neurite). In a previous report, we used a watershed based algorithm [110] for quantifying focal adhesions in neurons cultured on fibronectin or poly-L-lysine coated substrates and found that somas were characterized by numerous, large FACs whereas neurites exhibited smaller FACs and lower densities [30]. In agreement with those findings, examination of $FAC_{substrate}$ density in neurons grown on LM indicated large and numerous $FACs_{substrate}$ for the somas whereas neurites typically exhibited lower $FAC_{substrate}$ density. This observation suggested a higher threshold for mechanical failure in somas than in neurites. Based on this observation, we sought to determine the relative adhesion failures of the soma versus the neurite as

neurons were peeled from the substrate. We were able to use the magnetic tweezers to determine the maximum force required to break the $FACs_{substrate}$ that locally bound the neuron to the substrate and found that the force required for detaching the soma was roughly three-fold higher than that required to detach the neurite (Fig. 2-5D). Thus, the difference in the binding force between the neurite and the substrate compared to that of the soma and the substrate suggested a correlation between $FAC_{substrate}$ density and laminin binding affinity to the substrate as previously reported for fibronectin [30].

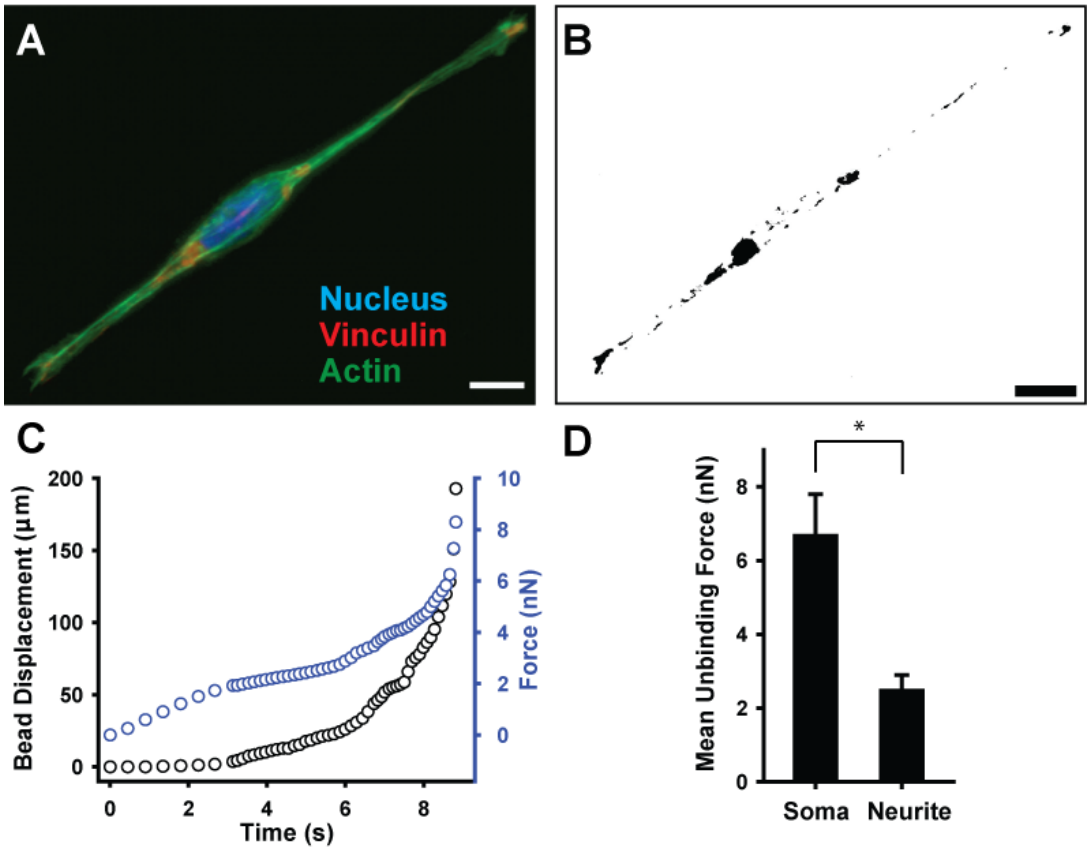

Figure 2-5: Properties of neuronal microcompartment adhesion to substrate. (A) Single bipolar shaped neuron grown on LM lines stained for DAPI (in blue), vinculin (in red), and actin (in green). (B) The spatial localization of focal adhesion sites is revealed by thresholded vinculin image from (A). Scale bars = 10µm. (C) Representative bead displacements (in black) and corresponding forces (in blue) as neurons were peeled from substrate. (D) The mean unbinding force required to detach the soma was three times greater than the mean force needed to detach the neurites of bipolar-shaped neurons. n = 5 for soma and n = 7 for neurite (error bars indicate SEM).

2.4 Discussion

Magnetic tweezers have been used extensively to mechanically manipulate multiple cell types. Through the ability to directly bind specific cell surface receptors, we probed specific mechanical properties of whole neurons in addition to their individual microcompartments. To date, magnetic tweezers have been primarily used to assess the mechanical properties of cells that are generally homogenous in structure [111-113]. Other magnetic bead systems, such as magnetic bead twisting cytometry, have also been utilized to reveal internal cell cytoskeleton dynamics [114]. While magnetic bead systems have led to successful advances in understanding how extracellular forces couple into the cytoskeleton of the cell as a whole, they have not been utilized in order to isolate and dynamically characterize specific microcompartments of cells.

In neurons, Atomic Force Microscopy (AFM) has been used to probe solely the soma [115], while separate instruments, such as optical tweezers, were utilized to assess the properties of distal growth cones [116]. Moreover, glass needles have also been utilized to both assess the mechanical properties of neurons and to elicit neurite outgrowth [117, 118]. Magnetic tweezers have also been used to elicit neurite extension in neurons [119], but they have also revealed microcompartment-specific differences in substrate adhesion failure strength [30]. Magnetic tweezers offer an alternative to current approaches of region specific mechanical manipulation of neurons, where investigators have turned to methods that mechanically stimulate or injure focal sections of neurons. For example, glass pipettes have been used to mechanically induce calcium waves and action potentials in neurons [120-123] and to transect axons [124]. Even more refined techniques utilized laser dissection in order to cut neuronal extensions [125, 126] and

have also disrupted subcellular components of the cytoskeleton [127]. However, all of these methods are invasive and traumatically injure neurons and may overlook the impact of more subtle and focal forces. Given the heterogeneous structure of neurons and evidence that neuronal injury can also be mediated by focal stimuli, magnetic tweezers systems provide an important means for better characterization of neuronal mechanics and ultimately an understanding of how they interact with extrinsic mechanical forces.

The design of the magnetic tweezers system focused on the induced magnetic field gradient and bead type. The steepness of the gradient depends on several factors, including the geometry and the material properties of the tweezers' tips, the number of wire turns in the solenoid, and the current supplied to the system [112]. The paramagnetic bead's total magnetic moment when in an external magnetic field is a function of the bead's volume and its magnetic susceptibility. By using paramagnetic beads 5 μm in diameter and with high magnetic susceptibility, the bead magnetic moment induced by the magnetic field was maximized. The steep magnetic field gradient generated by the bipolar tweezers and use of beads with high magnetic susceptibility helped increase the range of forces that could be applied to beads bound to neurons. Moreover, coating beads with ECM protein that bound neuronal surface integrins provided a direct link to the intracellular cytoskeleton as the focal contact between the bead and the neuron matured. Since integrin mediated effects on ion channel currents have been documented [128, 129]**,** the magnetic tweezers can also be used to assess the effects of local mechanical stimuli on action potential propagation.

In the present study, magnetic tweezers were used to determine both the local elastic properties of neurons and their substrate adhesion characteristics. By isolating the

properties of somas and neurites independently, this work suggests important differences in each microcompartment's response to mechanical stimuli. The relatively weaker substrate adhesions between the soma and neurite may have significant implications for the mechanical integrity of neurons during diffuse axonal injury [30, 130, 131] while also casting light on neuron and glial cell interactions via integrins during neuronal migration and development [132]. Furthermore, the sigmoidal behavior of peeling speed of neurons on LM, which was characterized by three well-defined phases (an initial delay, a rapid phase, and a plateau), is distinct from neurons grown on nonspecific coatings, such as poly-L-lysine [30]. This indicates that neurons grown on substrates with specific ECM coatings exhibit adhesion strengthening relative to neurons grown on non-specific ECMs (e.g., poly-L-lysine), underscoring the importance of neuron-substrate adhesion properties.

Super resolution microscopy has revealed unique patterns of actin and spectrin alignment in axons relative to dendrites, suggesting that these microcompartments exhibit unique local mechanical properties [133]. Though the peeling model allowed for direct measurement of Young's modulus of neurites, magnetic tweezers can be extended to permit the study of complex viscoelastic properties. To do so, a constant stress can be applied longer than characteristic viscoelastic time scales for neurites, allowing for strain over time to be recorded. Thus, time-dependent viscous properties can be assessed since the evolution of cellular creep due to a static force can be directly measured and fit to a power-law creep response, which reveals shear modulus and degree of viscoelasticity [134]. In addition, the degree of plastic deformation in the cytoskeleton due to creep may be determined by measuring the relaxation of beads following the creep experiment,

providing insight into the effects of long-term cytoskeletal remodeling. Since beads bound integrins and formed focal adhesions, this technique more directly reflects the properties of internal neuronal components when compared to microneedle-based neurite deflection platforms [106]. Furthermore, by coating magnetic beads with various antibodies and non-specific coatings, investigators may begin to assess the anisotropic mechanical stimulation of a myriad of neuronal surface receptors, which when combined with *in vitro* neural networks [135], provides a robust platform for the study of complex mechanotransduction processes in neurons.

3 A Possible Role for Integrin Signaling in Diffuse Axonal Injury

Over the past decade, investigators have attempted to establish the pathophysiological mechanisms by which non-penetrating injuries damage the brain. Several studies have implicated either membrane poration or ion channel dysfunction pursuant to neuronal cell death as the primary mechanism of injury. We hypothesized that traumatic stimulation of integrins may be an important etiological contributor to mild Traumatic Brain Injury. In order to study the effects of forces at the cellular level, we utilized two hierarchical, *in vitro* systems to mimic traumatic injury to rat cortical neurons: a magnetic tweezer system and magnetic twisting cytometry. In both systems, we used magnetic beads to directly simulate the abrupt injury forces endured by a focal adhesion on the neurite. The magnetic tweezers revealed variations in the rate and nature of neuronal injury as a function of focal adhesion density, direct integrin stimulation, and cytoskeletal pre-stress without membrane poration. Using magnetic twisting cytometry, we implicated a role for Src kinase as a downstream mediator of injury forces. These data suggest that integrin-mediated forces are distributed through the neuronal cytoskeleton to activate mechanically sensitive signaling cascades, contributing to the diffuse axonal injury reported in mild Traumatic Brain Injury.

3.1 Introduction

Blast-induced mild Traumatic Brain Injury (mTBI) is the most frequent wound of the conflicts in Afghanistan and Iraq [136]. Approximately 60% of total combat casualties are associated with blast events generated by improvised explosive devices,

and recent studies suggest that nearly 16% of US combatants have been diagnosed with mTBI [137]. Although how blast energy is transmitted to the brain is not well understood, *in vivo* studies and clinical reports have shown that exposure to blast can cause mTBI [137-139]. Interestingly, the neuronal injury observed in these studies resembles diffuse axonal injury (DAI), a common pathology observed following mTBI *in vivo* [140]. Diffusion tensor imaging studies have identified structural alteration in white matter tracts in military personnel who previously suffered blast-induced mTBI [131, 141], and experimental models have linked these structural alterations to DAI [142]. However, the cellular mechanisms which initiate this pathophysiological response are not well understood.

In vitro models of TBI may not fully recapitulate the complexity of the brain, but they provide unique insight into its cellular pathology. Previous models of mTBI have proposed that a disruption in ion homeostasis initiates a sequence of secondary events ultimately leading to neuronal death, however, membrane poration can only account for a portion of injured neurons [88, 143], and excitotoxicity due to changes in ion channel homeostasis [144] cannot account for observations of axonal retraction.

We hypothesized that mechanical perturbation of integrins in the neuronal membrane may represent an injury pathway that would account for DAI in mTBI. Integrins are transmembrane proteins that couple the cytoskeleton in the intracellular space to the matrix network in the extracellular space, providing mechanical continuity across the membrane [145]. Mechanical forces propagating through these coupled networks can activate signal transduction pathways, alter ion channel currents, and initiate pathological cascades [146, 147]. In the brain, integrin signaling is implicated in

development and memory potentiation [27, 43, 48, 69, 148, 149], however, there are no reports on the role of integrin signaling in mTBI.

To test our hypothesis, we built used magnetic tweezers and coated paramagnetic beads bound to neurons to demonstrate that focal adhesions are important contributors to how neurons interact with the local microenvironment. We demonstrated that neurites had significantly weaker attachments to the substrate relative to those of the soma. We then applied an abrupt force to these neurons and found that with fibronectin (FN)-coated beads neurite focal swelling, including abrupt mechanical failure in neurites, occurred 100s of microns away from the soma, suggesting that injury forces may propagate through the neuronal cytoskeleton without damaging the neuronal membrane. Conversely, poly-L-lysine (PLL)-coated beads attached to neurites induced only a local injury. Moreover, increasing the cytoskeletal pre-stress lowered the threshold for injury, whereas decreased cytoskeletal pre-stress delayed injury onset. Treatment with a Src kinase inhibiter also delayed neuronal injury, suggesting a role for downstream integrin-mediated cascade events in the injury mechanism.

3.2 Results

3.2.1 Neurites are More Susceptible to Injury

Given the focal nature of axonal swelling in DAI [150], it is reasonable to assume that there is heterogeneous vulnerability to injury within the various structures of a neuron, such as the dendrites, axons, and soma. Examination of FAC density in immunostained neurons [30] led us to hypothesize that the larger, more numerous FACs of the soma would endow it with a higher threshold for mechanical failure than those in neurites. We used magnetic tweezers to apply nanoNewton (nN) forces to 4.5 μm FN-

coated paramagnetic beads bound to specific segments of individual neurons (Figure 3-1A). By increasing the applied force with time (Figure. 3-1B), we peeled neurons from the PLL and FN coated substrates. After correcting for displacement of the paramagnetic bead position relative to the magnetic tweezer tip, we found a linear behavior in the speed with which neurons were peeled from PLL-coated substrates whereas neuronal peeling on FN-coated substrates was represented by a sigmoidal curve (Figure 3-1C). These differences can be directly related to the FAC density and thus suggest adhesion strengthening on FN-coated substrates. We sought to determine the relative vulnerabilities of the soma versus the neurite to strain injury and compared the failure strengths of FACs in these different regions. We reasoned that a relative difference in FAC failure strength between the soma and its neurites would serve as an indicator of vulnerability to mechanical injury. We used the magnetic tweezers to measure the maximum force required to break the FACs that bound the soma and neurites to the substrate. The force required to detach the soma was found to be higher than that required to detach the neurite for both coatings, and significantly larger for FN-coated substrates (Figure 3-1D). The contribution of FACs in the adhesion strengthening of the soma versus the neurite is illustrated by the linear relationship between mean unbinding force and focal adhesion size (Figure 3-1E). The differences in adhesion strength suggest that axonal and dendritic extensions have a vulnerability to integrin-mediated mechanical injury in axons.

3.2.2 Injury Extent Depends on Integrin Binding

Integrins provide mechanical continuity between the ECM and the cytoskeleton, thus mediating the possible propagation of mechanical forces bidirectionally across the

membrane. The cytoskeleton is an integrated polymer network that propagates mechanical forces throughout a cell. We asked whether a brief, traumatic pull to simulate injury forces via integrins (FN-coated paramagnetic beads), versus a nonspecific (PLL-coated paramagnetic beads) administration of the force to the cell, would result in different injury modalities. This was supported by the differential binding strengths of neurons grown either on FN or PLL-coated substrate. We reasoned that this experiment would reveal an injury threshold, similar to the force thresholds previously reported for integrin-mediated neurite formation [119]. Using magnetic tweezers, we administered abrupt (100 msec) (Figure 3-1F), 0.5-5.5 nN forces to FN-coated paramagnetic beads attached to the surfaces of cultured neurons and established an injury force dose response curve. These data revealed a focal adhesion injury threshold of 4nN (Figure 3-1G). Consistent with an integrin-mediated injury mechanism, 62% (n = 13) of neurons were injured with FN-coated beads, while 33% (n = 12) of neurons were injured with PLL-coated beads (Figure 3-1H). In neither case, membrane poration was observed and temperature rise due to magnetic tweezers operation was minimal (Figure 3-2). The ability of PLL-coated beads bound to the apical surface of the axon to injure despite their inability to specifically bind integrins was likely due to the fact that neurons attach to the substrate through integrins on the basal surface and local stretching of the cell membrane may activate these integrin complexes and induce injury, albeit at a lower rate. Furthermore, abrupt pull of bound FN-coated beads consistently induced formation of focal swellings on neurites extending from the opposite side of the soma, generating a global injury (100% of injured neurons, Figure 3-1I), where focal swellings appeared up to 150μm away from the bead pull site (Figures 3-1J , 3-3). Similar perturbations of

PLL-coated beads tended to injure near the point of attachment, generating a local injury (Figure 3-1K). We also tested a 1 sec bead pull and noted similar injury morphologies (Figure 3-4). It should be noted that neither the magnetic field alone, attached beads alone, nor Acetylated-LDL-coated beads (non-integrin receptor binding) were able to induce injury (Figures 3-5, 3-6). That integrin-bound beads were able to injure neurons globally, while PLL-coated beads tended to injure cells only locally, suggests that despite the local nature of the insult, integrin-mediated forces result in injury at a distance, leading to a global, cellular response propagated through the CSK.

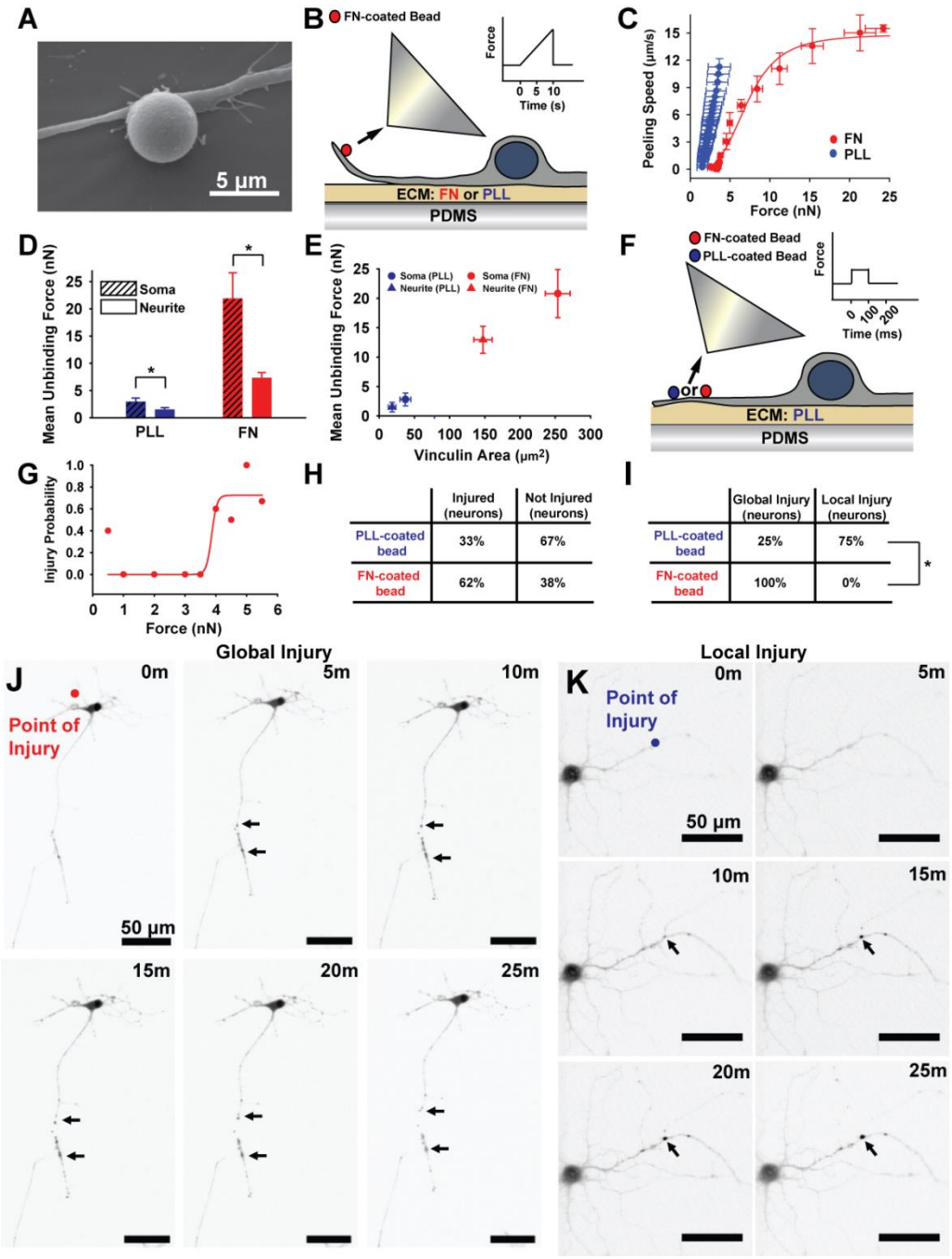

Figure 3-1: Role of integrins in adhesion strengthening and injury.

(A) Paramagnetic beads, as shown by SEM, were bound to neurons. (B) The failure strength of neuron/substrate adhesions was measured using either FN-coated (red) or PLL-coated (blue) substrates. The beads were pulled with an ascending ramp in force as

Figure 3-1 Cont.

indicated by the inset. (C) The speed at which neurons detached from the substrate (Peeling Speed) during the ascending pull was plotted as a function of the applied force for PLL-coated (blue) and FN-coated substrates (red) ($n \geq 4$). (D) The maximum force required for complete detachment (Mean Unbinding Force) for soma (dashed) and neurite (plain) was plotted for PLL-coated substrates (blue) and FN-coated substrates (red) ($n \geq 4$). (E) Mean unbinding forces for the soma (circles) and neurites (triangles) of cells on PLL or FN coated substrates was plotted as a function of mean vinculin area ($n \geq 4$). (F) Magnetic Tweezers were used to deliver a 100ms pulse (inset) to neurons with either FN (red) or PLL (blue) coated beads. (G) FN-coated beads were used to establish an injury dose response curve. (H) FN-coated beads were able to injure cells more often than PLL-coated beads and the extent of injury (I) depended upon bead coating. (J) FN-coated beads always caused global cellular injury (focal swellings indicated by black arrows extended throughout the cell), while (K) PLL-coated beads tended to injure locally to the bead-pull site ($n = 13$ for FN-coated beads and $n = 12$ for PLL-coated beads). Inverted fluorescence images from neurons loaded with Fluo-4 calcium dye. All bars SEM for all panels, * $p < 0.05$.

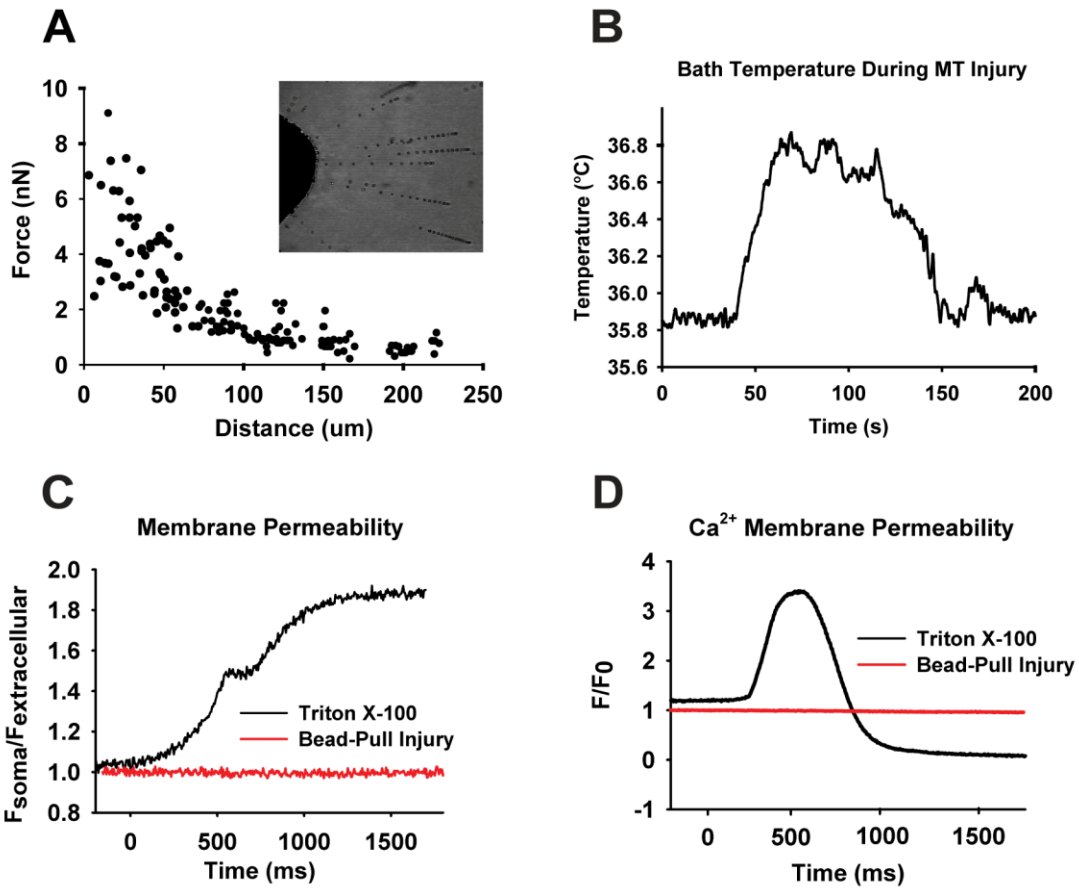

Figure 3-2: Magnetic Tweezers Calibration.

(A) Force calibration of 4.5 µm paramagnetic beads was conducted in 99% glycerol solution. The bead velocity was tracked and force was deduced through Stokes' formula for low Reynolds flow. (B) Induction of magnetic field in tweezers did not result in a large temperature increase after a 1 second 5 Ampere pulse. Pulling beads bound to neurons did not cause an increase in membrane permeability as evidenced by the lack of (C) rhodamine dye and (D) calcium ion entry into the cell during and after the injury pull.

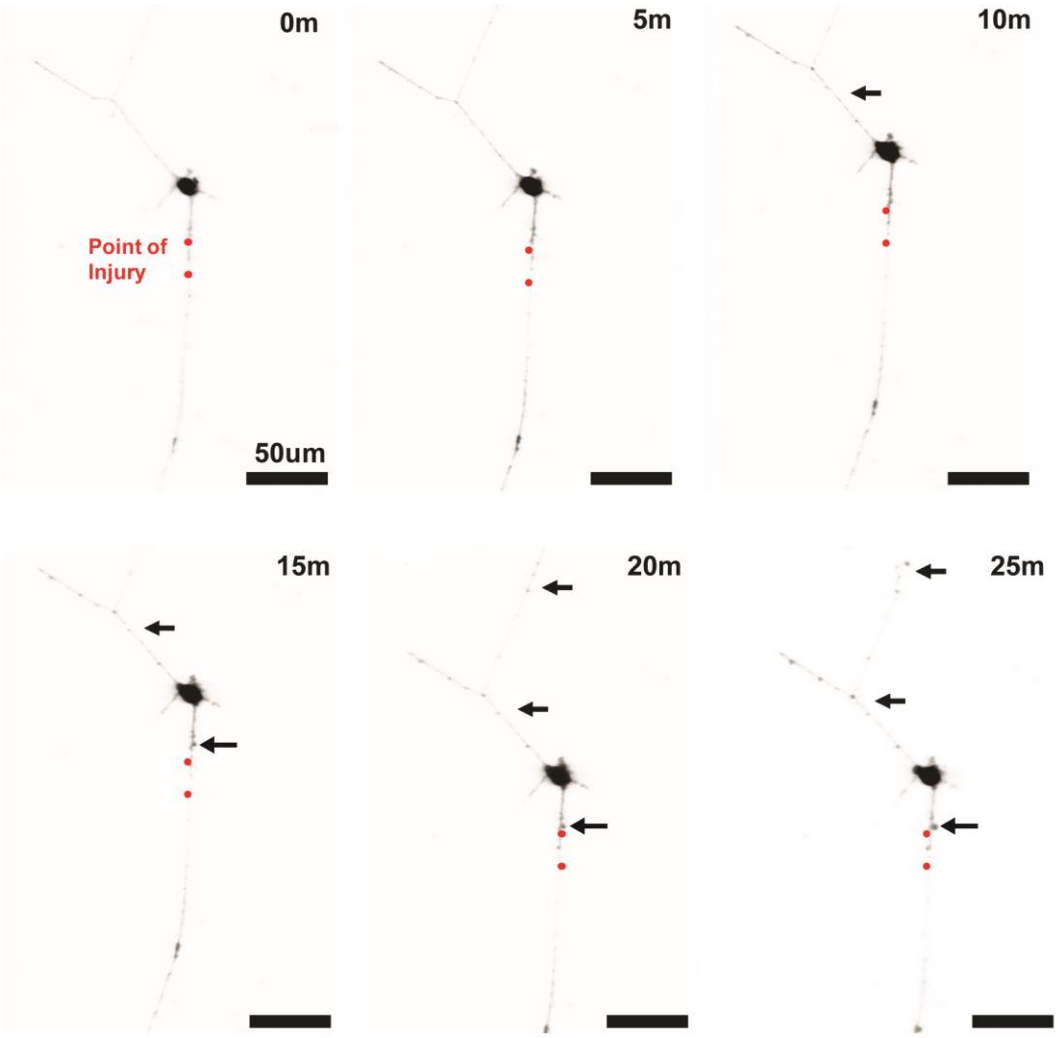

Figure 3-3: FN-coated Bead Injury.

Time series depicts focal swelling development due to a 3nN 100ms injury pulse applied at the red paramagnetic bead locations. Focal swellings occurred globally and in bi-directional fashion despite the focal nature of the injury.

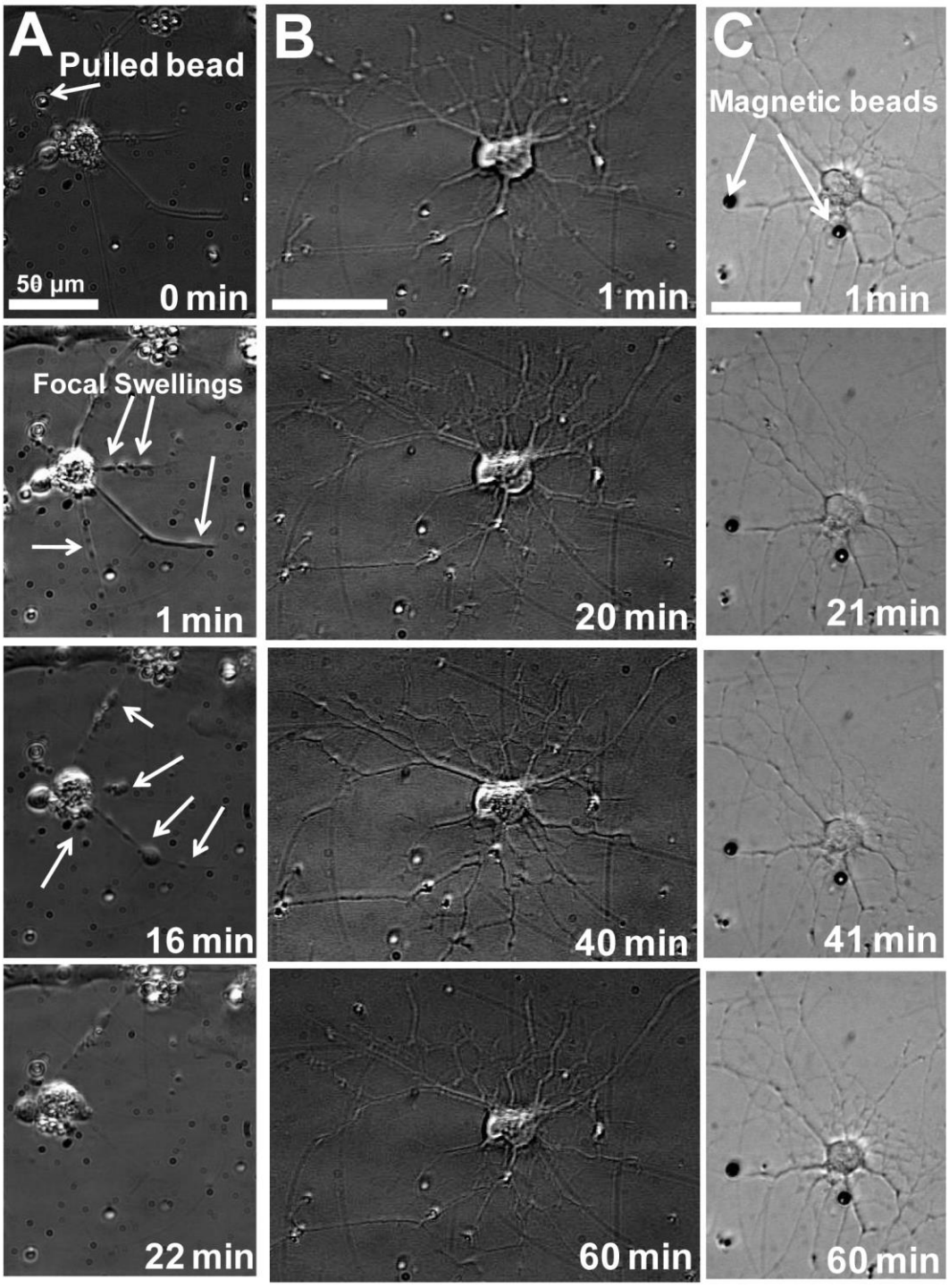

Figure 3-4: Tweezers Control Experiments.

(A) Panels depict the formation of focal swellings along neurites as seen by phase contrast microscopy following a 1 second 3nN pull on a bound bead. (B) Exposing a neuron to the magnetic field alone did not induce an injury. (C) The beads alone failed to produce injury without the presence of the magnetic field.

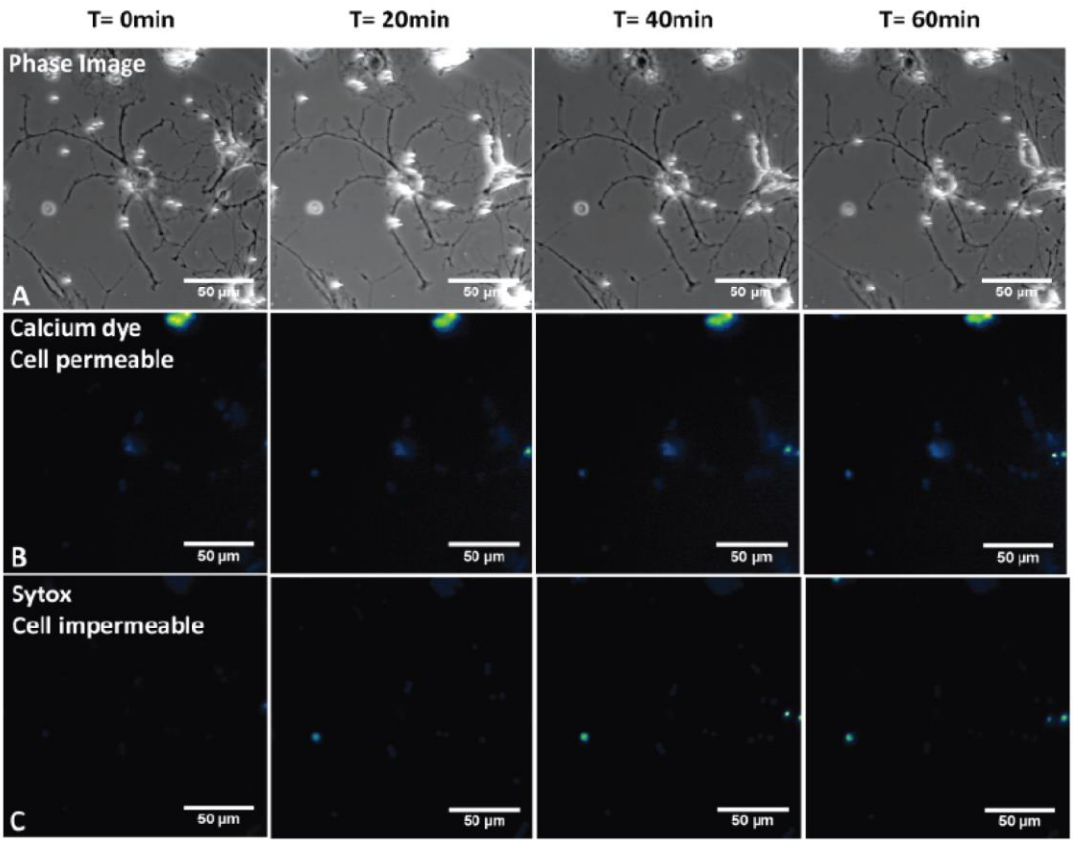

Figure 3-5: Magnetic Field Alone Did Not Induce Injury.

FN-coated paramagnetic beads were attached to neurons as previously described. With no magnetic field, cells did not show signs of injury as indicated by the lack of focal swellings, Ca2+ uptake, and Sytox uptake.

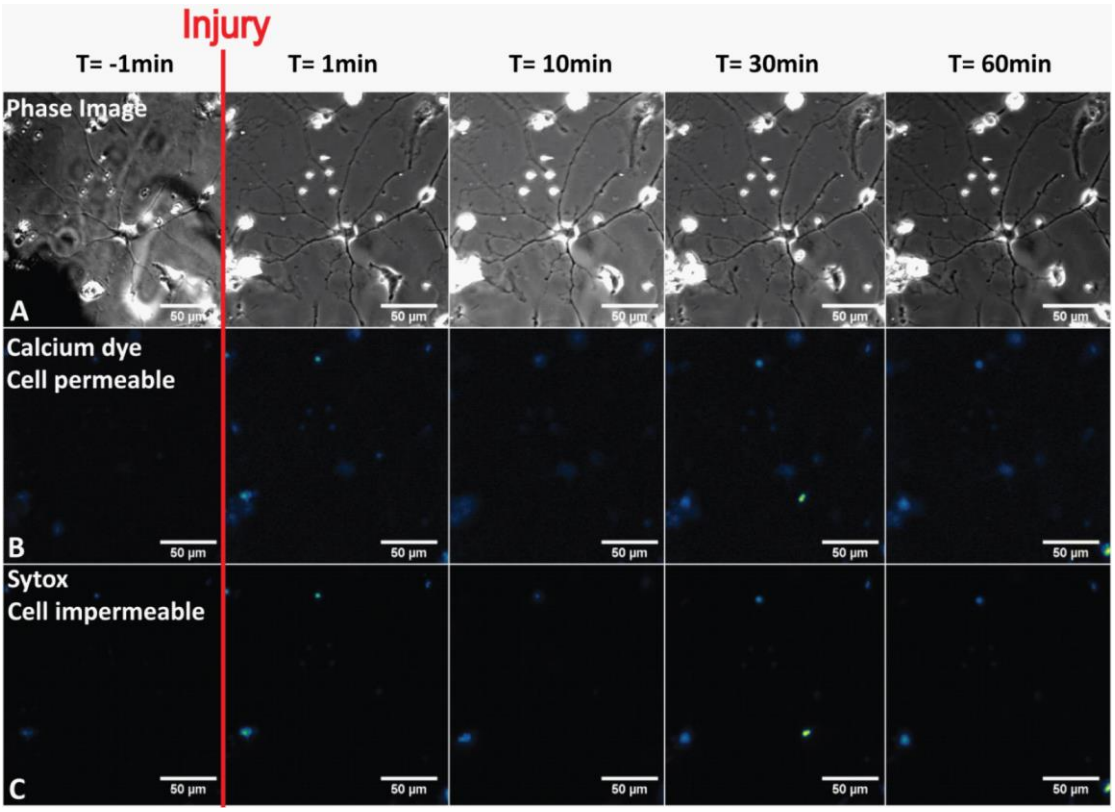

Figure 3-6: AcLDL-coated Beads Did Not Induce Injury.

Beads coated with Ac-LDL bind neurons nonspecifically through lipid interactions. Since focal adhesions did not form at the bead binding site, force applied to such beads failed to produce injury as indicated by the lack of focal swellings, Ca2+ uptake, and Sytox uptake.

3.2.3 Effects of the Neuronal Cytoskeleton on Injury

Since the formation of focal swellings globally in neurons was dependent on forces directed via integrins, we reasoned that the cytoskeleton (CSK) played an important role in propagating injury forces throughout neurons. To illustrate that forces applied to FN-coated beads were transmitted throughout neurons, we performed Traction Force Microscopy (TFM) on neurons as they were pulled with the magnetic tweezers (Figure 3-7A). As beads were pulled with the tweezers, traction forces developed throughout the neuron, distal to the site of bead attachment to neurons (Figure 3-7B). These data demonstrate that FN-coated beads transmit forces to the cytoskeleton, allowing injury forces to be propagated throughout the neuron. We next sought to determine the role of CSK pre-stress on injury. We reasoned that increasing pre-stress of the neuronal CSK would allow more efficient injury force propagation, while decreased pre-stress would dampen injury forces. To reduce pre-stress, we incubated neurons with HA-1077, a ROCK inhibitor that lowers cellular pre-stress and showed that the onset of injury was later as a result (Figure 3-8). On the other hand, increasing cellular pre-stress with calyculin, a ROCK mimicker increased cellular pre-stress (Figure 3-9A). When magnetic tweezer injury experiments were conducted in the presence of 1.5nM calyculin, the previous 4nN injury threshold was lowered and 2-3nN force was sufficient to induce injury (Figure 3-9B). Taken together, these data demonstrate that the neuronal CSK is a primary conduit for integrin-mediated injury forces in neurons.

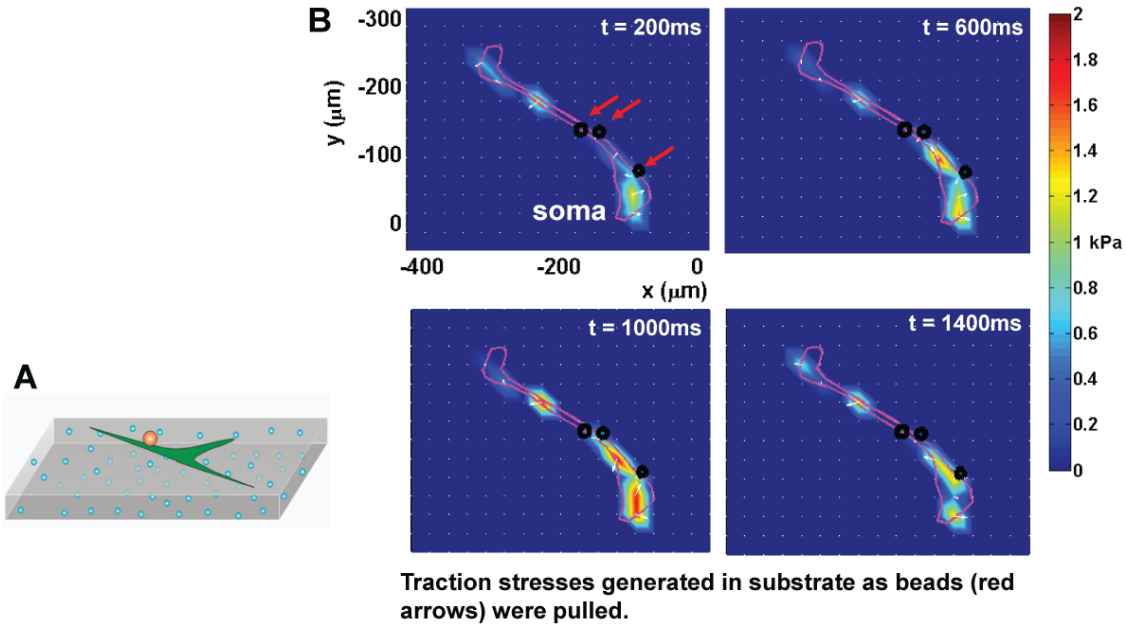

Figure 3-7: Magnetic Tweezers and Traction Force Microscopy.

(A) Schematic depicting bead bound to neuron cultured on polyacrylamide gel that is loaded with fluorescent beads. (B) Traction stresses develop throughout neuron when forces are applied to bound beads (red arrows).

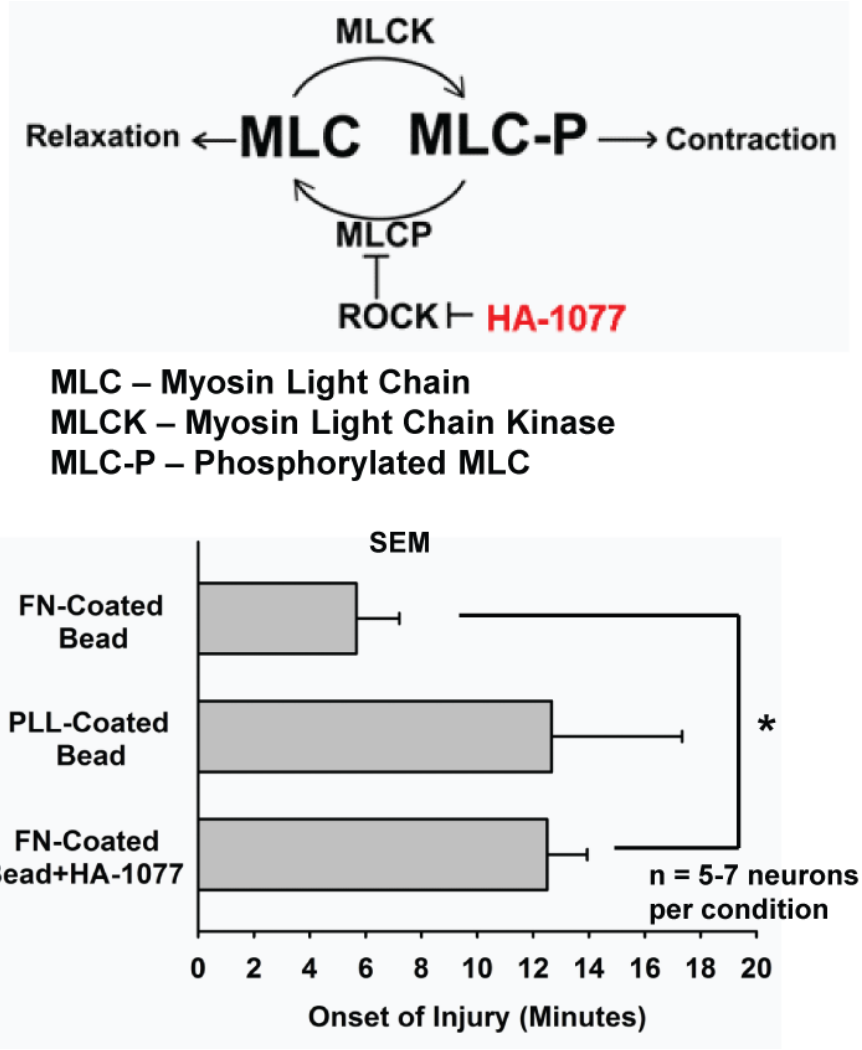

Figure 3-8: Reduced Pre-Stress Delays Injury

Neurons treated with HA-1077 to reduce cytoskeletal pre-stress exhibited delayed injury onset.

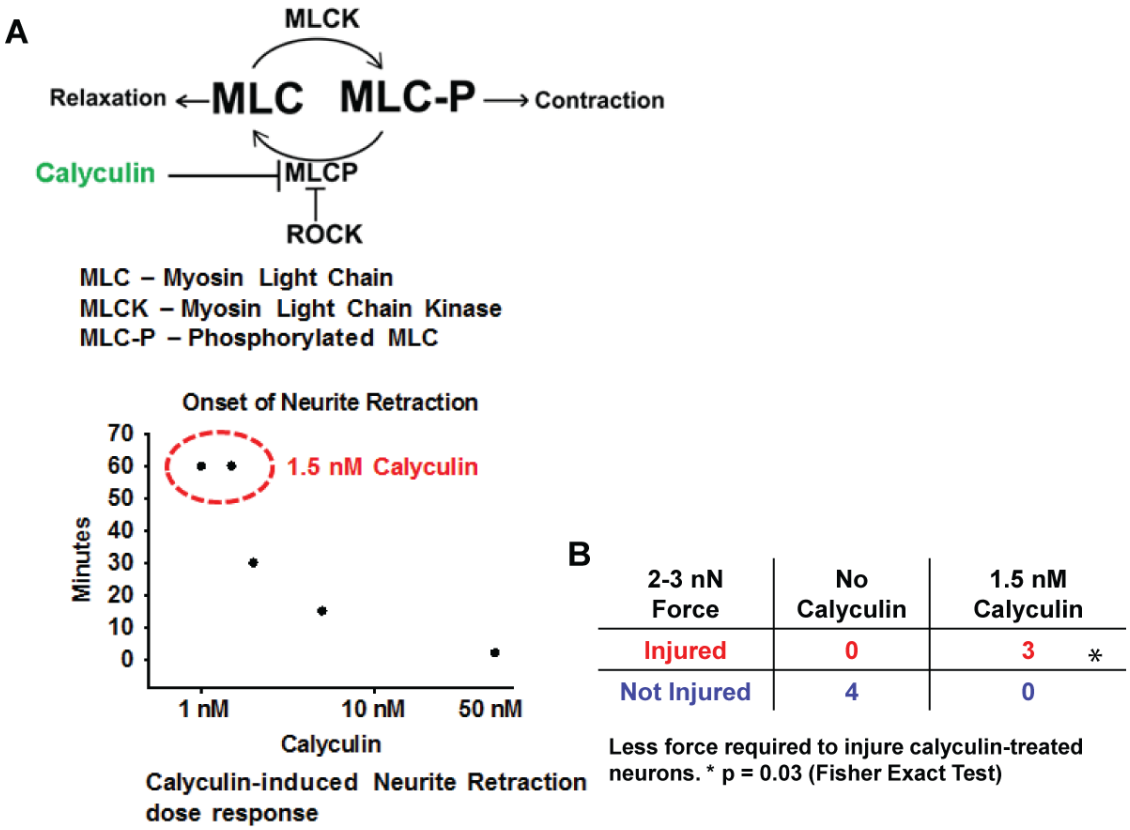

Figure 3-9: Increased Pre-Stress Lowered Injury Threshold.

(A) Calyculin, a ROCK mimicker, was used to increase the pre-stress of the neuronal cytoskeleton. 1.5nM was used since neurons remained stable during the course of the experiment in this concentration of calyculin. (B) Injury threshold was lowered from 4nN (without calyculin) to 2-3nN.

3.2.4 Src Kinase May Cause Downstream Injury

Although it is evident that injury forces couple into neurons via integrin proteins that relay forces to the rest of the neuron through its CSK, the ultimate outcome of this mechanical perturbation and its downstream biological effects are not well understood. Since Src kinase is known as a mechanically sensitive kinase [55, 151] that is associated with the CSK (Figure 3-10A), we hypothesized that its activity may result in hyperphosphorylation of tau protein and microtubule disruption (Figure 3-10B). Since Src kinase was expressed by neurons in culture (Figure 3-10C,D), we asked wheter its inhibition may mitigate injury (Figure 3-11A). To this end, neurons were pre-treated with PP2, a known inhibitor of Src kinase before injury (Figure 3-11B). To injure neurons, we still used magnetic beads bound to integrins, but used magnetic twisting cytometry (MTC) to apply forces to multiple neurons simultaneously [152]. Relative to neurons treated with vehicle only (DMSO), PP2-treated neurons exhibited a delayed onset in injury (Figure 3-11C). Though injury rates were significantly different 40 minutes after injury, no significant reduction in injury was noted after one hour (Figure 3-11D). These results indicate that although Src kinase may be implicated in the downstream biological signaling of integrin-mediated injury, the action of other mechanically sensitive kinases, such as Focal Adhesion Kinase and Integrin Linked Kinase may also be pertinent.

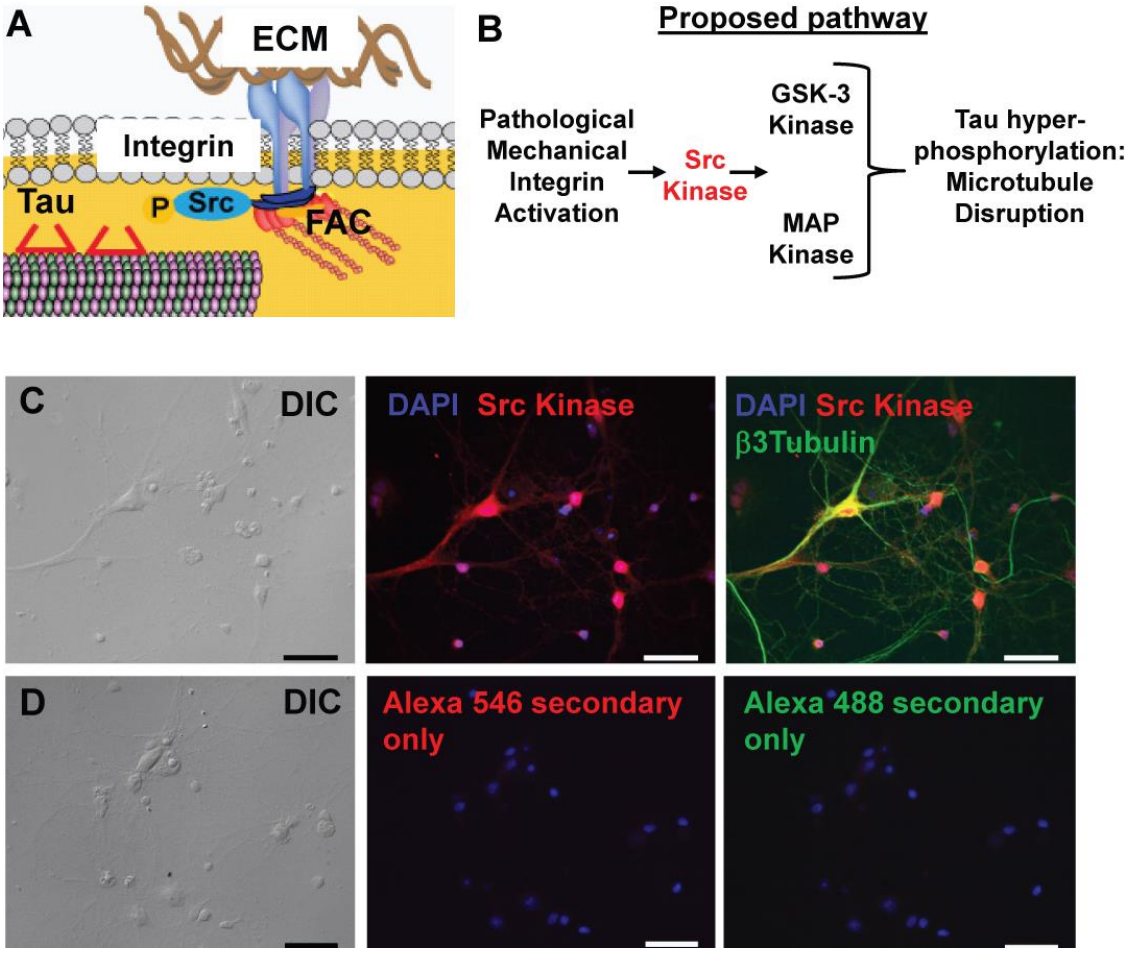

Figure 3-10: Src Kinase: A Potential Link between Integrin Activation and Injury.

(A) Src kinase is a mechanically sensitive kinase associated with the focal adhesion complex (FAC) and the cytoskeleton, where it can act to phosphorylate tau protein and cause microtubule disassembly (B). (C) Src kinase is expressed in neurons *in vitro*. (D) Control staining with secondary antibodies only. Scale Bars = 50 µm.

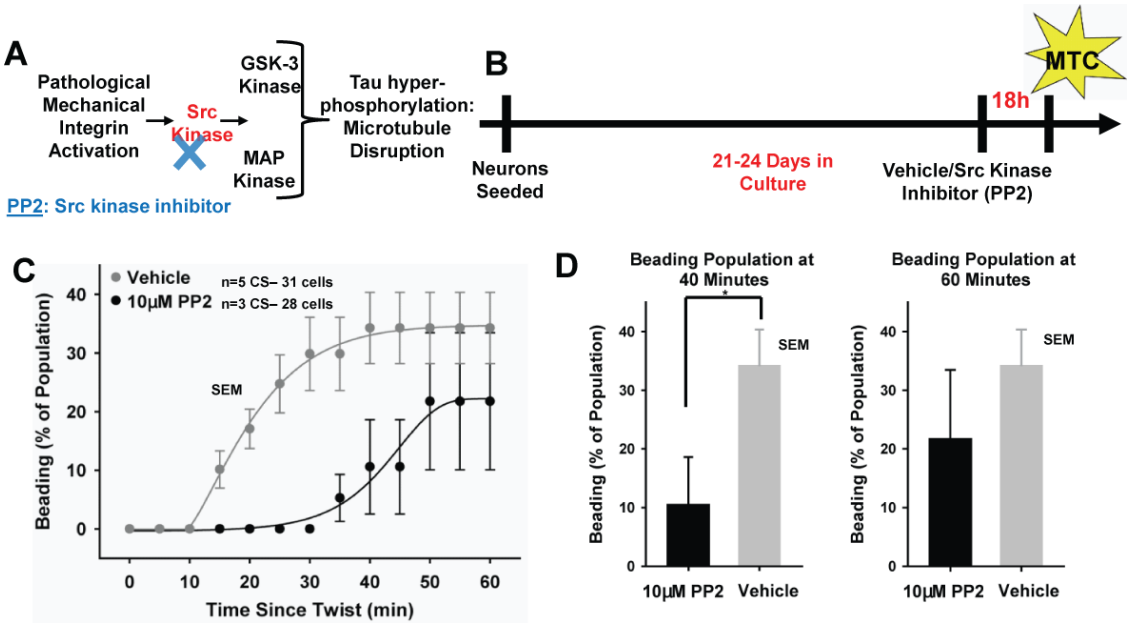

Figure 3-11: Inhibiting Src Kinase Delayed Injure Onset.

(A) PP2, a known inhibitor of src kinase was incubated with neurons before injury (B) experiments. (C). PP2 delayed the onset of focal swellings relative to vehicle (DMSO) treated neurons.

3.3 Discussion

Here we have shown that an acute mechanical perturbation of neuronal integrins is sufficient to induce neuronal focal swelling, reminiscent of DAI *in vivo*. Previous studies have attributed this injury to a loss of ionic homeostasis caused by either a disruption of the cell membrane [88, 143, 153] or changes in ion channel function [144, 154]. However, we have shown that injury can be induced by applying small strains, less than what can disrupt the cell membrane, at high rates directly through mechanically sensitive FACs. A recent *in vitro* study directly linked focal swelling to the pathological influx of calcium and activation of calpains which degrade the cytoskeleton [88]. Other studies have shown that not all neuronal injury is dependent on membrane disruption and calpain activity [143, 155], but offer little evidence for an alternative. Our *in-vitro* study indicates that integrin mediated src kinase activation may account for calpain independent pathways of injury.

Integrins are expressed heterogeneously throughout the brain and have been shown to be differentially expressed in the adult rat brain [27, 41]. Integrins are highly expressed in synaptic regions [49, 156] and can modulate synaptic plasticity by regulating ion channel currents [48, 149, 157]. In the developing nervous system, integrins are involved in dendrite and axon outgrowth [26, 158-160] and guide synaptogenesis [149, 157], and in mature neurons, they play a role in remodeling dendritric spines [157, 161]. Their ability to modify Ca^{2+} handling and modulate synaptic strength has also been linked to stabilizing long term memory potentiation [29], suggesting that integrins may be key players in memory and learning [27, 149]. In this study, we showed that axons may be more vulnerable to injury than the soma because the

failure strength of FACs in neurites is significantly lower than in the soma. Furthermore, neuronal injury was dependent upon FAC density, and force transmission via integrin binding proteins always produced widespread focal swelling, whereas non-specific force transmission through the membrane produced only local injury. A previous study has demonstrated a similar sensitivity of neuronal injury to ECM composition in the 3D cell microenvironment [43]. Neurons embedded in a 3-D gel composed of collagen conjugated to agarose exhibited increased cell death following an acute, high rate deformation when the collagen concentration was increased, indicating that the degree of cell-ECM contacts may influence neuronal injury [162]. In another study, the threshold for mechanically induced action potentials was found to be lower in neurons cultured on FN compared to those cultured on PLL, underscoring the important role of cell-ECM contacts in neurons [122]. Cell-matrix interactions have also been shown to be involved in pathological processes following acute mechanical stimulation in other cell types such as vascular smooth muscle cells [163] and epithelial cells [164, 165]. These reports, coupled with the data reported herein, suggest integrins are a reasonable conduit for mechanical cell trauma.

Since integrins mechanically link the ECM to the cytoskeleton of neurons, we also reasoned that the state of pre-stress in the neuronal cytoskeleton may affect injury force propagation in neurons. Mechanical signaling within cells relies on stress wave propagation through the cytoskeleton, and its efficiency is proportional to the stiffness of the components of the cytoskeleton (e.g., actin and microtubules) [166]. In smooth muscles cells, mechanical signal propagation is evidenced by integrin-mediated signaling that occurs at time scales faster than may be accounted by chemical diffusion or the

action of molecular motors [55]. Stress propagation in neurons via growth cones has been measured using traction force microscopy, where the forces transmitted to the underlying substrate via tension within the neuronal cytoskeleton are quantified [167]. Using this technique, we showed that forces applied locally to integrin-bound beads resulted in global cytoskeletal deformation in neurons, pointing to the cytoskeleton as an intracellular mediator of injury forces. Therefore, we reasoned that the mechanical properties of the cytoskeleton may affect injury dynamics. ROCK inhibition and treatment with calyculin have been shown to reduce and increase cytoskeletal pre-stress in myofibroblasts, respectively [168]. By using ROCK inhibitors to reduce cytoskeletal pre-stress, we showed that the onset of injury slowed. Conversely, increasing cytoskeletal pre-stress with calyculin lowered the force required for injury. Taken together, these data and previous reports suggest an injury mechanism that utilizes the neuronal cytoskeleton as a conduit for distributing forces throughout neurons.

Previous reports suggest a role for calpains in neuronal injury [88, 143, 155]. In our low strain model, we were unable to mitigate neuronal injury with a calpain inhibitor. However, we were successful in reducing neurite injury with the use of a ROCK inhibitor. Integrin stimulation can activate many signaling cascades [169], but activation of the Rho-ROCK pathway is of particular interest because of its known effects on the cell cytoskeleton. ROCK activation can affect cytoskeleton remodeling by activating downstream targets which regulate cytoskeleton tension [170], actin polymerization [171], neurofilament depolymerization [172], and microtubule stability [173]. Interestingly, studies have shown that axon focal swelling may be a result of the breakdown of microtubules and impairment of the axonal transport system [87].

Furthermore, axon retraction following mTBI can be linked to active remodeling of the neuronal cytoskeleton [174]. The activation of RhoA in *in vitro* studies has demonstrated neurite retraction in neuroblastoma cell lines [175] and dendritic retraction in brain slices [176]. A genetic study in *Drosophila* indicates that in mature neurons, the RhoA-mediated axon retraction pathway is actively repressed by negative regulators [177]. The synaptic degeneration associated with DAI implies that the activation of RhoA is a maladaptive response. Blocking activation with a Rho antagonist can reduce injury related apoptosis in the CNS [178], suggesting that blocking Rho activation may be effective in treating TBI. Furthermore, since the mechanical activation of integrin leads to the activation of src kinase [55], and src kinase activity may also lead to microtubule disruption [61], other therapeutic options beyond Rho signaling are available. This was evidenced by the slowed onset of injury when we pre-treated neurons with a src kinase inhibitor. With the growing concern about the lack of therapeutic options for treating mTBI [179], our results suggest that further exploration of integrin mediated neuronal injury may identify novel therapeutic opportunities.

3.4 Materials and Methods

3.4.1 Ethics Statement

All procedures were approved by the Harvard Animal Care and Use Committee under Animal Experimentation Protocol permit number 24-01. This protocol, entitled "Harvest and Culture of Neural and Cardiac Tissue from Neonatal Rats and Mice for In Vitro Disease Models," meets the guidelines for the use of vertebrate animals in research and teaching of the Faculty of Arts and Sciences of Harvard University. It also follows recommendations included in the NIH Guide for the care and use of laboratory animals

and is in accordance with existing Federal (9 CFR Parts 1,2&3), state and city laws and regulations governing the use of animals in research and teaching.

3.4.2 Neuron Harvest and Culture

Cortical neurons were isolated from 2-day old neonatal Sprague-Dawley rats (Charles River Laboratories, Boston, MA). Reagents were obtained from Sigma-Aldrich (St. Louis, MO) unless otherwise indicated. Cortices were surgically isolated and minced in Hanks' balanced salt solution (Invitrogen, Carlsbad, CA) followed by digestion with trypsin (USB, Santa Clara, CA) overnight at 4°C. The cell suspension was then filtered though a nylon filter of 40µm pore size (BD Bioscience) and finally separated using a Percoll gradient (GE Healthcare Life Sciences, Piscataway, NJ). Subsequently, cells were re-suspended in DMEM culture medium (Invitrogen) supplemented with 10% (v/v) heat-inactivated fetal bovine serum (Invitrogen), 30 mM Glucose, 2mM L-glutamine, 25 mM KCl, 50 mU Insulin, 7µM *p*-Aminobenzoic acid, 100 U/mL penicillin, and 100µg/mL streptomycin. Cells were seeded at a density of 30,000 cells per cm^2 and supplemented with 10 µM cytosine arabinoside for the first 48 hours of culture on substrates coated with either 100µg/ml PLL or 50 µg/ml FN. Samples were incubated under standard conditions at 37°C and 5% CO_2. After 48 hours cells were washed 3 times with PBS to remove non-adherent cells. Media was replaced every 48 hours until experiments were executed. All experiments were performed on either day 4 or 5 post seeding.

3.4.3 Immunofluorescent Staining and Microscopy

Cells were washed 3 times in PBS at 37^{o}C and fixed for 10 minutes in 4% paraformaldehyde and 2.5% TritonX-100 in PBS at 37^{o}C. Cells were then washed 3 times in PBS and an initial blocking step using 5% Bovine Serum Albumin (Jackson ImmunoResearch, West Grove, PA) in PBS was performed for 1 hour at 37^{o}C. The blocking solution was aspirated away and the primary antibody solution was immediately added and incubated for 1.5 hours at room temperature. The primary antibodies used were either anti-β-Tubulin III (1:200), monoclonal anti-Vinculin (1:200), or anti-glial fibrillary acidic protein (1:200). Primary antibodies were added to a 0.5% BSA in PBS solution. Following primary staining, cells were washed 3 times, and the secondary staining solution consisting of either goat anti-mouse conjugated to Alexa-Fluor 488 or goat anti-rabbit conjugated to Alexa-Fluor 546 and 4',6-diamidino-2-phenylindole (DAPI) was added to the cells for 30 minutes at room temperature. Samples were then washed 3 times. For samples seeded on silicon sheets, a scalpel was used to cut out an 18mm circular section of the substrate which was placed on a glass slide. For glass bottom samples, the glass was removed from the dish and placed on a glass slide. ProLong Gold Antifade reagent (Invitrogen) was added to preserve the samples and glass coverslips are affixed using nail polish (company info). Prepared slides were either imaged immediately or stored at -20^{o}C. Imaging was performed on a LSM 5 LIVE confocal microscope (Carl Zeiss, Oberkochen, Germany) with appropriate filter cubes.

3.4.4 Magnetic Tweezer Fabrication and Control

The magnetic tweezer was fabricated using a permalloy core (MμShield, Londonderry, NH) that was equipped with a 720-turn solenoid (Magnetic Sensor

Systems, Van Nuys, CA). The tweezer ensemble was mounted on an Axio Observer.Z1 microscope (Carl Zeiss) and was controlled by a micromanipulator system (Eppendorf, Hamburg, Germany). Current in the solenoid was produced by a voltage-controlled current supply (Kepco Model # BOP 100-4M, Flushing, NY) that transformed voltage signals from a function generator into a current signal with amplitudes up to 5A. LabVIEW (National Instruments, Austin, TX) software was used to program the desired voltage waveform. The magnetic tweezer was calibrated using methods outlined in [180]. Briefly, beads were placed in a 99% glycerol solution and the tweezer was engaged at various current levels. Utilizing Stoke's formula and magnetic bead velocities, we calculated force as a function of distance from tweezer tip for each current level (fig S4A). Temperature rise of the extracellular media as a result of the Joule effect in the tweezer's coil was determined to be approximately one degree Celsius (Figure 3-2). Mechanoporation during bead pull experiments was assessed through rhodamine dye uptake [143] and intracellular rises in calcium concentration (fig. S4C-D), revealing no increase in cell membrane permeability.

3.4.5 Bead Functionalization and Attachment

In order to deliver necessary forces for neuron adhesion strength and peeling experiments, the super paramagnetic beads (Bioclone, San Diego, CA) were coated with fibronectin (10 μg/ml) according to manufacturer's specifications. For bead-induced neuronal injury studies, much less force was required and Dynabeads paramagnetic beads (Invitrogen) were used and coated with either PLL or fibronectin (PLL: 100 μg/ml; FN:

10 µg/ml). For both cases beads were incubated with neurons for a total of 1 hour before experiments.

3.4.6 Neuronal Magnetic Tweezer Injury Experiments

Cells were plated onto PDMS-coated coverslips coated with 100µg/mL Poly-L-Lysine. Cells were loaded with Fluo-4 (Invitrogen) so that calcium activity during the pull could be measured. The magnetic tweezers captured individual beads and applied a short 100ms pulse between 0.5nN and 5.5nN. Each cell was imaged every minute following bead pull to determine injury outcome. All experiments were conducted in normal Tyrode's solution at 37º C.

3.4.7 Magnetic Tweezer Membrane Poration Studies

Normal Tyrode's solution was supplemented with 12.5µM carboxytetramethylrhodamine dye (Invitrogen). Cells were imaged during and after bead pull to assess changes in intracellular dye concentration as an indicator of cell membrane poration, which would allow the dye to rush into the cell. Given the high ratio of extracellular to intracellular calcium concentration, Fluo-4 (Invitrogen) was also used to determine if smaller pores-those that could let calcium ions pass- formed by checking for a rise in intracellular calcium concentration during the bead pull.

3.4.8 Scanning Electron Microscopy

After beads were attached to neurons they were rinsed twice with PBS fixed with 2.5% Glutaraldehyde for 2 hours. After rinsing again, cells were treated with 1% OsO_4 for 2 hours. After another rinse with PBS, cells were gradually dehydrated with increasing dilutions of ethanol up to 100%. After critical point drying was completed,

cells were gold sputter coated for 2 minutes at 30mA. All imaging was done on Quanta 200 scanning electron microscopy (FEI, Hillsboro, OR).

3.4.9 Pharmacological Interventions

Rho-associated Kinase (ROCK) inhibitor HA-1077 (Sigma) was prepared by dissolving in water and neurons were treated with concentration ranging between 1 nM and 100 μM in Tyrode's solution 15 minutes prior to injury. 1.5 nM calyculin (Enzo Life Sciences, Farmingdale, NY) was added to neuron to increase pre-stress prior to injury. Neurons were treated with 10 μM PP2 (Enzo Life Sciences) 18 hours to inhibit src kinase activity prior to injury experiments.

3.4.10 Traction Force Microscopy

Cells were cultured on polyacrylamide gels. Acrylamide and bis-acrylamide (Fisher Scientific, Pittsburgh, PA) solutions are prepared to contain a constant polymer mass of 5% and bis-acrylamide concentrations of 0.2% to reach a final modulus of 1.5 kPa (Brain: E~0.1–1 kPa). Acrylamide, bis-acrylamide, ammonium persulfate, and N,N,N,N-tetramethylethylenediamine (TEMED) under a nonaqueous layer of toluene containing 0.5% acrylic acid N-hydroxy succinimide ester were mixed with 200 nm fluorescent beads (Invitrogen) and polymerized between two coverslips, chemically modified as previously described [95]. After washing with HEPES buffer to remove traces of unpolymerized solvent, wells containing the polyacrylamide (PA) gels were filled with sterile water and keep at 4°C until use.

In order to coat the polyacrylamide gel with ECM, a few drops of 1 mM Sulfo-SANPAH (sulfosuccinimidyl-6- (4-azido-2-nitrophenyl-amino) hexanoate); (Pierce/ThermoFisher Scientific, Waltham, MA) in 200 mM HEPES were added to

activate the free surface of the gel. The system was then irradiated with the UV light of a sterile hood (254 nm wave length) for 5 min to link the SANPAH to the gel by photoactivation. The solution containing excess SANPAH was removed by aspiration, and the process of adding SANPAH and exposing to vacuum and UV light was repeated once moreThe ECM protein was held in place by the chamber on the surface of the activated gel overnight at 4°C and excess of solution was removed by washing the gels.

Traction forces were quantified by measuring the displacement within the gel substrate by tracking fluorescent bead motion as described previously [181]. Briefly, displacement fields of the gel were determined by tracking the motion of individual grids on beads. The motion of the grid as tension developed within neurons provided the displacement of the gel due to forces acting on it from the attached neuron.

3.4.11 Statistical Analysis

Statistical significance was measured by ANOVA and subsequent pairwise comparison when comparing multiple values. Fisher's exact test was used to analyze data in contingency tables [182]. $p<0.05$ for all statistically significant differences.

4 The Structural and Functional Effects of Integrin-Mediated Traumatic Axonal Injury

4.1 Introduction

The mechanisms underlying mild Traumatic Brain Injury (mTBI)-induced structural and functional effects are not well understood. As the most common form of TBI, mTBI accounts for 75% of the 1.7 million individuals affected by TBI in the Unites States annually [3]. A mechanically initiated disease process, mTBI initiates pathological remodeling of the cytoskeletal of neurons, disrupting microtubule and neurofilament networks [183, 184]. The disrupted cytoskeleton leads to the formation of focal swellings along axons, creating a "beads on a string" pattern [15, 185]. These swellings result from cytoskeletal dysfunction and remodeling that has been attributed to several processes, including cell membrane poration, inappropriate cleavage of ion channels, and integrin signaling [30, 52, 87]. Moreover, clinical measures of brain function in patients suffering from mTBI have revealed network-level functional deficits [186]. Assessing brain activity through magnetoecephalography and functional magnetic resonance imaging (fMRI) has demonstrated altered neuronal network connectivity in injured patients [141, 187]. Such direct functional measures of brain function are supplemented by clinical indicators of brain dysfunction, where patients who have suffered mTBI exhibit reduced reaction time and cognitive decline [188, 189]. Thus, the dysfunction associated with mTBI correlates with known structural injuries, which suggest that the forces from mechanical insults of mTBI lead to structural remodeling that ultimately hinders neuronal function.

Assessing the direct relationship between structural and functional injury during and following mechanical injury in neurons is hampered by limitations in obtaining functional readouts from neurons undergoing mechanical deformation. Previous reports have relied on *in vitro* and *in situ* settings, where dissociated neuronal cultures and brain slices have been utilized, respectively [190, 191]. Such studies injure neurons by directly straining dissociated neurons or organotypic slices uniformly on an elastomeric substrates. Functional measures of activity, including patch clamp and calcium-sensitive dyes, are used to assess neuronal function before and after injury [144, 187, 188, 192]. Similarly, neurons or slices from animal models of injury, such as cortical impact or fluid percussion, may be isolated for functional analysis with microelectrode arrays and patch clamp [193, 194]. These models of injury have demonstrated that neurons, whose membrane integrity has been compromised as a result of the applied mechanical strains, are marked by reduced coordinated activity and disrupted function in specific circuitry, like those found in the hippocampus. Previously, we reported that mechanical insults directed through specific transmembrane and mechanically sensitive integrin proteins also injured neurons [30]. We utilized magnetic beads coated with adhesive protein in order to deliver mechanical insults without increasing neuronal membrane permeability. This mode of injury resulted in focal swellings, reminiscent of the diffuse axonal injury reported in animal models of mTBI and implicated integrin signaling in mTBI. Although integrin-mediated injury forces recapitulated the structural deficits of mTBI, its functional effects have not been described.

We hypothesized that in addition to initiating structural deficits in neurons, mechanical insults directed into neurons via integrin proteins may reduce spontaneous

neuronal electrical activity. To test this, we utilized ferromagnetic beads coated to bind transmembrane integrin proteins, which afforded mechanical continuity between the bead and the cytoskeleton of the neuron. The beads were mechanically actuated by adapting Magnetic Twisting Cytometry (MTC), which rotated beads bound to neurons with prescribed temporal characteristics designed to mimic injury during mTBI. We demonstrated that the MTC injury system caused structural injury without increases in membrane poration. Because the MTC injury system enables measurement of neuronal electrical function during the mechanical insult, we showed that injury forces did not induce electrical dysfunction during injury. Moreover, we showed that spontaneous neuronal electrical activity, as measured by the activity of calcium transients, was reduced after the formation of swellings in axons. This reduction was associated with lowered coordinated electrical activity of neurons *in vitro*, suggesting that mechanical injury directed into neurons via integrin proteins confers both structural and functional deficits in neurons.

4.2 Results

4.2.1 Magnetic Twisting Cytometry Injury in Neurons

We previously reported that forces directed into neurons via integrin-bound beads with magnetic tweezers initiated the formation of focal swellings, reminiscent of Diffuse Axonal Injury [30]. To simultaneously injure multiple neurons, we adapted magnetic twisting cytometry (MTC) [145, 195] to apply injury forces to beads bound to axons. After incubating beads with neurons, the MTC system was used to magnetize axon bound

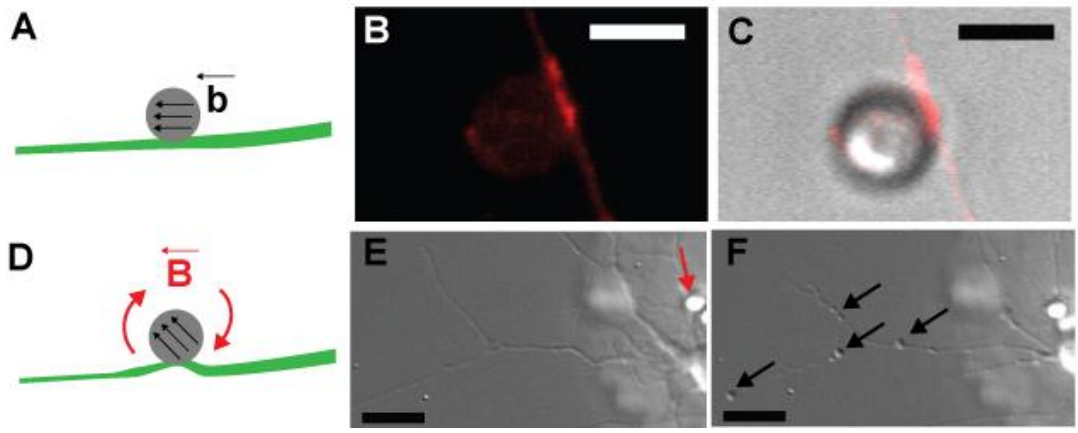

Figure 4-1: Magnetic Twisting Cytometry Induced Traumatic Axonal Injury. (A) Ferromagnetic beads coated to bind integrins in the neuronal membrane were uniformly magnetized with an external magnetic field ($\overrightarrow{\boldsymbol{b}}$). (B-C) β1 integrin clustering at the site of bead binding was confirmed by immunostaining. Scale Bars = 5μm (D) After binding to axons, beads were twisted with the Magnetic Twisting Cytometery system to apply mechanical stimuli to integrins by applying an external magnetic field ($\overrightarrow{\boldsymbol{B}}$). Uninjured neurons (E) exhibited smooth axons with bound bead (red arrow), but 60 minutes following injury (F) focal swellings appeared (black arrows). Scale Bars = 10 μm.

beads (Figure 4-1A). To test whether fibronectin (FN)-coated beads bound to integrins in the neuronal membrane, we immunostained for β1 integrins, a known ligand for FN [196] and revealed that β1 integrins integrins clustered in proximity to the site of bead binding (Figure 4-1B,C). This indicated that the bead had bound integrins and initiated their clustering as a focal adhesion complex formed, which serves to mechanically couple

the integrin's extracellular binding domain to the intracellular cytoskeleton [197]. Through the mechanical continuity between bound beads and the neuronal cytoskeleton, injury forces applied via the MTC system delivered injury forces into neurons through specific attachment points.

The MTC system rapidly applied injury forces to neurons through controlling custom-built capacitor banks. The system delivered 125 Pa of shear force to beads for duration of 50 ms to injure neurons as previously reported [152]. The temporal profile of the applied mechanical stimulus was chosen to mimic the ranges reported in TBI events [5]. Since beads were uniformly magnetized, beads attached to neurons were uniformly twisted (Figure 4-1D). One hour following injury, the smooth axons of uninjured neurons (Figure 4-1E) developed focal swellings (Figure 4-1F). It is noteworthy that the swellings occurred distal to the site of bead binding, demonstrating that injury forces propagate through the cytoskeleton of the neuron, as had been reported with the magnetic tweezer induced injuries previously reported [30]. Taken together, these results indicated that the MTC recapitulated the morphological characteristics of *in vitro* traumatic axonal injury.

The morphological injuries produced in neurons by the MTC system parallels the swellings seen in histological analysis of brain tissue in animal models of mTBI. Previous reports have indicated that these swellings are associated microtubule disassembly [184, 185]. To determine whether the focal swellings produced by injury with the MTC model, we assessed the integrity of microtubules in uninjured and injured neurons. We reasoned that during microtubule disassembly, regions of unpolymerized tubulin (Figure 4-2A) would also stain positive for tubulin in with traditional fixation protocols, which would

retain tubulin monomers in injured neurons. To circumvent this, we employed an alternate microtubule staining protocol that removed unpolymerized tubulin while stabilizing assembled microtubules [198, 199]. This technique would produce gaps where unpolymerized tubulin has been rinsed away, leaving only intact microtubules to bind tubulin antibodies (Figure 4-2B).Using this technique, we observed that neurons prior to injury exhibited smooth staining along axons, indicating intact microtubules along their length without any gaps (Figure 4-2C). This was in contrast to injured neurons, which displayed numerous gaps along axons and indicated regions where microtubule architecture had been compromised (Figure 4-2D). Thus, mechanical insults applied to neurons with the MTC injury model were associated with damaged microtubule architecture, providing a link to the morphological swellings that have been previously reported in this injury model.

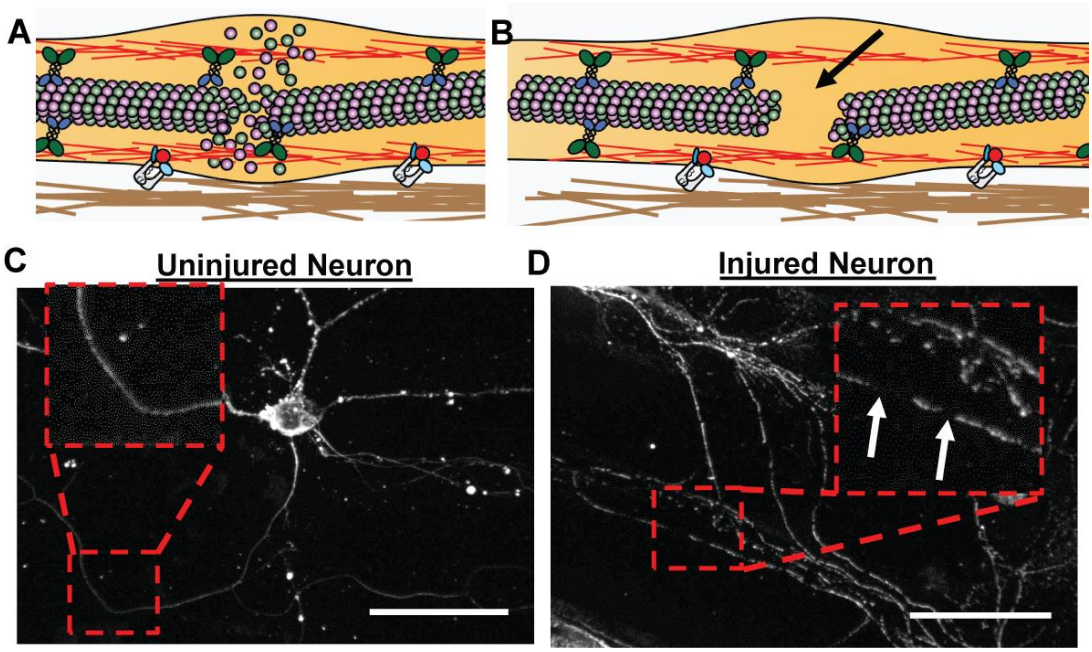

Figure 4-2: Microtubule Disassembly in Injured Neurons.

(A) Schematic depicting microtubule disassembly at sites of focal swellings. (B) Immunostaining protocol removes unpolymerized tubulin monomers while preserving intact microtubules in order to expose sites of microtubule disassembly (black arrows). (C-D) Stabilized microtubule staining of uninjured and injured neurons revealed gaps in microtubule staining in injured neurons (white arrows). Scale Bars = 50 µm.

4.2.2 Functional Activity of Patterned Neurons

In order to determine the functional effects of the MTC injury model, it was important to determine the functionality of neurons in culture. As electrically active cells, neuronal action potentials are an important aspect of neuronal function. To assess whether the cultures formed functional networks *in vitro*, we cultured neurons on microelectrode arrays. Neurons formed interconnected networks in culture, as indicated by phase contrast imaging (Figure 4-3A). After two weeks in culture, cultures were characterized by spontaneous action potential spikes, which represented the isolated activity of several neurons in proximity to microelectrodes (Figure 4-3B). As neurons matured after two weeks in culture, the individual spikes were replaced by robust bursting patterns (Figure 4-3C). Closer temporal examination of the electrical activity revealed that spikes from immature cultures represented single action potentials (Figure 4-3D), while bursting, mature cultures displayed pockets of closely spaced action potentials from the coordinated firing of multiple cells surrounding each microelectrode (Figure 4-3E). Taken together, these data demonstrate that although dissociated neurons are initially functionally isolated, they form robust networks characterized by spontaneous electrical activity as they mature beyond two weeks.

Measuring the functionality of axons in the MTC injury model required patterned cultures that allowed for axons to be isolated. To this end, neurons were initially seeded into a prescribed PDMS mask, where neurons were isolated to the peripheral regions of the glass coverslip (Figure 4-4A). Once the masks were removed, axonal extensions bridged the gap between the regions of neuronal cell bodies.

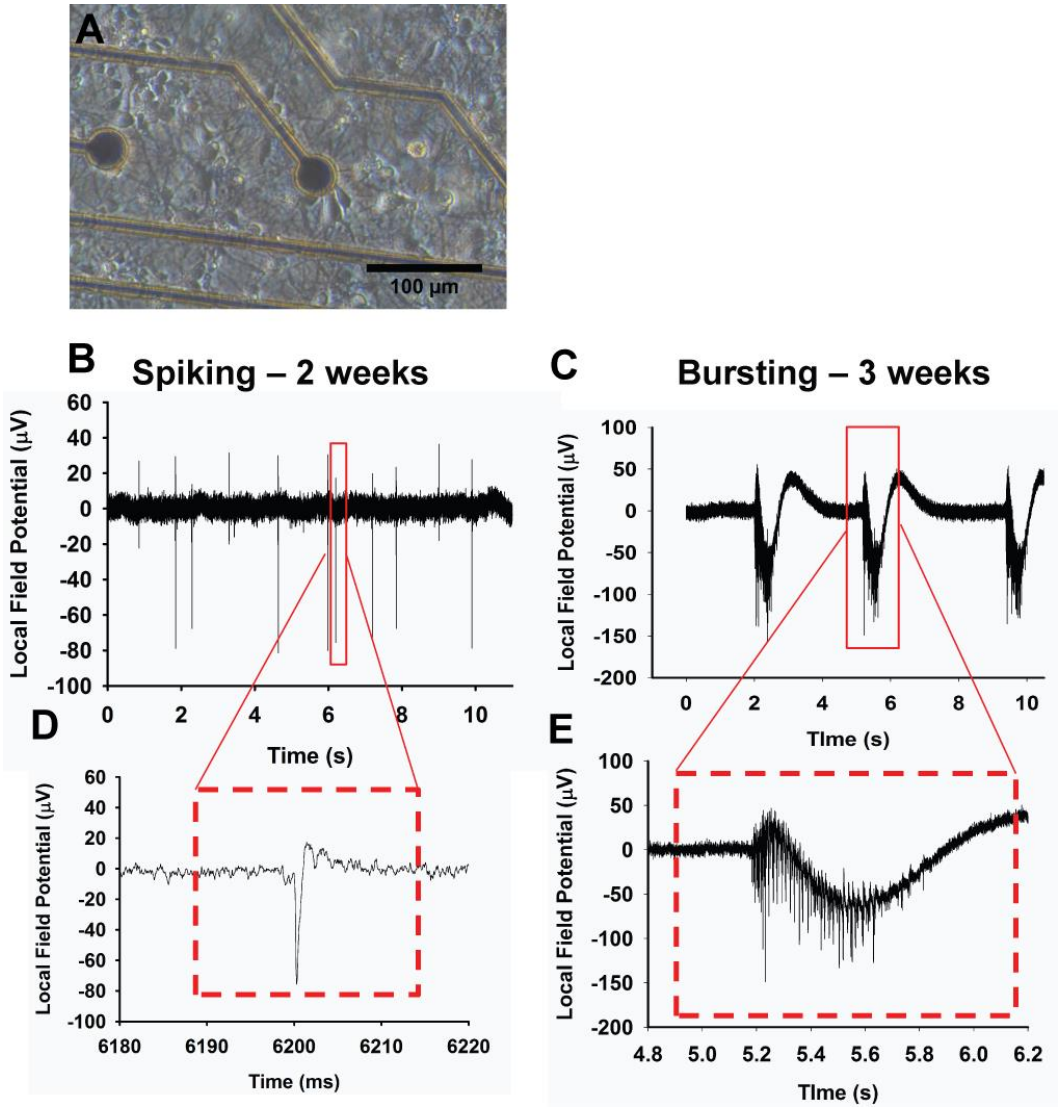

Figure 4-3: Spontaneous Neuronal Electrical Activity.

(A) Neurons grown on microelectrode arrays exhibited spontaneous spiking activity approximately two weeks after culture (B). As cultures matured beyond two weeks, they developed robust bursting activity (C). Spiking (D) and bursting (E) plotted to identify individual spikes.

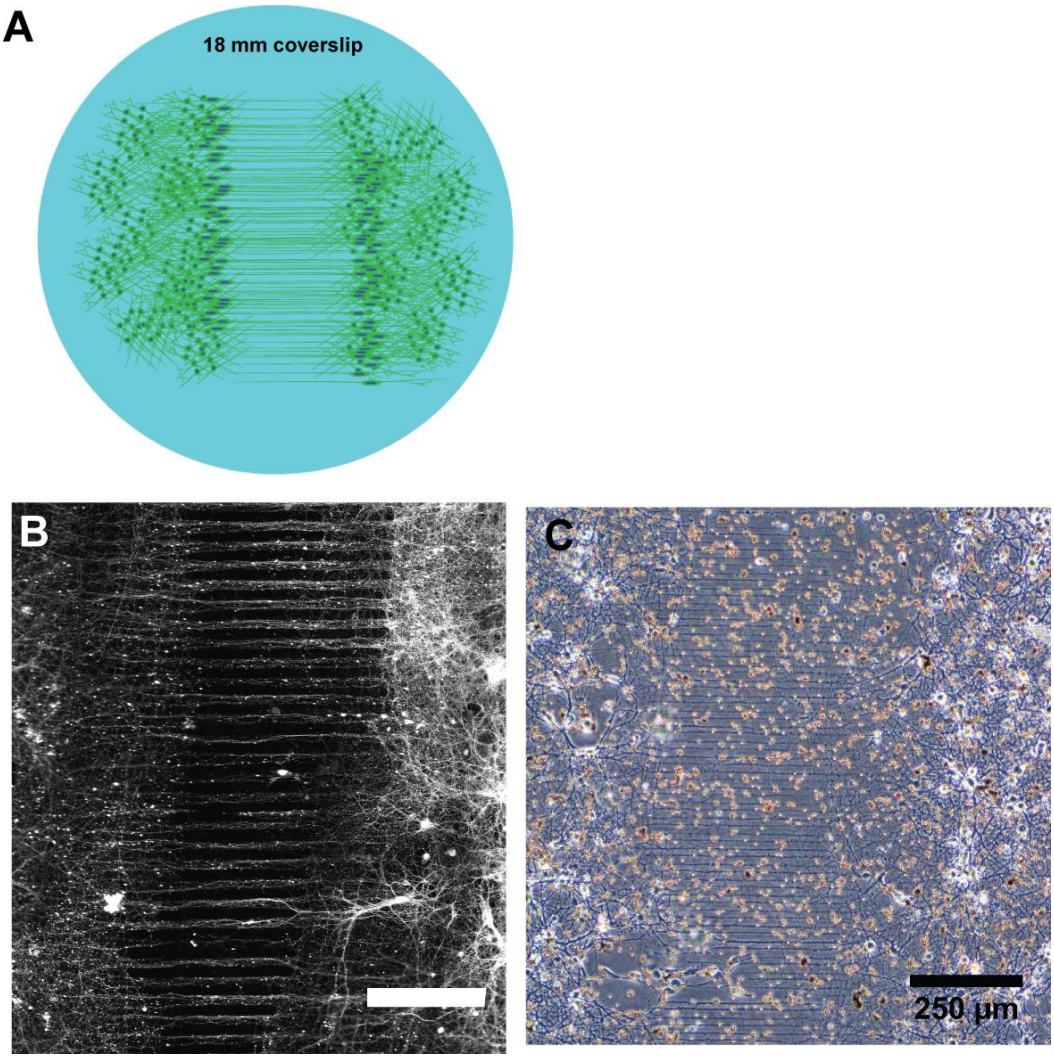

Figure 4-4: Patterned Neuronal Culture.

(A) Schematic depicting isolated regions of somas and dendrites connecteted by isolated axons. (B) β3 staining in culture revealed well aligned axonal regions surrounded by isotropic regions containing somas. (C) Phase contrast image of neurons patterned to isolate axons with beads attached to neurons throughout the field of view. Scale Bars = 250µm.

This well-defined pattern was evident when cultures were stained for neuron-specific β3-tubulin antibody (Figure 4-4B). Magnetic beads designated for the MTC injury model were incubated with the neurons and axons (Figure 4-4C) prior to injury. Although beads are incubated with all neurons and are allowed to settle throughout the coverslip, only the functionality of the regions enriched for axons was assessed before and after MTC induced injury. Thus, the patterned culture of neurons provided direct access to the functional behavior of axons before and after injury.

Although we established that the neuronal cultures were electrically active by directly measuring extracellular voltage, simultaneous injury with the MTC injury model and voltage measurements were not possible given the sensitivity of the microelectrode array to external electromagnetic fields. Given that the neurons in culture displayed bursting activity (see Figure 4-3) and that this bursting activity is also correlated with neuronal calcium transients [200], we reasoned that the spontaneous electrical activity of the patterned neuronal networks may be measured by loading the neurons with Fluo-4, a calcium sensitive dye. After incubating Fluo-4 with neurons and rinsing neurons, axons were visualized with the calcium dye (Figure 4-5A). Closer examination of the individual axons revealed spontaneous calcium transients (Figure 4-5B,C). These calcium transients matched the temporal characteristics of the electrical busting, effectively providing a proxy for the electrical activity within the axon-enriched regions of the neuronal culture. Combined with the MTC injury model, this imaging modality permitted direct access to the electrical activity of axons before, during, and after the injury.

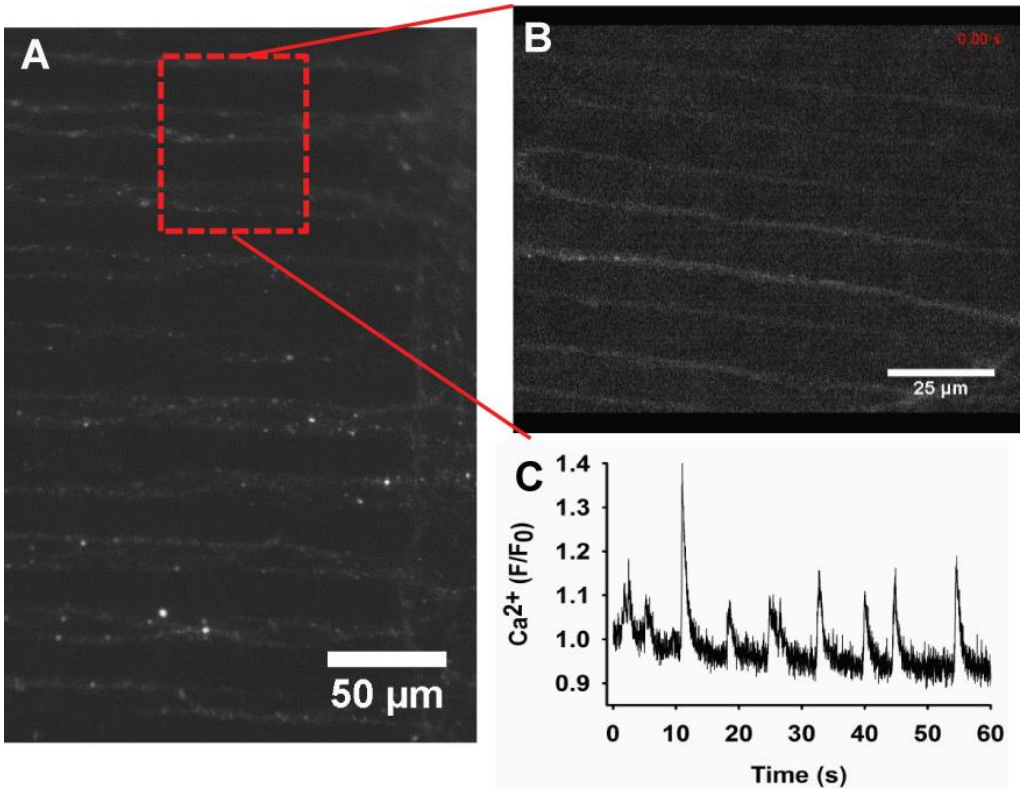

Figure 4-5: Spontaneous Calcium Transients in Neurons.

(A) Axonal regions of patterned neurons were loaded with fluo-4, a calcium sensitive dye. (B) Zoom in on axonal regions of axons loaded with calcium dye. (C) Axonal regions depicted spontaneous calcium transients.

4.2.3 Deficits in Axonal Function Due to MTC Injury

To determine functional consequences of MTC injury, we sought to measure the electrical activity of axons before, during, and immediately following the injury. To this end, we imaged neuronal calcium activity while simultaneously using the MTC system to twist beads bound to axons. Multiple beads bound to axons were twisted (Figure 4-6A), and the deformation caused negligible out of plane motion of axons. This allowed steady measurement of calcium activity in Fluo-4 loaded axons (Figure 4-6B). Bead twist was traced by the motion of the beads as they were actuated by the external magnetic field induced by the MTC system. By plotting the calcium activity in individual axonal segments, we noted no calcium activity in response to the bead twist (Figure 4-6C). This indicated that the mechanical perturbation of beads bound to integrins in the neuronal membrane failed to activate mechanically sensitive ion channels, which would have resulted in a calcium transient that directly corresponded with the bead twist injury. Moreover, a lack of calcium increase during the twist also demonstrated that the injury did not perturb cell membrane integrity, since calcium ions would have travelled down the $[Ca^{2+}]$ gradient if any pores had formed in the cell membrane. The fact that axons still exhibited calcium transients in the seconds following the injury also indicated that no immediate negative functional deficits were present immediately following the injury. Taken together, these data demonstrate that the MTC injury system does not initiate immediate electrical dysfunction in axons.

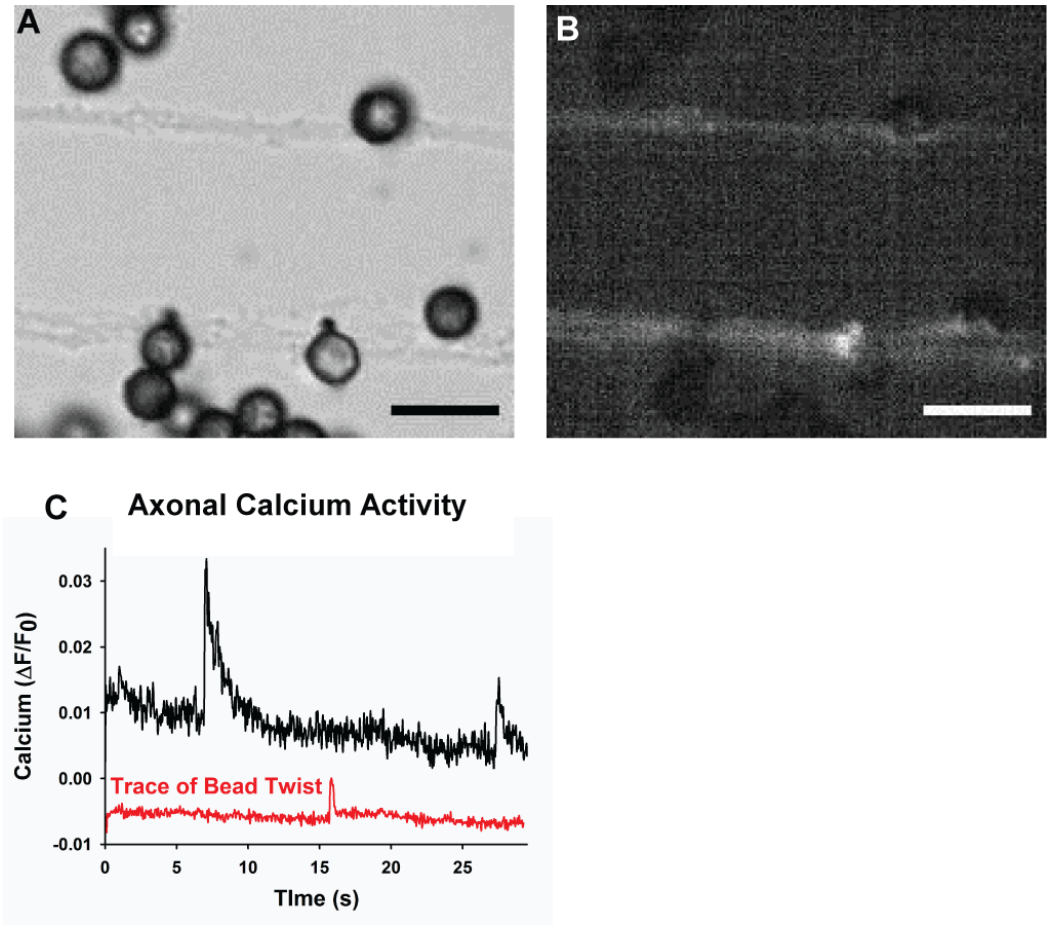

Figure 4-6: Electrical Activity During MTC Injury

(A) Brightfield image depicting bead attached to patterned axons (B) Axons loaded with fluo-4 (calcium-sensitive dye). (C) Calcium transients (black trace) recorded during bead twist (red trace).

Since the structural deficits caused by the MTC injury model appeared in the hour following injury, we asked how the electrical function of neurons throughout this period maybe affected. The electrical activity of axons bound to FN-coated beads was assessed before and at 15 minute intervals following MTC injury (Figure 4-7A). During each

recording, one minute of spontaneous calcium activity was recorded per field of view, which was divided into multiple grids (Figure 4-7B). The proportion of regions that were active in each field of view was tabulated and all subsequent activity was normalized to pre-injury levels. When the proportion of active regions in injured neurons was compared to control samples, where beads were bound to neurons without any magnetic field to twist them, significant reductions in spontaneous calcium activity were noted 45 and 60 minutes following injury (Figure 4-8A). The axons with reduced electrical activity were correlated with those that also exhibited swellings, which was determined by the morphological changes apparent in Fluo-4-loaded neurons (Figure 4-8B). The reduction in electrical activity was not immediate, and for the first 30 minutes following injury it was comparable to control activity levels. Therefore, the formation of focal swellings in axons that were initiated by injury forces directed through integrin proteins correlated with reductions in spontaneous electrical activity.

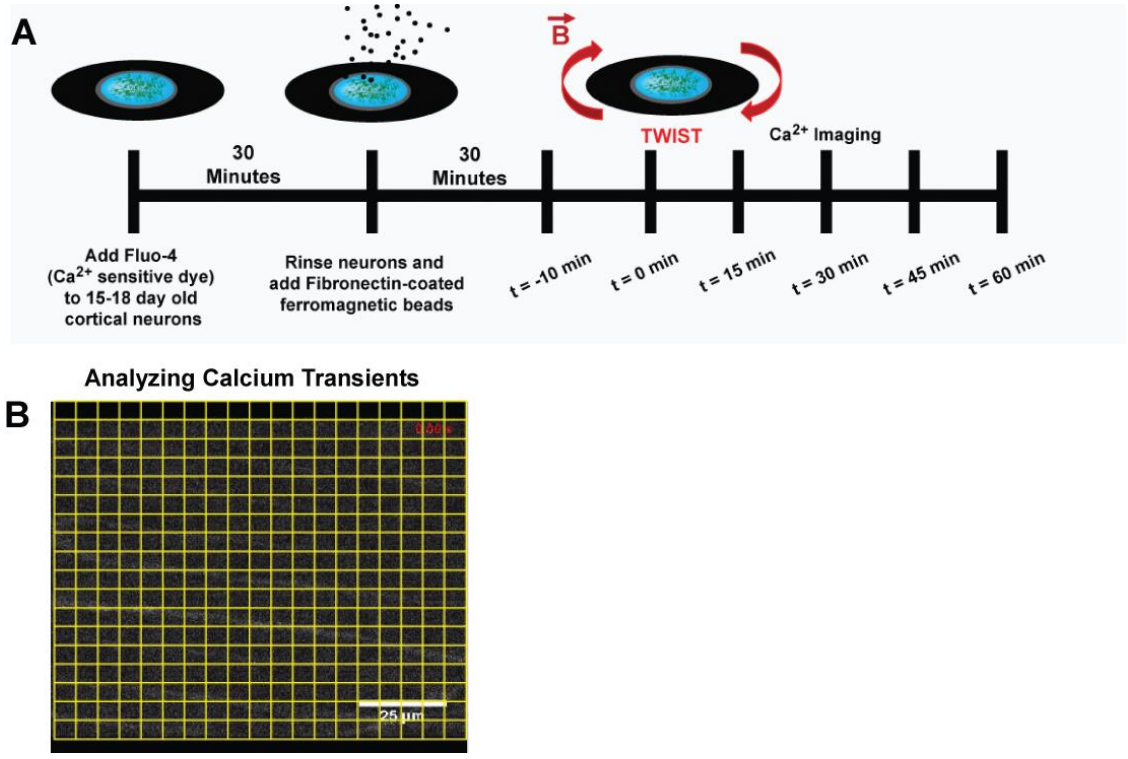

Figure 4-7: Schematic of MTC Injury and Calcium Imaging.

(A) Neurons were loaded with calcium sensitive dye (fluo-4) prior to magnetic bead incubation and injury. (B) Each field of view containing axons was divided into grids. The proportion of active grids was used to indicate axonal activity.

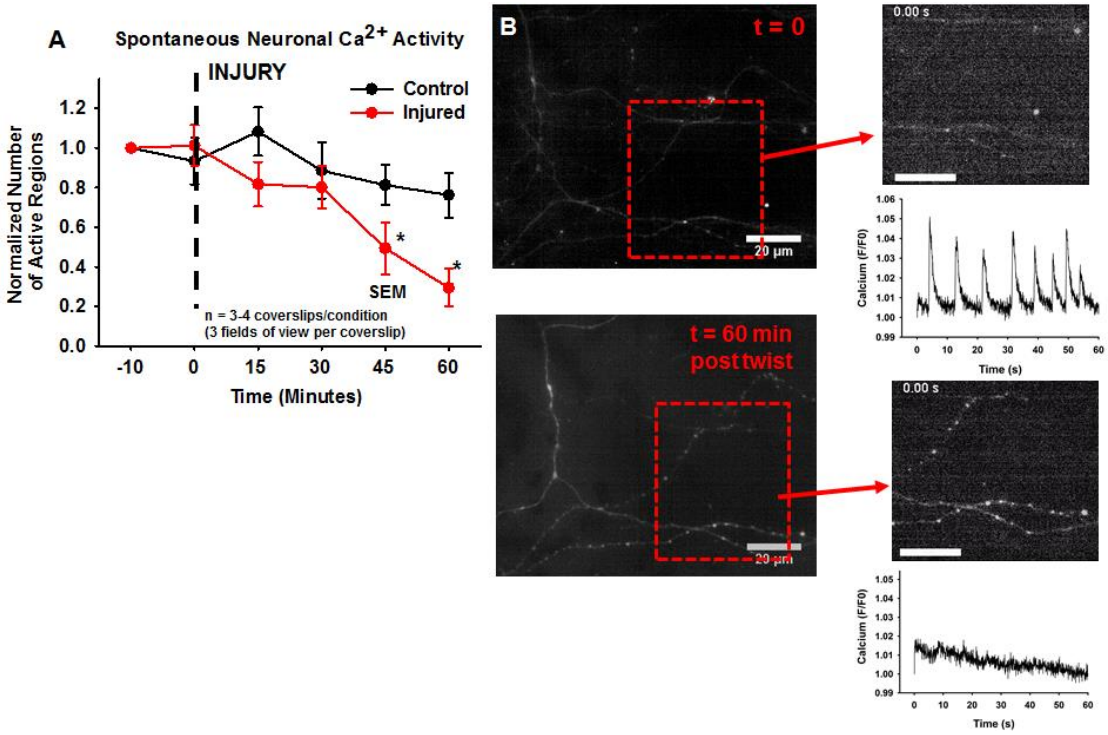

Figure 4-8: MTC Injury Reduces Calcium Transients.

(A) Aggregate calcium activity normalized to pre-twist proportion of active grids/total grids. Error bars SEM. (B) Sample calcium transients before injury (top panel) and 60 min post injury (bottom panel) – note swellings in neurites and lost calcium transients. Inset scale bar = 10 µm.

4.2.4 Coordinated Neuronal Activity is Disrupted Following MTC Injury

The coordinated electrical activity of neuronal networks represents a system with robust connectivity, which may be disrupted by axons that are injured within the network. To assess the effects of MTC induced injury on coordinated neuronal function, we interrogated the activity of multiple neurons in individual fields of view. The electrical function of neurons may be monitored by soma calcium transients [201]. Within a single field of view, the activity of multiple neurons was captured (Figure 4-9A). These calcium traces from individual neurons were collected in order to determine the degree of coordinated firing among neurons (Figure 4-9B). This collection of activity from multiple neurons may be tabulated into a cross correlation matrix, which depicts the level of coordinated activity between neurons (Figure 4-10A,B). Through this analysis, we formed representative cross-correlation matrices for a single field of view before, 30 minutes, and 60 minutes following MTC injury (Figure 4-11A-C). There was a noticeable decrease in neuronal activity that was well correlated, which was exemplified by the predominately negative percent change in cross correlation when post and pre injury activity was compared (Figure 4-11D). This trend was reinforced by aggregated data, which revealed that coordinated activity of injured neurons decreased relative to that of control neurons, where bound beads were not twisted (Figure 4-11E). These results mirror the reduced axonal activity, relating changes in activity at the single axon level to the coordinated activity of multiple neurons in a local network.

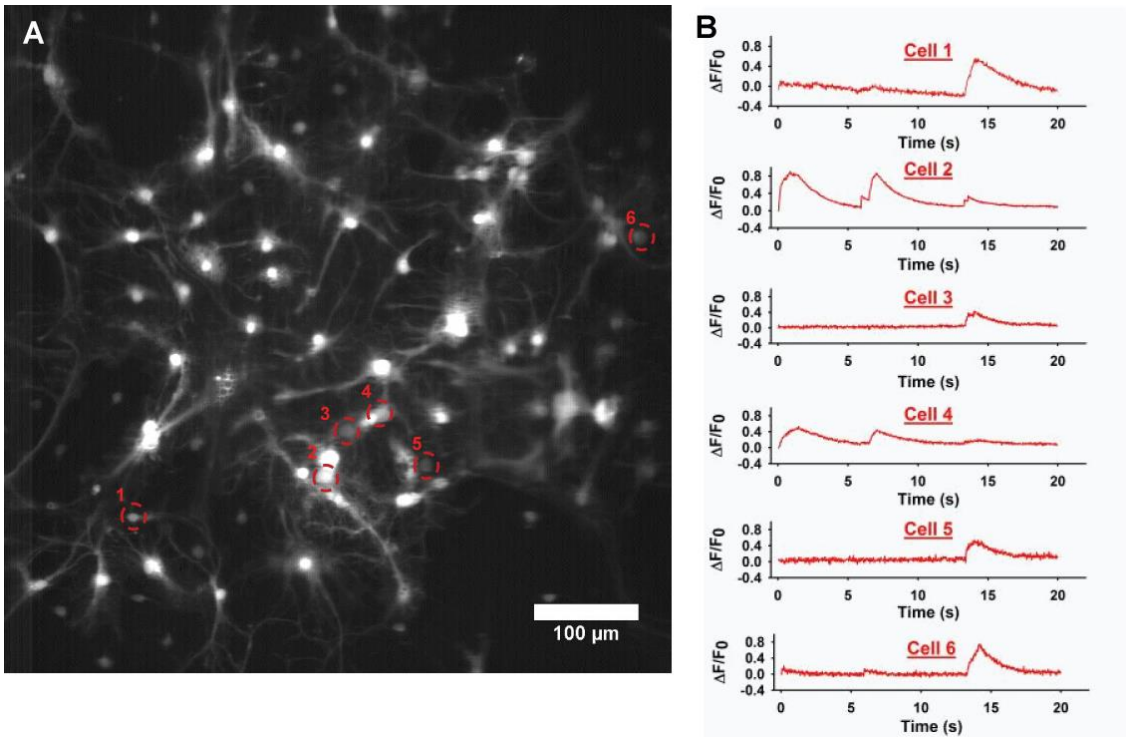

Figure 4-9: Measuring Activity of Neuronal Networks

A) Neuronal activity was obtained from measuring calcium activity via fluo-4 dye in somas of neurons in field of view. (B) Sample calcium traces from neurons.

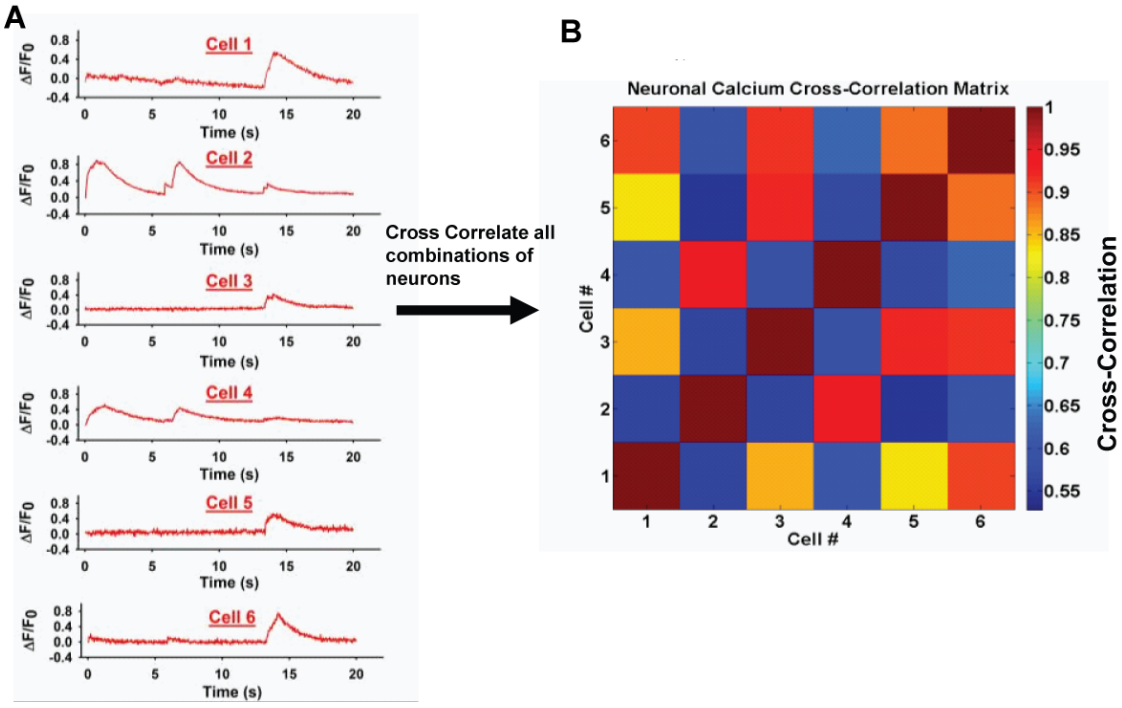

Figure 4-10: Neuronal Network Cross Correlation

A) Calcium traces from field of view in Figure 4-9 were cross correlated to form example cross-correlation matrix (B).

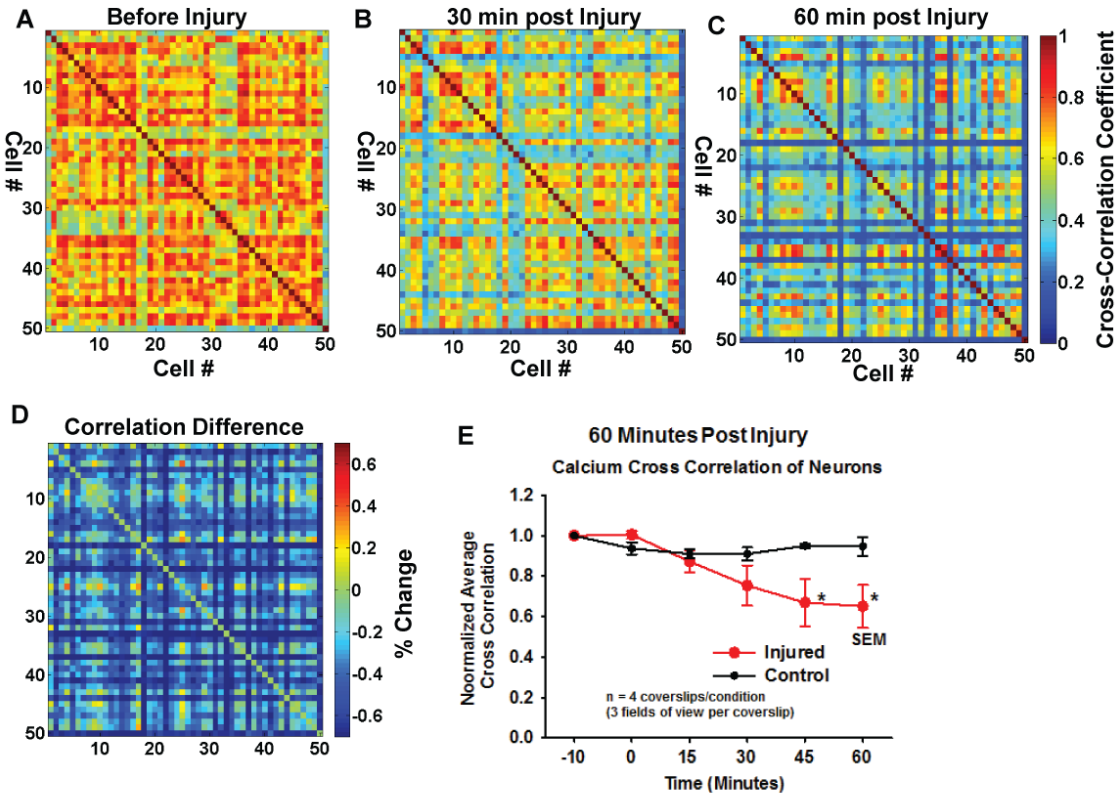

Figure 4-11: Neuronal Network Cross-Correlation following MTC Injury.

(A-C) Representative cross-correlation matrices before, 30 minutes, and 60 minutes after MTC injury. (D) Percent change between before and after cross-correlations of representative field of view. (E) Aggregated and normalized cross-correlations indicated decreased coordinated neuronal network activity following MTC injury.

4.3 Discussion

Here, we have shown that MTC induced forces directed into neurons via integrin proteins produced focal swellings in neurons. This injury was similar to those reported in previous *in vitro* models of Traumatic Axonal Injury (TAI), where swellings formed following stretcher or fluid shear induced forces [87, 88, 202]. However, MTC induced injury without altering neuronal membrane integrity. We have previously reported that injury forces directed into neurons with magnetic tweezers and beads bound to integrins also induced focal swelling formation without changes in cell membrane permeability [30]. With the MTC injury model, multiple neurons were injured simultaneously and we were able to demonstrate indications of microtubule disassembly in injured neurons by rinsing unpolymerized tubulin before fixation and staining. This procedure revealed gaps in intact microtubules along axons, suggesting that integrin-mediated injury forces also cause microtubule disorganization, similar to other models of TAI [184, 185]. Taken together, these results indicate an injury mechanism by which integrin-mediated injury forces recapitulate focal swelling injury in the absence of membrane poration.

The mechanical insults associated with mTBI have been also shown to induce functional deficits. Stretching hippocampal slices *in situ* has demonstrated significant alterations in currents required to activate circuitry [203, 204]. Moreover, stretching neuronal networks grown from dissociated cultures of neurons has demonstrated losses in coordinated activity as measured by calcium sensitive dyes [192]. However, these reports utilized uniform stretching models, where membrane poration has been shown to be a significant contributor to the underlying injury. By using the MTC injury model, we showed that forces that do not cause membrane poration were also capable of reducing

spontaneous neuronal activity and disrupting the coordinated activity of neuronal networks *in vitro*. Therefore, integrin-mediated injury forces present an injury mechanism that supplements existing membrane poration or ion channel dysfunction modes of injury. Since multiple degrees of injury exist within mTBI, it is possible that different mechanisms are responsible for different injury severities.

4.4 Materials and Methods

4.4.1 Neuronal Harvest and Culture

All procedures were approved by the Harvard Animal Care and Use Committee under Animal Experimentation Protocol permit number 24-01. Cortical neurons were harvested from two day old Sprague-Dawley Rats (Charles River Laboratories, Boston, MA) as reported previously [205]. Briefly, freshly isolated cortices were minced into one mm^3 sections and placed in Papain (Worthington) dissolved in calcium-free Hibernate A (Life Technologies) at 34 U/mL supplemented with 0.5mM Glutamax (Life Technologies) in 30°C for 30 minutes with gentle agitation. Digested tissues were then transferred to Hibernate A/B27 supplemented with 0.5 mM Glutamax to deactivate protease activity. Digested tissues were then triturated with fire-polished Pasteur pipette in order to gently release neurons from tissue sections. Following trituration, dissociated neurons were loaded onto OptiPrep density gradient (Sigma) and centrifuged for 15 minutes at 800*g* at room temperature. The neuronal fraction resulting from the centrifuged density gradient was rinsed and centrifuged again at 200*g* before cell counting and seeding in Neurobasal A medium (Life Technologies), supplemented with B27, 0.5 mM Glutamax, and 10 μg/mL gentamicin.

Culture substrates were prepared by rinsing 18 mm glass coverslips (VWR) with 70% ethanol. Cleaned coverslips were UV-Ozone (Jetlight) treated for 8 minutes to surface activation and sterilization. In order to isolate neuronal populations and to induce aligned axonal extensions between them, polydimethylsiloxane (PDMS) (Sylgard 184, Dow Corning) stamps featuring 10 μm wide lanes separated by 10 μm gaps were generated using soft lithography as previously described [96]. The stamps were then laser cute so that two separate oval regions for neuronal cell bodies separated by a 750 μm gap created a PDMS 'stencil' to be placed on each coverslip (see Fig. 4-4A). The line features of the stamp were coated with 50 μg/mL laminin (Life Technologies) dissolved in 0.1 % w/v poly-L-lysine (PLL) (Sigma) for one hour. After UV-Ozone treating coverslips, the coated PDMS stencils were placed line-feature side down onto each coverslip. The exposed glass regions of the coverslip were filled with PLL and allowed to coat for one hour. The coverslips were then rinsed with PBS (Life Technologies) and 60,000 neurons were seeded per region. After 1 hour, PDMS stencils were removed and neurons were rinsed. Coverslips were maintained in 12 well culture plates in 1 mL of media. Half of the culture medium was replaced every 72 hours and experiments were carried out on day 17-19.

4.4.2 Magnetic Beads Functionalization and Attachment

4.5 μm carboxyl ferromagnetic beads (Spherotech) were coated to bind integrins in the membrane of neurons. with Fibronectin (BD Sciences). 500 μL of stalk bead solution (1.996×10^8 beads/mL) was centrifuged briefly to remove supernatant. 980 μL of sodium acetate buffer was added to the beads. then 10 μL of Sulfo-NHS (10 mg/mL, Sigma) and 10 μL of EDC (10 mg/mL, TCI America) was mixed with the bead solution

and allowed to incubate with gentle mixing at room temperature for one hour. After centrifuging to remove supernatant, the beads were rinsed once with isosaline buffer solution. 10 μg/mL Fibronectin (BD Sciences) in isosaline buffer was added to beads and allowed to incubate with gentle mixing for at least two hours at 4 °C. Beads were rinsed and stored in 10% BSA until use. For each 18 mm coverslip, 200 μL of bead solution (~ 4 million beads) was incubated with neurons for 30 minutes to allow sufficient integrin binding.

4.4.3 Magnetic Twisting Cytometry Injury System

Custom built magnetizing coils were used to magnetize protein-coated beads and to twist beads attached to neurons to deliver mechanical injury forces to neurons via integrins as previously described [152]. Briefly, a magnetizing loop consisting of 9 layers of eight 22 AWG loops is used to generate 0.1 Tesla for 10 μs to magnetize beads. For twisting beads, a coil made up of 22 layers of 18 AWG loops is used to generate 0.01 Tesla for 50 ms. Calibration was conducted in solution of known viscosity (glycerol) as previously described [206], revealing 125 Pa of shear stress generated per bead.

4.4.4 Immunofluorescence and Microscopy

For β1 integrin staining, neurons were rinsed in PBS at room temperature and fixed for 30 minutes in 4% paraformaldehyde on ice. No detergent was used since the primary β1 integrin is a transmembrane protein and the antibody used targeted its extracellular domain. After rinsing neurons, 1% Bovine Serum Albumin (Jackson ImmunoResearch, West Grove, PA) in PBS was incubated with neurons for 30 minutes are room temperature to block nonspecific binding. The blocking solution was aspirated

away and the primary antibody solution was added and incubated for one hour at room temperature. The primary antibody solution consisted of the anti-β1 Integrin (1:50, CD29 Mouse Monocloncal, LifeSpan Biosciences) dissolved in 0.5% BSA in PBS solution. After primary staining, cells were washed 3 times with PBS, and either goat anti-mouse Alexa-Fluor 488 and 4',6-diamidino-2-phenylindole (DAPI) was added to the cells for one hour at room temperature. After rinsing, ProLong Gold Antifade reagent (Invitrogen) was added to preserve the samples.

For imaging microtubules, we utilized microtubule stabilization and staining protocols as outline previously [198, 199]. Briefly, neurons were rinsed in microtubule stabilizing buffer (60 mM Pipes, 25 mM Hepes, 10 mM EGTA, 2 mM MgCl2, pH 6.9) and treated with 0.5% Triton X-100 in the stabilizing buffer and 10 μM taxol for 3 minutes at 37°C. The neurons were then fixed by adding equal volume of 8% paraformaldehyde for 10 minutes. The cultures were then blocked with BSA as before and primary polyclonal anti β3 tubulin antibody (1:200, Sigma) was added overnight at 4°C. Secondary goat anti-mouse Alexa-Fluor 488 was incubated with neurons for 30 minutes at room temperature before rinsing and mounting neurons in ProLong Gold.

Prepared slides were either imaged immediately or stored at -20^{o}C. Imaging was performed on a Olympus IX-83 microscope equipped with the CSU -W1 Andor spinning disc confocal module and Andor Neo Camera.

4.4.5 Calcium Imaging and Analysis

To image electrical activity of neurons, calcium-sensitive Fluo-4 dye (Life Technologies) was used. 2 mM aliquots of dye were made using Pluronic F-127 (Life Technologies) and a final 2.3 μM concentration of dye was incubated in neurons with

culture medium for 30 minutes. Neurons were then rinsed with warmed Hibernate A Low Fluorescence (Brain Bits) and transferred to heated microscope imaging chamber in Hibernate A Low Florescence. Neurons were allowed to equilibrate for another 30 minutes while protein-coated magnetic beads bound. Activity from fields of view was recorded two separate time points prior to injury at 20Hz for one minute. Fields of view were then imaged for one hour following injury at 15 minute intervals.

Custom-written Matlab (Mathworks) software was used in conjunction with ImageJ to tabulate active regions in each field of view and to tabulate cross-correlation between individual neurons. All spontaneous activity and cross correlation values were normalized to pre-injury levels for each field of view.

4.4.6 Microelectrode Array Recordings

To confirm that the dissociated cultures were electrically active, 400,000 neurons were seeded isotropically onto an 8x8 microelectrode array (Multichannel Systems) coated with PLL. After two weeks in culture, electrical activity was recorded at 37 °C using the MEA 2100 recording system (Multichannel Systems). Each recording lasted 90 seconds and was sampled at 25 kHz. Custom written Matlab software was used to extract spiking and bursting activity of electrodes.

4.4.7 Statistical Analysis

Statistical significance was measured by ANOVA and subsequent pairwise comparison when comparing multiple values. $p<0.05$ for all statistically significant differences.

5 Conclusions

5.1 Integrin Signaling in mTBI

As a mechanically initiated disease process, mTBI initiates multiple, complex signaling cascades that ultimately lead to neuronal dysfunction. It is important to note that while severe injuries may surpass the mechanical failure strengths of brain and cellular tissue and result in direct axonal shearing, membrane poration, or microtubule damage, more subtle injury forces also correlate with clinical deficits and predispose individuals to neurodegenerative disease later in life. A central question that arises in this setting is how can such forces result in injury? As mechanically sensitive proteins, integrins link the CSK of cells to the surrounding microenvironment, which may include extracellular matrix proteins and other cells. Not only do integrins serve as mechanical conduits to the intracellular space, but their mechanical activation can also activate mechanosensitive biological cascades. Therefore, it is imperative to consider integrin signaling in the context of mTBI, especially where injury forces do not result in overt pathology associated with simple mechanical failure of brain tissue. Moreover, integrin signaling provides a means for understanding how mTBI is a risk factor for neurodegenerative diseases like Alzheimer's Disease. Since integrin signaling links amyloid beta aggregates to tau pathology in AD, it stands to reason that the mechanical activation of integrins in mTBI may potentiate similar neuropathological cascades. As such, the study of integrin signaling in the context of mTBI offers considerable mechanistic and therapeutic insights.

5.2 Magnetic Tweezers for Accessing Neuronal Microcompartments

In order to test whether integrin signaling plays a role in mTBI, we had to build custom designed magnetic tweezers capable of directly tying forces to the neuronal CSK at specific points. To test whether this was possible, we first utilized tweezers and beads bound to integrins to interrogate the mechanical properties of neuronal microcompartments (e.g., soma and neurites). We were able to obtain the mechanical properties of neurites with the tweezers, obtaining values that were in agreement with other modes of measurement, such as glass needle pipet deflection. This result provided evidence that the magnetic tweezers were a viable means of mechanically coupling to the neuronal CSK. Moreover, the tweezers allowed for the interrogation of the adhesive properties of neuronal microcompartments, which demonstrated that this tool can directly apply forces at specific points *within* a single neuron. This was an important distinction from other methods of injury, which uniformly apply forces to neurons (e.g., cell stretchers and fluid shear forces).

5.3 Integrin and CSK Signaling in Traumatic Axonal Injury

Using the magnetic tweezers, we prescribed specific pulses at specified currents to apply injury forces to neurons via integrins. The temporal characteristics of the applied force were chosen to match those found in mTBI and we showed that by varying the intensity of the force, we changed the probability of injury. By assessing the relationship between force and injury probability, we demonstrated that injury forces may utilize integrins to gain access to the intracellular space without damaging the neuronal cell membrane. We also demonstrated this by showing that similar mechanical deformation applied to beads that bound to neurons nonspecifically (i.e., not bound to integrins)

injured neurons less efficiently. This phenomenon was evident by the fact that beads bound to integrins transmit forces directly to the CSK of the neuron, efficiently distributing energy from the injury throughout the cell. We illustrated this by measuring traction forces that were generated distal to the bead binding site when the tweezers applied forces to neurons grown on TFM substrates. Lastly, we implicated this physical perturbation to the activation of mechanically sensitive kinases like as src kinase, which may ultimately lead to the CSK disorganization associated with the formation of focal swellings in injured axons.

5.4 Functional Effects of Integrin-Mediated TAI

The structural deficits (e.g., focal swellings and axonal retraction) of mTBI must have functional effects. This is evident in patients suffering from mTBI where many suffer from cognitive impairment. These clinical deficits are echoed by more direct measures of brain activity, where disrupted network activity following injury has been noted in fMRI and magnetoencephalography studies. To assess whether integrin-mediated injuries may also disrupt neuronal network activity, we adapted Magnetic Twisting Ctyometry (MTC) to apply injury forces simultaneously to beads bound to multiple neurons. The MTC injury model recapitulated the focal swellings we induced with the magnetic tweezer model. Moreover, we demonstrated that the focal swellings were associated with reduced axonal electrical activity, which was measured using calcium-sensitive Fluo-4 dye. More importantly, we sought to understand neuronal network function following injury by assessing the coordinated activity of multiple neurons simultaneously. We found that MTC injured neurons were less coordinated, which was supported by our finding that the axons, which form the physical basis for the

network, were also functionally compromised. Taken together, these results indicate that integrin-mediated injury forces incite both structural and functional deficits and thus affect the intracellular (CSK injury) as well as intercellular function (coordinated electrical activity) of neurons.

5.5 Outlook and Limitations

This dissertation has demonstrated that the mechanical activation of integrins is sufficient for inducing traumatic axonal injury *in vitro*. This is significant because previous reports relied on traumatic failure of cellular components to achieve TAI. For example, forces that cause membrane poration were required to produce CSK damage that would ultimately lead to focal swellings along axons. Prior to this work, the focal swellings that are reminiscent of the findings in Diffuse Axonal Injury were primarily ascribed to the mechanical failure of various neuronal elements, including the cell membrane and the cytoskeleton. We have shown that forces not exceeding mechanical failure thresholds of neurons can also cause injury when directed into neurons through integrins.

Although we demonstrated general CSK damage and functional impairment as a result of injury forces mediated by integrins, more detailed analysis of the specific mediators of this injury mechanisms have yet to be described. For example, how do injury forces ultimately exert their biological effects? We posited that src kinase may represent one such mediator, as its mechanical activation initiates pathological biological cascades that ultimately result in injury. However, assays utilizing more specific inhibitors of various pathways, including siRNA or neurons from transgenic animals, are required to fully characterize more specific downstream injury mechanisms. Transgenic

animals permit live visualization of kinases via FRET imaging, allowing the direct visualization of mechanically-induced biological signaling cascades. Moreover, our injury model did not address the role of astrocytes in our mixed neuronal cultures. Astrocytes provide integral metabolic support to neurons, and given evidence of excitotoxicity and metabolic dysfunction in mTBI, their role must be closely examined. Lastly, this work did not utilize proteins that are predominately responsible for interacting with neurons *in vivo*. Fibronectin was used as a tool for binding integrins, mimicking *in vivo* interactions between neurons and brain extracellular matrix proteins (ECM), which also contain integrin-binding domains. Coating magnetic beads directly with brain ECM proteins will reveal more accurate characteristics of integrin-mediated injury in mTBI.

It is important to note that current treatment strategies for mTBI are only supportive and serve to simply alleviate symptoms. Because the underlying mechanisms of this disease process have yet to be fully characterized, treatments that address them are also lacking. Integrin signaling provides an exciting array of therapeutic options since it has been heavily scrutinized in various biological processes, ranging from development to cancer. Although the blood brain barrier provides a challenge for easy therapeutic access to the brain, strategies involving pathways associated with integrins provide a heretofore unexplored source of treatments for mTBI.

5.6 Funding Sources

This work was supported by the Defense Advance Research Projects Agency's PREVENT Program (Office of Naval Research SPAWAR N66001-09-c-2064), Congressionally Directed Medical Research Programs (CDMRP) grant W81XWH-11-2-0057, the Emerald Foundation, the Harvard School of Engineering and Applied Sciences, and the Harvard's Center for Nansocale Systems (CNS).

6 References

1. Faul, M., et al., *Traumatic brain injury in the United States: emergency department visits, hospitalizations and deaths 2002–2006.* Atlanta, GA: Centers for Disease Control and Prevention, National Center for Injury Prevention and Control, 2010: p. 2-70.

2. Thom, T., et al., *Heart disease and stroke statistics--2006 update: a report from the American Heart Association Statistics Committee and Stroke Statistics Subcommittee.* Circulation, 2006. **113**(6): p. e85-151.

3. Prevention, N.C.f.I. and Control, *Report to Congress on mild traumatic brain injury in the United States: Steps to prevent a serious public health problem*2003: Centers for Disease Control and Prevention.

4. Franz, G., et al., *Amyloid beta 1-42 and tau in cerebrospinal fluid after severe traumatic brain injury.* Neurology, 2003. **60**(9): p. 1457-61.

5. Goldstein, L.E., et al., *Chronic traumatic encephalopathy in blast-exposed military veterans and a blast neurotrauma mouse model.* Sci Transl Med, 2012. **4**(134): p. 134ra60.

6. Tran, H.T., et al., *Controlled cortical impact traumatic brain injury in 3xTg-AD mice causes acute intra-axonal amyloid-beta accumulation and independently accelerates the development of tau abnormalities.* J Neurosci, 2011. **31**(26): p. 9513-25.

7. Tran, H.T., et al., *Distinct temporal and anatomical distributions of amyloid-beta and tau abnormalities following controlled cortical impact in transgenic mice.* PLoS One, 2011. **6**(9): p. e25475.

8. Aoki, Y., et al., *Diffusion tensor imaging studies of mild traumatic brain injury: a meta-analysis.* J Neurol Neurosurg Psychiatry, 2012. **83**(9): p. 870-6.

9. Mayer, A.R., et al., *A prospective diffusion tensor imaging study in mild traumatic brain injury.* Neurology, 2010. **74**(8): p. 643-50.

10. Wilde, E.A., et al., *Diffusion tensor imaging of acute mild traumatic brain injury in adolescents.* Neurology, 2008. **70**(12): p. 948-55.

11. Baugh, C.M., et al., *Chronic traumatic encephalopathy: neurodegeneration following repetitive concussive and subconcussive brain trauma.* Brain Imaging Behav, 2012. **6**(2): p. 244-54.

12. Conde, C. and A. Caceres, *Microtubule assembly, organization and dynamics in axons and dendrites.* Nat Rev Neurosci, 2009. **10**(5): p. 319-32.

13. da Silva, J.S. and C.G. Dotti, *Breaking the neuronal sphere: regulation of the actin cytoskeleton in neuritogenesis.* Nat Rev Neurosci, 2002. **3**(9): p. 694-704.

14. Lendahl, U., L.B. Zimmerman, and R.D. McKay, *CNS stem cells express a new class of intermediate filament protein.* Cell, 1990. **60**(4): p. 585-95.

15. Johnson, V.E., W. Stewart, and D.H. Smith, *Axonal pathology in traumatic brain injury.* Exp Neurol, 2013. **246**: p. 35-43.

16. McKee, A.C., et al., *Chronic traumatic encephalopathy in athletes: progressive tauopathy after repetitive head injury.* J Neuropathol Exp Neurol, 2009. **68**(7): p. 709-35.

17. Yamada, K.M. and S. Miyamoto, *Integrin transmembrane signaling and cytoskeletal control.* Curr Opin Cell Biol, 1995. **7**(5): p. 681-9.

18. Alenghat, F.J. and D.E. Ingber, *Mechanotransduction: all signals point to cytoskeleton, matrix, and integrins.* Sci STKE, 2002. **2002**(119): p. pe6.

19. Wang, N., J.P. Butler, and D.E. Ingber, *Mechanotransduction across the cell surface and through the cytoskeleton.* Science, 1993. **260**(5111): p. 1124-7.

20. DuFort, C.C., M.J. Paszek, and V.M. Weaver, *Balancing forces: architectural control of mechanotransduction.* Nat Rev Mol Cell Biol, 2011. **12**(5): p. 308-19.

21. Hynes, R.O., *Integrins: versatility, modulation, and signaling in cell adhesion.* Cell, 1992. **69**(1): p. 11-25.

22. Shimizu, Y., et al., *Regulated expression and binding of three VLA (beta 1) integrin receptors on T cells.* Nature, 1990. **345**(6272): p. 250-3.

23. Wang, N., J.D. Tytell, and D.E. Ingber, *Mechanotransduction at a distance: mechanically coupling the extracellular matrix with the nucleus.* Nat Rev Mol Cell Biol, 2009. **10**(1): p. 75-82.

24. Myers, J.P. and T.M. Gomez, *Focal adhesion kinase promotes integrin adhesion dynamics necessary for chemotropic turning of nerve growth cones.* J Neurosci, 2011. **31**(38): p. 13585-95.

25. Myers, J.P., M. Santiago-Medina, and T.M. Gomez, *Regulation of axonal outgrowth and pathfinding by integrin-ECM interactions.* Dev Neurobiol, 2011. **71**(11): p. 901-23.

26. Robles, E. and T.M. Gomez, *Focal adhesion kinase signaling at sites of integrin-mediated adhesion controls axon pathfinding.* Nat Neurosci, 2006. **9**(10): p. 1274-83.

27. Chan, C.S., et al., *Integrin requirement for hippocampal synaptic plasticity and spatial memory.* J Neurosci, 2003. **23**(18): p. 7107-16.

28. Kramar, E.A., et al., *Integrin-driven actin polymerization consolidates long-term potentiation.* Proc Natl Acad Sci U S A, 2006. **103**(14): p. 5579-84.

29. Staubli, U., D. Chun, and G. Lynch, *Time-dependent reversal of long-term potentiation by an integrin antagonist.* J Neurosci, 1998. **18**(9): p. 3460-9.

30. Hemphill, M.A., et al., *A possible role for integrin signaling in diffuse axonal injury.* PLoS One, 2011. **6**(7): p. e22899.

31. Caltagarone, J., Z. Jing, and R. Bowser, *Focal adhesions regulate Abeta signaling and cell death in Alzheimer's disease.* Biochim Biophys Acta, 2007. **1772**(4): p. 438-45.

32. Guskiewicz, K.M., et al., *Association between recurrent concussion and late-life cognitive impairment in retired professional football players.* Neurosurgery, 2005. **57**(4): p. 719-26; discussion 719-26.

33. Lehman, E.J., et al., *Neurodegenerative causes of death among retired National Football League players.* Neurology, 2012. **79**(19): p. 1970-4.

34. Plassman, B.L., et al., *Documented head injury in early adulthood and risk of Alzheimer's disease and other dementias.* Neurology, 2000. **55**(8): p. 1158-66.

35. Fleminger, S., et al., *Head injury as a risk factor for Alzheimer's disease: the evidence 10 years on; a partial replication.* J Neurol Neurosurg Psychiatry, 2003. **74**(7): p. 857-62.

36. Ballatore, C., V.M. Lee, and J.Q. Trojanowski, *Tau-mediated neurodegeneration in Alzheimer's disease and related disorders.* Nat Rev Neurosci, 2007. **8**(9): p. 663-72.

37. Ittner, L.M. and J. Gotz, *Amyloid-beta and tau--a toxic pas de deux in Alzheimer's disease.* Nat Rev Neurosci, 2011. **12**(2): p. 65-72.

38. Drubin, D.G. and M.W. Kirschner, *Tau protein function in living cells.* J Cell Biol, 1986. **103**(6 Pt 2): p. 2739-46.

39. Lindwall, G. and R.D. Cole, *Phosphorylation affects the ability of tau protein to promote microtubule assembly.* J Biol Chem, 1984. **259**(8): p. 5301-5.

40. Hynes, R.O., *Integrins: bidirectional, allosteric signaling machines.* Cell, 2002. **110**(6): p. 673-87.

41. Pinkstaff, J.K., et al., *Integrin subunit gene expression is regionally differentiated in adult brain.* J Neurosci, 1999. **19**(5): p. 1541-56.

42. Stevens, G.R., et al., *CNS neuronal focal adhesion kinase forms clusters that co-localize with vinculin.* J Neurosci Res, 1996. **46**(4): p. 445-55.

43. Su, L., X. Lv, and J. Miao, *Integrin beta 4 in neural cells.* Neuromolecular Med, 2008. **10**(4): p. 316-21.

44. Ingber, D.E., *Mechanobiology and diseases of mechanotransduction.* Ann Med, 2003. **35**(8): p. 564-77.

45. Clements, J.M., et al., *Identification of a key integrin-binding sequence in VCAM-1 homologous to the LDV active site in fibronectin.* J Cell Sci, 1994. **107 (Pt 8)**: p. 2127-35.

46. Brocke, S., et al., *Antibodies to CD44 and integrin alpha4, but not L-selectin, prevent central nervous system inflammation and experimental encephalomyelitis by blocking secondary leukocyte recruitment.* Proc Natl Acad Sci U S A, 1999. **96**(12): p. 6896-901.

47. Sims, T.N. and M.L. Dustin, *The immunological synapse: integrins take the stage.* Immunol Rev, 2002. **186**: p. 100-17.

48. Lin, C.Y., et al., *Integrin regulation of cytoplasmic calcium in excitatory neurons depends upon glutamate receptors and release from intracellular stores.* Mol Cell Neurosci, 2008. **37**(4): p. 770-80.

49. Nishimura, S.L., et al., *Synaptic and glial localization of the integrin alphavbeta8 in mouse and rat brain.* Brain Res, 1998. **791**(1-2): p. 271-82.

50. DeRidder, M.N., et al., *Traumatic mechanical injury to the hippocampus in vitro causes regional caspase-3 and calpain activation that is influenced by NMDA receptor subunit composition.* Neurobiol Dis, 2006. **22**(1): p. 165-76.

51. Geddes-Klein, D.M., et al., *Pharmacologically induced calcium oscillations protect neurons from increases in cytosolic calcium after trauma.* J Neurochem, 2006. **97**(2): p. 462-74.

52. Singh, P., et al., *N-methyl-D-aspartate receptor mechanosensitivity is governed by C terminus of NR2B subunit.* J Biol Chem, 2012. **287**(6): p. 4348-59.

53. Juliano, R.L., *Signal transduction by cell adhesion receptors and the cytoskeleton: functions of integrins, cadherins, selectins, and immunoglobulin-superfamily members.* Annu Rev Pharmacol Toxicol, 2002. **42**: p. 283-323.

54. Torsoni, A.S., et al., *RhoA/ROCK signaling is critical to FAK activation by cyclic stretch in cardiac myocytes.* Am J Physiol Heart Circ Physiol, 2005. **289**(4): p. H1488-96.

55. Na, S., et al., *Rapid signal transduction in living cells is a unique feature of mechanotransduction.* Proc Natl Acad Sci U S A, 2008. **105**(18): p. 6626-31.

56. Poh, Y.C., et al., *Rapid activation of Rac GTPase in living cells by force is independent of Src.* PLoS One, 2009. **4**(11): p. e7886.

57. Alford, P.W., et al., *Blast-induced phenotypic switching in cerebral vasospasm.* Proc Natl Acad Sci U S A, 2011. **108**(31): p. 12705-10.

58. Haass, C. and D.J. Selkoe, *Soluble protein oligomers in neurodegeneration: lessons from the Alzheimer's amyloid beta-peptide.* Nat Rev Mol Cell Biol, 2007. **8**(2): p. 101-12.

59. Sabo, S., et al., *Interaction of beta-amyloid peptides with integrins in a human nerve cell line.* Neurosci Lett, 1995. **184**(1): p. 25-8.

60. Pena, F., et al., *Beta-amyloid protein (25-35) disrupts hippocampal network activity: role of Fyn-kinase.* Hippocampus, 2010. **20**(1): p. 78-96.

61. Williamson, R., et al., *Rapid tyrosine phosphorylation of neuronal proteins including tau and focal adhesion kinase in response to amyloid-beta peptide exposure: involvement of Src family protein kinases.* J Neurosci, 2002. **22**(1): p. 10-20.

62. Han, H.Y., et al., *alphanu and beta1 integrins mediate Abeta-induced neurotoxicity in hippocampal neurons via the FAK signaling pathway.* PLoS One, 2013. **8**(6): p. e64839.

63. Wright, S., et al., *Alpha2beta1 and alphaVbeta1 integrin signaling pathways mediate amyloid-beta-induced neurotoxicity.* Neurobiol Aging, 2007. **28**(2): p. 226-37.

64. Thaxton, L. and M.A. Myers, *Sleep disturbances and their management in patients with brain injury.* J Head Trauma Rehabil, 2002. **17**(4): p. 335-48.

65. Trinh, N.H., et al., *Efficacy of cholinesterase inhibitors in the treatment of neuropsychiatric symptoms and functional impairment in Alzheimer disease: a meta-analysis.* JAMA, 2003. **289**(2): p. 210-6.

66. Polman, C.H., et al., *A randomized, placebo-controlled trial of natalizumab for relapsing multiple sclerosis.* N Engl J Med, 2006. **354**(9): p. 899-910.

67. Reardon, D.A., et al., *Randomized phase II study of cilengitide, an integrin-targeting arginine-glycine-aspartic acid peptide, in recurrent glioblastoma multiforme.* J Clin Oncol, 2008. **26**(34): p. 5610-7.

68. Clegg, D.O., et al., *Integrins in the development, function and dysfunction of the nervous system.* Front Biosci, 2003. **8**: p. d723-50.

69. Milner, R. and I.L. Campbell, *The integrin family of cell adhesion molecules has multiple functions within the CNS.* J Neurosci Res, 2002. **69**(3): p. 286-91.

70. Bradshaw, A.D., et al., *Integrin alpha 2 beta 1 mediates interactions between developing embryonic retinal cells and collagen.* Development, 1995. **121**(11): p. 3593-602.

71. McKerracher, L., M. Chamoux, and C.O. Arregui, *Role of laminin and integrin interactions in growth cone guidance.* Mol Neurobiol, 1996. **12**(2): p. 95-116.

72. Weaver, C.D., et al., *Expression and in vitro function of beta 1-integrin laminin receptors in the developing avian ciliary ganglion.* J Neurosci, 1995. **15**(7 Pt 2): p. 5275-85.

73. Lois, C., J.M. Garcia-Verdugo, and A. Alvarez-Buylla, *Chain migration of neuronal precursors.* Science, 1996. **271**(5251): p. 978-81.

74. Rakic, P., *Principles of neural cell migration.* Experientia, 1990. **46**(9): p. 882-91.

75. Schmid, R.S., et al., *alpha3beta1 integrin modulates neuronal migration and placement during early stages of cerebral cortical development.* Development, 2004. **131**(24): p. 6023-31.

76. Marui, T., et al., *Association of the neuronal cell adhesion molecule (NRCAM) gene variants with autism.* Int J Neuropsychopharmacol, 2009. **12**(1): p. 1-10.

77. O'Dushlaine, C., et al., *Molecular pathways involved in neuronal cell adhesion and membrane scaffolding contribute to schizophrenia and bipolar disorder susceptibility.* Mol Psychiatry, 2011. **16**(3): p. 286-92.

78. Arcangeli, A. and A. Becchetti, *Complex functional interaction between integrin receptors and ion channels.* Trends Cell Biol, 2006. **16**(12): p. 631-9.

79. Chiquet, M., et al., *From mechanotransduction to extracellular matrix gene expression in fibroblasts.* Biochim Biophys Acta, 2009. **1793**(5): p. 911-20.

80. Christ, K.V., et al., *Measurement of single-cell adhesion strength using a microfluidic assay.* Biomed Microdevices, 2010. **12**(3): p. 443-55.

81. Engler, A.J., et al., *A novel mode of cell detachment from fibrillar fibronectin matrix under shear.* Journal of Cell Science, 2009. **122**(10): p. 1647-1653.

82. Griffin, M.A., et al., *Patterning, prestress, and peeling dynamics of myocytes.* Biophys J, 2004. **86**(2): p. 1209-22.

83. Fu, G., et al., *Shear assay measurements of cell adhesion on biomaterials surfaces.* MATER SCI ENG: C, 2009. **29**(4): p. 1293-1301.

84. Irmscher, M., et al., *The influence of inhomogeneous adhesion on the detachment dynamics of adhering cells.* Eur Biophys J, 2013. **42**(6): p. 419-26.

85. Rocha, A., M. Hahn, and H. Liang, *Critical fluid shear stress analysis for cell-polymer adhesion.* Journal of Materials Science, 2010. **45**(3): p. 811-817.

86. Tsang, P.H., et al., *Adhesion of single bacterial cells in the micronewton range.* Proc Natl Acad Sci U S A, 2006. **103**(15): p. 5764-8.

87. Kilinc, D., G. Gallo, and K.A. Barbee, *Mechanically-induced membrane poration causes axonal beading and localized cytoskeletal damage.* Exp Neurol, 2008. **212**(2): p. 422-30.

88. Kilinc, D., G. Gallo, and K.A. Barbee, *Mechanical membrane injury induces axonal beading through localized activation of calpain.* Exp Neurol, 2009. **219**(2): p. 553-61.

89. Alenghat, F.J. and D.E. Ingber, *Mechanotransduction: all signals point to cytoskeleton, matrix, and integrins.* Sci STKE, 2002. **2002**(119): p. e6(1-4).

90. Loulier, K., et al., *beta1 integrin maintains integrity of the embryonic neocortical stem cell niche.* PLoS Biol, 2009. **7**(8): p. e1000176.

91. Nasu, M., et al., *Robust Formation and Maintenance of Continuous Stratified Cortical Neuroepithelium by Laminin-Containing Matrix in Mouse ES Cell Culture.* PLoS One, 2012. **7**(12): p. e53024.

92. Rico, B., et al., *Control of axonal branching and synapse formation by focal adhesion kinase.* Nat Neurosci, 2004. **7**(10): p. 1059-69.

93. Parker, K.K., et al., *Directional control of lamellipodia extension by constraining cell shape and orienting cell tractional forces.* FASEB J, 2002. **16**(10): p. 1195-204.

94. Miller, K., et al., *Mechanical properties of brain tissue in-vivo: experiment and computer simulation.* J Biomech, 2000. **33**(11): p. 1369-76.

95. Pelham, R.J., Jr. and Y. Wang, *Cell locomotion and focal adhesions are regulated by substrate flexibility.* Proc Natl Acad Sci U S A, 1997. **94**(25): p. 13661-5.

96. Adams, W.J., et al., *Engineering design of a cardiac myocyte.* J Comput-Aided Mater Des, 2007. **14**(1): p. 19-29.

97. Grevesse, T., et al., *A simple route to functionalize polyacrylamide hydrogels for the independent tuning of mechanotransduction cues.* Lab Chip, 2013. **13**(5): p. 777-80.

98. Ovadia, H., P.Y. Paterson, and J.R. Hale, *Magnetic microspheres as drug carriers: factors influencing localization at different anatomical sites in rats.* Isr J Med Sci, 1983. **19**(7): p. 631-7.

99. Yagi, K., *The mechanical and colloidal properties of amoeba protoplasm and their relations to the mechanism of amoeboid movement.* Comp Biochem Physiol, 1961. **3**(2): p. 73-91.

100. Parsons, J.T., A.R. Horwitz, and M.A. Schwartz, *Cell adhesion: integrating cytoskeletal dynamics and cellular tension.* Nat Rev Mol Cell Biol, 2010. **11**(9): p. 633-43.

101. Salgin, S., U. Salgin, and S. Bahadir, *Zeta Potentials and Isoelectric Points of Biomolecules: The Effects of Ion Types and Ionic Strengths.* Int. J. Electrochem. Sci., 2012. **7**(12): p. 12404-12414.

102. Schultz, N., et al., *Zeta potential measurement as a diagnostic tool in enzyme immobilisation.* Colloids Surf B Biointerfaces, 2008. **66**(1): p. 39-44.

103. Thielbeer, F., K. Donaldson, and M. Bradley, *Zeta potential mediated reaction monitoring on nano and microparticles.* Bioconjug Chem, 2011. **22**(2): p. 144-50.

104. Lu, Y.B., et al., *Viscoelastic properties of individual glial cells and neurons in the CNS.* Proc Natl Acad Sci U S A, 2006. **103**(47): p. 17759-64.

105. Sanchez, D., et al., *Noncontact measurement of the local mechanical properties of living cells using pressure applied via a pipette.* Biophys J, 2008. **95**(6): p. 3017-27.

106. Bernal, R., P.A. Pullarkat, and F. Melo, *Mechanical properties of axons.* Phys Rev Lett, 2007. **99**(1): p. (018301)1-4.

107. Xu, G., P.V. Bayly, and L.A. Taber, *Residual stress in the adult mouse brain.* Biomech Model Mechanobiol, 2009. **8**(4): p. 253-62.

108. Xu, G., et al., *Axons pull on the brain, but tension does not drive cortical folding.* J Biomech Eng, 2010. **132**(7): p. 071013.

109. Bernal, R., F. Melo, and P.A. Pullarkat, *Drag force as a tool to test the active mechanical response of PC12 neurites.* Biophys J, 2010. **98**(4): p. 515-23.

110. Versaevel, M., T. Grevesse, and S. Gabriele, *Spatial coordination between cell and nuclear shape within micropatterned endothelial cells.* Nat Commun, 2012. **3**: p. 671.

111. Alenghat, F.J., et al., *Analysis of cell mechanics in single vinculin-deficient cells using a magnetic tweezer.* Biochem Biophys Res Commun, 2000. **277**(1): p. 93-9.

112. Kollmannsberger, P. and B. Fabry, *High-force magnetic tweezers with force feedback for biological applications.* Rev Sci Instrum, 2007. **78**(11): p. 114301.

113. Vonna, L., et al., *Local force induced conical protrusions of phagocytic cells.* J Cell Sci, 2003. **116**(5): p. 785-90.

114. Wang, N., et al., *Mechanical behavior in living cells consistent with the tensegrity model.* Proc Natl Acad Sci U S A, 2001. **98**(14): p. 7765-70.

115. Bernick, K.B., et al., *Biomechanics of single cortical neurons.* Acta Biomater, 2011. **7**(3): p. 1210-9.

116. Dai, J. and M.P. Sheetz, *Mechanical properties of neuronal growth cone membranes studied by tether formation with laser optical tweezers.* Biophys J, 1995. **68**(3): p. 988-96.

117. Chada, S., et al., *Cytomechanics of neurite outgrowth from chick brain neurons.* J Cell Sci, 1997. **110 (Pt 10)**: p. 1179-86.

118. Dennerll, T.J., et al., *The cytomechanics of axonal elongation and retraction.* J Cell Biol, 1989. **109**(6 Pt 1): p. 3073-83.

119. Fass, J.N. and D.J. Odde, *Tensile force-dependent neurite elicitation via anti-beta1 integrin antibody-coated magnetic beads.* Biophys J, 2003. **85**(1): p. 623-36.

120. Charles, A.C., et al., *Intercellular signaling in glial cells: calcium waves and oscillations in response to mechanical stimulation and glutamate.* Neuron, 1991. **6**(6): p. 983-92.

121. Regan, R.F. and D.W. Choi, *The effect of NMDA, AMPA/kainate, and calcium channel antagonists on traumatic cortical neuronal injury in culture.* Brain Res, 1994. **633**(1-2): p. 236-42.

122. Lin, Y.W., et al., *Understanding sensory nerve mechanotransduction through localized elastomeric matrix control.* PLoS One, 2009. **4**(1): p. e4293.

123. Cheng, C.M., et al., *Probing localized neural mechanotransduction through surface-modified elastomeric matrices and electrophysiology.* Nat Protoc, 2010. **5**(4): p. 714-24.

124. Mukhin, A., L. Fan, and A.I. Faden, *Activation of metabotropic glutamate receptor subtype mGluR1 contributes to post-traumatic neuronal injury.* J Neurosci, 1996. **16**(19): p. 6012-20.

125. Lucas, J.H., et al., *Neuronal survival or death after dendrite transection close to the perikaryon: correlation with electrophysiologic, morphologic, and ultrastructural changes.* Cent Nerv Syst Trauma, 1985. **2**(4): p. 231-55.

126. Rosenberg, P.A. and M.A. Dichter, *Extracellular cAMP accumulation and degradation in rat cerebral cortex in dissociated cell culture.* J Neurosci, 1989. **9**(8): p. 2654-63.

127. Heisterkamp, A., et al., *Pulse energy dependence of subcellular dissection by femtosecond laser pulses.* Opt Express, 2005. **13**(10): p. 3690-6.

128. Davis, M.J., et al., *Regulation of ion channels by integrins.* Cell Biochem Biophys, 2002. **36**(1): p. 41-66.

129. Dabiri, B.E., H. Lee, and K.K. Parker, *A potential role for integrin signaling in mechanoelectrical feedback.* Prog Biophys Mol Biol, 2012. **110**(2-3): p. 196-203.

130. Bennett, R.E., C.L. Mac Donald, and D.L. Brody, *Diffusion tensor imaging detects axonal injury in a mouse model of repetitive closed-skull traumatic brain injury.* Neurosci Lett, 2012. **513**(2): p. 160-5.

131. Mac Donald, C.L., et al., *Detection of blast-related traumatic brain injury in U.S. military personnel.* N Engl J Med, 2011. **364**(22): p. 2091-100.

132. Anton, E., J.A. Kreidberg, and P. Rakic, *Distinct functions of alpha3 and alpha(v) integrin receptors in neuronal migration and laminar organization of the cerebral cortex.* Neuron, 1999. **22**(2): p. 277-89.

133. Xu, K., G. Zhong, and X. Zhuang, *Actin, spectrin, and associated proteins form a periodic cytoskeletal structure in axons.* Science, 2013. **339**(6118): p. 452-6.

134. Kollmannsberger, P. and B. Fabry, *Linear and Nonlinear Rheology of Living Cells.* Annu. Rev. Mater. Res., 2011. **41**: p. 75-97.

135. Vogt, A.K., et al., *Synaptic plasticity in micropatterned neuronal networks.* Biomaterials, 2005. **26**(15): p. 2549-57.

136. Bhattacharjee, Y., *Neuroscience. Shell shock revisited: solving the puzzle of blast trauma.* Science, 2008. **319**(5862): p. 406-8.

137. Hoge, C.W., et al., *Mild traumatic brain injury in U.S. Soldiers returning from Iraq.* N Engl J Med, 2008. **358**(5): p. 453-63.

138. Elder, G.A. and A. Cristian, *Blast-related mild traumatic brain injury: mechanisms of injury and impact on clinical care.* Mount Sinai Journal of Medicine: A Journal of Translational and Personalized Medicine, 2009. **76**(2): p. 111-118.

139. Cernak, I., et al., *Ultrastructural and functional characteristics of blast injury-induced neurotrauma.* Journal of Trauma-Injury Infection and Critical Care, 2001. **50**(4): p. 695-706.

140. Gennarelli, T.A., et al., *Diffuse axonal injury and traumatic coma in the primate.* Annals of Neurology, 1982. **12**(6): p. 564-574.

141. Sponheim, S.R., et al., *Evidence of disrupted functional connectivity in the brain after combat-related blast injury.* NeuroImage, 2011. **54**(Supplement 1): p. S21-S29.

142. Mac Donald, C.L., et al., *Detection of traumatic axonal injury with diffusion tensor imaging in a mouse model of traumatic brain injury.* Exp Neurol, 2007. **205**(1): p. 116-131.

143. Farkas, O., J. Lifshitz, and J.T. Povlishock, *Mechanoporation induced by diffuse traumatic brain injury: an irreversible or reversible response to injury?* J Neurosci, 2006. **26**(12): p. 3130-40.

144. Spaethling, J.M., et al., *Calcium-permeable AMPA receptors appear in cortical neurons after traumatic mechanical injury and contribute to neuronal fate.* J Neurotrauma, 2008. **25**(10): p. 1207-16.

145. Wang, N., et al., *Mechanical behavior in living cells consistent with the tensegrity model.* Proc Natl Acad Sci U S A, 2001. **98**(14): p. 7765-70.

146. Jaalouk, D.E. and J. Lammerding, *Mechanotransduction gone awry.* Nat Rev Mol Cell Biol, 2009. **10**(1): p. 63-73.

147. Meyer, C.J., et al., *Mechanical control of cyclic AMP signalling and gene transcription through integrins.* Nat Cell Biol, 2000. **2**(9): p. 666-8.

148. Schmid, R.S. and E.S. Anton, *Role of integrins in the development of the cerebral cortex.* Cereb Cortex, 2003. **13**(3): p. 219-24.

149. Watson, P.M., et al., *Integrin-binding RGD peptides induce rapid intracellular calcium increases and MAPK signaling in cortical neurons.* Mol Cell Neurosci, 2007. **34**(2): p. 147-54.

150. Povlishock, J. and C. Christman, *The pathobiology of traumatically induced axonal injury in animals and humans: a review of current thoughts.* Journal of neurotrauma, 1995. **12**(4): p. 555-564.

151. Seong, J., S. Lu, and Y. Wang, *Live Cell Imaging of Src/FAK Signaling by FRET.* Cell Mol Bioeng, 2011. **2**(4): p. 138-147.

152. Hemphill, M.A., J.A. Goss, and K.K. Parker,
An in vitro Magnetic Twisting Cytometry Model for Studying the Role of Specific Cell Adhesion Molecules in Traumatic Brain Injury Proceedings of the International IRCOBI Conference on the Biomechanics of Impact, 2013.

153. Geddes, D.M., R.S. Cargill, 2nd, and M.C. LaPlaca, *Mechanical stretch to neurons results in a strain rate and magnitude-dependent increase in plasma membrane permeability.* J Neurotrauma, 2003. **20**(10): p. 1039-49.

154. Wolf, J.A., et al., *Traumatic axonal injury induces calcium influx modulated by tetrodotoxin-sensitive sodium channels.* J Neurosci, 2001. **21**(6): p. 1923-30.

155. Stone, J.R., et al., *Impaired axonal transport and altered axolemmal permeability occur in distinct populations of damaged axons following traumatic brain injury.* Exp Neurol, 2004. **190**(1): p. 59-69.

156. Rodriguez, M.A., et al., *Colocalization of integrin receptors and reelin in dendritic spine postsynaptic densities of adult nonhuman primate cortex.* Proc Natl Acad Sci U S A, 2000. **97**(7): p. 3550-5.

157. Shi, Y. and I.M. Ethell, *Integrins control dendritic spine plasticity in hippocampal neurons through NMDA receptor and Ca2+/calmodulin-dependent protein kinase II-mediated actin reorganization.* Journal of Neuroscience, 2006. **26**(6): p. 1813-1822.

158. Tomaselli, K.J., et al., *N-cadherin and integrins: two receptor systems that mediate neuronal process outgrowth on astrocyte surfaces.* Neuron, 1988. **1**(1): p. 33-43.

159. Hoang, B. and A. Chiba, *Genetic analysis on the role of integrin during axon guidance in Drosophila.* J Neurosci, 1998. **18**(19): p. 7847-55.

160. Schmidt, C.E., et al., *Integrin-cytoskeletal interactions in neuronal growth cones.* J Neurosci, 1995. **15**(5 Pt 1): p. 3400-7.

161. Webb, D.J., et al., *alpha5 integrin signaling regulates the formation of spines and synapses in hippocampal neurons.* J Biol Chem, 2007. **282**(10): p. 6929-35.

162. Cullen, D.K., M.C. Lessing, and M.C. LaPlaca, *Collagen-dependent neurite outgrowth and response to dynamic deformation in three-dimensional neuronal cultures.* Annals of Biomedical Engineering, 2007. **35**(5): p. 835-846.

163. Wernig, F., M. Mayr, and Q.B. Xu, *Mechanical stretch-induced apoptosis in smooth muscle cells is mediated by beta(1)-integrin signaling pathways.* Hypertension, 2003. **41**(4): p. 903-911.

164. Tzima, E., et al., *Activation of integrins in endothelial cells by fluid shear stress mediates Rho-dependent cytoskeletal alignment.* EMBO J, 2001. **20**(17): p. 4639-47.

165. Birukova, A.A., et al., *Mechanotransduction by GEF-H1 as a novel mechanism of ventilator-induced vascular endothelial permeability.* Am J Physiol Lung Cell Mol Physiol, 2010. **298**(6): p. L837-48.

166. Hwang, Y., C.L. Gouget, and A.I. Barakat, *Mechanisms of cytoskeleton-mediated mechanical signal transmission in cells.* Commun Integr Biol, 2012. **5**(6): p. 538-42.

167. Betz, T., et al., *Growth cones as soft and weak force generators.* Proc Natl Acad Sci U S A, 2011. **108**(33): p. 13420-5.

168. Tomasek, J.J., et al., *Contraction of myofibroblasts in granulation tissue is dependent on Rho/Rho kinase/myosin light chain phosphatase activity.* Wound Repair Regen, 2006. **14**(3): p. 313-20.

169. Schwartz, M.A. and S.J. Shattil, *Signaling networks linking integrins and Rho family GTPases.* Trends in Biochemical Sciences, 2000. **25**(8): p. 388-391.

170. Kimura, K., et al., *Regulation of Myosin Phosphatase by Rho and Rho-Associated Kinase (Rho- Kinase).* Science, 1996. **273**(5272): p. 245-248.

171. Ohashi, K., et al., *Rho-associated Kinase ROCK Activates LIM-kinase 1 by Phosphorylation at Threonine 508 within the Activation Loop.* Journal of Biological Chemistry, 2000. **275**(5): p. 3577-3582.

172. Hashimoto, R., et al., *Domain- and Site-Specific Phosphorylation of Bovine NF-L by Rho-Associated Kinase.* Biochemical and Biophysical Research Communications, 1998. **245**(2): p. 407-411.

173. Amano, M., et al., *Identification of Tau and MAP2 as novel substrates of Rho-kinase and myosin phosphatase.* J Neurochem, 2003. **87**(3): p. 780.

174. Luo, L. and D.D. O'Leary, *Axon retraction and degeneration in development and disease.* Annu Rev Neurosci, 2005. **28**: p. 127-56.

175. Jalink, K., et al., *Inhibition of lysophosphatidate- and thrombin-induced neurite retraction and neuronal cell rounding by ADP ribosylation of the small GTP-binding protein Rho.* J Cell Biol, 1994. **126**(3): p. 801-10.

176. Bito, H., et al., *A critical role for a Rho-associated kinase, p160ROCK, in determining axon outgrowth in mammalian CNS neurons.* Neuron, 2000. **26**(2): p. 431-41.

177. Billuart, P., et al., *Regulating axon branch stability: the role of p190 RhoGAP in repressing a retraction signaling pathway.* Cell, 2001. **107**(2): p. 195-207.

178. Dubreuil, C.I., M.J. Winton, and L. McKerracher, *Rho activation patterns after spinal cord injury and the role of activated Rho in apoptosis in the central nervous system.* J Cell Biol, 2003. **162**(2): p. 233-43.

179. Janowitz, T. and D.K. Menon, *Exploring new routes for neuroprotective drug development in traumatic brain injury.* Sci Transl Med, 2010. **2**(27): p. 27rv1.

180. Matthews, B.D., et al., *Cellular adaptation to mechanical stress: role of integrins, Rho, cytoskeletal tension and mechanosensitive ion channels.* J Cell Sci, 2006. **119**(Pt 3): p. 508-18.

181. Butler, J.P., et al., *Traction fields, moments, and strain energy that cells exert on their surroundings.* Am J Physiol Cell Physiol, 2002. **282**(3): p. C595-605.

182. Upton, G.J.G., *Fisher's exact test.* Journal of the Royal Statistical Society. Series A (Statistics in society), 1992. **155**(3): p. 395-402.

183. Marmarou, C.R., et al., *Quantitative analysis of the relationship between intra-axonal neurofilament compaction and impaired axonal transport following diffuse traumatic brain injury.* J Neurotrauma, 2005. **22**(10): p. 1066-80.

184. Tang-Schomer, M.D., et al., *Mechanical breaking of microtubules in axons during dynamic stretch injury underlies delayed elasticity, microtubule disassembly, and axon degeneration.* FASEB J, 2010. **24**(5): p. 1401-10.

185. Tang-Schomer, M.D., et al., *Partial interruption of axonal transport due to microtubule breakage accounts for the formation of periodic varicosities after traumatic axonal injury.* Exp Neurol, 2012. **233**(1): p. 364-72.

186. Sharp, D.J., G. Scott, and R. Leech, *Network dysfunction after traumatic brain injury.* Nat Rev Neurol, 2014. **10**(3): p. 156-66.

187. Zouridakis, G., et al., *Functional connectivity changes in mild traumatic brain injury assessed using magnetoencephalography.* J. Mech. Med. Biol., 2012. **12**(02).

188. Brenner, L.A., et al., *Neuropsychological test performance in soldiers with blast-related mild TBI.* Neuropsychology, 2010. **24**(2): p. 160-7.

189. Luukinen, H., et al., *Head injuries and cognitive decline among older adults: a population-based study.* Neurology, 1999. **52**(3): p. 557-62.

190. Morrison, B., 3rd, et al., *An in vitro model of traumatic brain injury utilising two-dimensional stretch of organotypic hippocampal slice cultures.* J Neurosci Methods, 2006. **150**(2): p. 192-201.

191. Smith, D.H., et al., *High tolerance and delayed elastic response of cultured axons to dynamic stretch injury.* J Neurosci, 1999. **19**(11): p. 4263-9.

192. Patel, T.P., S.C. Ventre, and D.F. Meaney, *Dynamic changes in neural circuit topology following mild mechanical injury in vitro.* Annals of Biomedical Engineering, 2012. **40**(1): p. 23-36.

193. Eakin, K. and J.P. Miller, *Mild traumatic brain injury is associated with impaired hippocampal spatiotemporal representation in the absence of histological changes.* J Neurotrauma, 2012. **29**(6): p. 1180-7.

194. Greer, J.E., J.T. Povlishock, and K.M. Jacobs, *Electrophysiological abnormalities in both axotomized and nonaxotomized pyramidal neurons following mild traumatic brain injury.* J Neurosci, 2012. **32**(19): p. 6682-7.

195. Wang, N. and D.E. Ingber, *Probing transmembrane mechanical coupling and cytomechanics using magnetic twisting cytometry.* Biochem Cell Biol, 1995. **73**(7-8): p. 327-35.

196. Plow, E.F., et al., *Ligand binding to integrins.* J Biol Chem, 2000. **275**(29): p. 21785-8.

197. Matthews, B.D., et al., *Mechanical properties of individual focal adhesions probed with a magnetic microneedle.* Biochem Biophys Res Commun, 2004. **313**(3): p. 758-64.

198. Ahmad, F.J. and P.W. Baas, *Microtubules released from the neuronal centrosome are transported into the axon.* J Cell Sci, 1995. **108 (Pt 8)**: p. 2761-9.

199. Ahmad, F.J., et al., *An essential role for katanin in severing microtubules in the neuron.* J Cell Biol, 1999. **145**(2): p. 305-15.

200. Bengtson, C.P., et al., *Calcium responses to synaptically activated bursts of action potentials and their synapse-independent replay in cultured networks of hippocampal neurons.* Biochim Biophys Acta, 2013. **1833**(7): p. 1672-9.

201. Ikegaya, Y., M. Le Bon-Jego, and R. Yuste, *Large-scale imaging of cortical network activity with calcium indicators.* Neurosci Res, 2005. **52**(2): p. 132-8.

202. LaPlaca, M.C., et al., *High rate shear insult delivered to cortical neurons produces heterogeneous membrane permeability alterations.* Conf Proc IEEE Eng Med Biol Soc, 2006. **1**: p. 2384-7.

203. Cater, H.L., et al., *Stretch-induced injury in organotypic hippocampal slice cultures reproduces in vivo post-traumatic neurodegeneration: role of glutamate receptors and voltage-dependent calcium channels.* J Neurochem, 2007. **101**(2): p. 434-47.

204. Yu, Z. and B. Morrison, 3rd, *Experimental mild traumatic brain injury induces functional alteration of the developing hippocampus.* J Neurophysiol, 2010. **103**(1): p. 499-510.

205. Brewer, G.J. and J.R. Torricelli, *Isolation and culture of adult neurons and neurospheres.* Nat Protoc, 2007. **2**(6): p. 1490-8.

206. Wang, N. and D.E. Ingber, *Control of cytoskeletal mechanics by extracellular matrix, cell shape, and mechanical tension.* Biophys J, 1994. **66**(6): p. 2181-9.

7 List of Publications

1. Mosadegh B, **Dabiri BE**, Lockett MR, Derda R, Campbell P, Parker KK and Whitesides GM. Three-Dimensional Paper-Based Model for Cardiac Ischemia. *Advanced Healthcare Materials*. 2014; (3) 2

2. **Dabiri BE**, Lee H, & Parker KK. A potential role for integrin signaling in mechanoelectrical feedback. *Progress in biophysics and molecular biology*. 2012. 110(2-3):196-203.

3. Hemphill MA*, **Dabiri BE***, Gabriele S*, Kerscher L, Franck C, Goss JA, Alford PW, Parker KK. A possible role for integrin signaling in diffuse axonal injury. *PLoS One*. 2011;6(7):e22899.

4. Alford PW, **Dabiri BE**, Goss JA, Hemphill MA, Brigham MD, Parker KK . Blast-induced phenotypic switching in cerebral vasospasm. *Proc Natl Acad Sci U S A* 2011;108(31):12705-12710.

5. Kennedy B, Okon A, Aghazarian H, Badescu M, Bao X, Bar-Cohen Y, Chang Z, **Dabiri BE**, Garrett M, Magnone L, Sherrit S. Lemur IIb: a robotic system for steep terrain access. *Industrial Robot-an International Journal*. 2006;33(4):265-269.

*Contributed Equally